6th International Conference on Magnetic Resonance Microscopy

"The Heidelberg Conference"

Organised by:

The Spatially Resolved Magnetic Resonance Division of The Groupment Ampère

2nd – 5th September 2001
Jubilee Campus
University of Nottingham
UK

Welcome !

Welcome to the 6th International Conference on Magnetic Resonance Microscopy – the Heidelberg Conference. Following its return to Heidelberg in 1999, the 2001 meeting moves westwards in location to Nottingham in the East Midlands of the United Kingdom.

The conference is organised under the auspices of the "Division of Spatially Resolved Magnetic Resonance" of the Groupement Ampère. It provides a unique forum for the discussion of the latest advances in NMR and EPR techniques for imaging and localised spectroscopy and their application to chemistry, physics, biology, and medicine, as well as to materials and earth sciences.

The meeting takes place at the recently constructed Jubilee Campus of the University of Nottingham, with the main focus of the meeting being The Exchange (CTF) located at lake-side and close to the conference accommodation in Southwell Hall. Talks will be presented in Lecture Theatre 3 (LT3) of this building, while the posters and industrial exhibition will be sited in the CTF Foyer. The conference registration and information desk will also be located in this area.

The conference begins with a one-day Educational Session on Sunday 2nd September, in which eight invited speakers will cover topics ranging from k-space to q-space and back again. The main meeting is spread over the following three days comprising nine sessions of oral presentations and two poster sessions. There are ten invited presentations by leading practitioners and thirty oral presentations selected from the submitted abstracts. Over 50 posters will be on display. Each abstract was considered by two referees drawn from the organising committee and their combined scores used to award oral or poster presentations.

Following the precedent set by the previous meeting in Heidelberg, we are holding a 'Young Investigators' competition. Four abstracts, by young researchers, have therefore been selected for oral presentation. These 'finalists' have already had their conference fee waived. Their extended presentations will be 30 minutes long and will be judged by a panel of experts to determine an overall winner. A presentation will be made (after 26 hours of deliberation!) to the winner at the conference dinner.

In addition to all the hard work, we have planned a full social programme, including an excursion to Nottingham Castle, a barbecue and the conference dinner.

The Organising Committee of the 6th ICMRM would like to acknowledge the generous support of this meeting by Bruker; Doty Scientific; Rapid Biomedical and Resonance Instruments.

We hope you have an enjoyable and rewarding time here in Nottingham.

Conference Local Organising Committee:

Co-Chairmen:	Prof. Peter McDonald (University of Surrey)
	Prof. Richard Bowtell (University of Nottingham)
Committee:	Dr. Paul Glover (University of Nottingham)
	Dr. Walter Köckenberger (University of Nottingham)
	Prof. John Strange (University of Kent)
	Prof. Peter Morris (University of Nottingham)
	Dr. Simon Doran (University of Surrey)

Conference Programme

Abstracts for the scientific programme will be found in this book. The abstracts are numbered as *L-n* for invited contributions, *C-nn* for oral presentations, *Y-n* for the 'young investigator' presentations, and *P-nn* for posters. The chronological day-by-day programme guide gives the abstract number. There is an alphabetic list of first authors in the index at the back of this book.

Oral Presentations

If you are a presenter then please ensure that the technician in charge of the audio-visual equipment is aware of your requirements. If data needs to be loaded onto the computer provided, this operation should be carried out well in advance. The following presentation facilities are available: overhead projection, dual 35mm slide projection and computer data projection. Facilities are available for loading and checking slide carousels in room C34. Carousels should be labelled and delivered to the projection room before the start of the session. PC based Microsoft PowerPoint (97/2000) is provided for computer based presentations. Files may be provided on floppy, CDROM or Iomega Zip disks.

Posters and Poster Sessions

The posters should be attached to the boards using Velcro sticky pads, and these will be provided. Posters can be put up on Sunday 2nd September from 4:00pm onwards, and should be in place by 9:00am on Monday 3rd September. Posters should remain in place for the duration of the scientific conference, but must be removed by 9:00am on Thursday 6th September. Any posters remaining after this time will be removed and disposed of.

There are two poster sessions planned where it is expected that presenters will 'stay close' to their own poster (Monday evening (with drinks) and Tuesday late morning). We understand that poster presenters need to talk to other presenters, so we are going to try and bring people together in the following way: near the poster boards, there will be 'index sheets', and you can put your name by a poster title to alert the presenter that you want to see them. If you are a presenter then you can then put a time by the name and arrange a meeting. Sticky 'Post-it' notes are also available for leaving details on posters.

Meals

All meals will be served in The Atrium cafeteria located near Southwell Hall, except for the barbecue and the conference dinner. Tea and coffee during the day will be served in the foyer in The Exchange adjacent to posters and exhibitors.

The 'welcome' barbecue will take place in the courtyard of Newark Hall.

Bars

The bar in Southwell Hall will be open until 12:00pm during the conference (except Sunday when we are using Newark Hall). After the conference dinner, there will be a late bar until 01:00am.

Excursion to Nottingham Castle

A trip to Nottingham Castle and its caves, followed by a visit to the oldest pub in England has been planned for Tuesday evening. A bus has been organised to take delegates to and from Nottingham.

Conference Dinner

The conference dinner will take place at 7:30pm in the Portland Building Dining Room on the university main campus (19 on map). Transport will be available, but you may wish to walk – particularly if you would like to visit the MR Centre en-route (near 25 on map). Return transport will be available. Dress is casual. Further details will be announced during the conference.

Computing Facility

Computers are available (in room B4 of The Exchange on the second floor) for Internet or Telnet access. Five PCs are available for the _afternoons only_ during the conference.

Telephones

To make telephone calls from the 'phone in your room, you will need to buy a card from the Hall Manager or porter. These are available in various denominations. You may want to buy as a group for efficient usage. Incoming calls do not require you to purchase a card. Unfortunately, it will not be possible to connect laptop modems to the 'phone socket – apparently this facility just doesn't work yet.

Checking out

You should vacate your room by 10:00am on the day of departure (Thursday 6th for most delegates). There is a secure room should you wish to leave luggage until later in the day.

Exhibitors

Bruker, Doty Scientific and Resonance Instruments will be exhibiting during the meeting. Please visit their stands in the foyer by the posters and their web-sites when you get home. Links may be followed from the meeting web-site. Literature of interest to the NMR community has been supplied by other commercial organisations and is displayed in the foyer area.

Doty Scientific

RAPID
Biomedical

Biomedizinische Geräte GmbH

BRUKER

RESONANCE

Scientific Conference Programme

Monday September 3rd 2001 (Morning)

Time	Presenter	Affiliation	Title	Abstract
8:45			Welcome and opening remarks	
	Opening Lecture			
9:00 – 9:40	**Sir Peter Mansfield**	University of Nottingham	Aspects of NMR Microscopy	L1
	Oral Session 1	**Porous Media**	**Chair: Rainer Kimmich**	
9:40 – 10:20	**Lynn Gladden**	Cambridge University, UK	Magnetic resonance imaging of single- and two-phase flow in packed bed reactors	L2
10:20 – 10:40	**J Stepisnik**, A Mohoric, A Duh	Universities of Ljubljana and Maribor. SLO	Molecular transport in a porous media by the pulse-gradient-spin-echo spectral analysis	C1
10:40 – 11:00	**M. Britton**, R. Graham and K. Packer	Universities of Cambridge and Nottingham, UK	Correlation of Displacements and Relaxation Behaviour of Fluids in Porous Media	C2
11:00 – 11:25	Tea and Coffee		Served in the Foyer Poster Area on Ground Floor	
	Oral Session 2	**Liquids Behaviour**	**Chair: Richard Bowtell**	
11:25 – 11:45	**H. Van As**, A Heibel, T W J Scheenen, J J Heiszwolf *et al*	Wageningen University, NL and others	MRI of liquid phase distribution and its effect on reactor performance in the film flow monolith reactor	C3
11:45 – 12:05	**F Grinberg**, R Kimmich	University of Ulm, GER	Monitoring Ultraslow Dipolar Correlations in Organised Liquids	C4
12:05 – 12:25	**C Heine**, S Stapf, B Blümich	RWTH Aachen, GER	3D wave analysis in thin falling liquid films - an NMR study	C5
12:25 – 13:40	Lunch		Served in the Atrium Cafeteria	

Monday September 3rd 2001 (Afternoon)

Time	Presenter	Affiliation	Title	Abstract
	Oral Session 3	**Biomedical**	**Chair: Robert Wind**	
13:40 – 14:25	**R. Jacobs**	Beckman Institute, Caltech, CA, USA	Looking Deeper into Vertebrate Development: Micro-MRI Applications in Developmental Biology	L3
14:25 – 14:45	**L W Hedlund**, B Fubara, G P Cofer, S J Kelly	Duke University, NC, USA	Using 3-D MR Microscopy for Morphologic Phenotyping: Analysis of a Uricase Knockout Mouse	C6
14:45 – 15:05	**S Köhler**, K-H Hiller, C Waller *et al*	University of Würzburg, GER	High resolution T_2^* imaging of the chronic infarcted isolated rat heart at 11.75T	C7
15:05 – 15:25	**J-M Bonny**, L Maunier, J-P Renou	INRA Unité STIM, FRA	Optimisation of high resolution MR imaging of muscle structure at 4.7 T	C8
15:25 – 15:45	A T Kryzak, **A Jasinski**, D Adamek *et al*	Inst. Of Nuclear Physics, Kraków, POL	Application of diffusion tensor microscopy to study spinal cord nervous tracts in a rat model of spinal cord injury	C9
15:45 – 16:00	Tea and Coffee		Served in the Foyer Poster Area on Ground Floor	
	Oral Session 4	**Techniques**	**Chair: Katsumi Kose**	
16:00 – 16:40	**Oleg Grinberg**	Dartmouth Medical School, New Hampshire, USA	Spatially Resolved EPR Oximetry *in-vivo*	L4
16:40 – 17:00	**I Sersa**, S Macura	Jozef Stefan Inst. SLO and Mayo Clinic, MN, USA	Spatially Selective NMR Observation with a High Spectral and Spatial Resolution	C10
17:00 – 17:20	**S Gutteridge**, C Ramanatha, R Bowtell	University of Nottingham, UK	Microscopic Susceptibility Contrast in the CRAZED Experiment	C11
17:20 – 17:40	**U Mikac**, A Demsar, I Sersa, F Demsar	Jozef Stefan Inst. and University of Ljubljana, SLO	Electric Current Density Imaging of a Tablet Dissolution	C12
17:40 – 17:45	**R. Valiullin** and I Furó	Royal Inst. of Technology, Stockholm, SWE	Liquid-liquid phase Separation in Porous Systems as seen by NMR cryoporometry	C13
19:00 – 20:00	Dinner		Served in the Atrium Cafeteria	
20:00 – 21:30	**Poster Reception**		Foyer	

Tuesday September 4th 2001 (Morning)

Time	Presenter	Affiliation	Title	Abstract
	Oral Session 5	**Plants and Animals**	**Chair: Walter Köckenberger**	
8:45 – 9:25	**A Haase**	University of Würzburg, GER	NMR Microimaging in Small Animals and Applications to Cardiovascular Research	L5
9:25 – 9:45	**H Shinar**, K Keinan-Adamsky, U Eliav, G Navon *et al*	Tel Aviv University ISR and Kyoto Prefectural University of Medicine, Kyoto, JPN	Double Quantum Filtered and Quadrupolar Echo MRI Microscopy of Cartilage	C14
9:45 – 10:05	**Y Seo**, H Shinar, Y Morita *et al*	Kyoto Prefectural University of Medicine, Kyoto, JPN and others	Degeneration of Neurofilament of Rat Sciatic Nerve Detected by ^{2}H Double Quantum Filtered NMR Spectroscopy and Microscopy	C15
10:05 – 10:25	**K Potter**, R D Leapman, P J Basser *et al*	Armed Forces Inst. of Pathology, Maryland, USA and others	Bone Formation Studied by Proton NMR Microscopy	C16
10:25 - 10:45	**S M Glidewell**, D Masson, B Williamson *et al*	Scottish Crop Res. Inst., Dundee, UK and others	NMR Imaging as a Tool in Podocarp Taxonomy	C17
10:45 – 11:05	**L van der Weerd**, F J Vergeldt, S M Melnikov *et al*	Wageningen University, NL	Interpretation of relaxation and diffusion parameters of plants during osmotic stress	C18
11:05 – 11:25	Tea and Coffee		Served in the Foyer Poster Area on Ground Floor	
	Posters			
	Division Meeting			
12:30 – 13:30	Lunch		Served in the Atrium Cafeteria	

Tuesday September 4th 2001 (Afternoon)

Time	Presenter	Affiliation	Title	Abstract
	Invited Lecture		**Session chair: Axel Haase**	
13:30 – 14:10	Timothy Havel	MIT, Cambridge USA	Quantum Information Processing and NMR	L6
	Young Investigator 1			
14:10 – 14:40	Song-I Han	RWTH Aachen, GER	NMR Imaging of a Falling Drop	Y1
14:40 – 15:10	Steven Beyea	New Mexico Resonance, USA	Spatially Resolved Isotherms of Thermally Polarised Gases in Mesoporous Solids using NMR Imaging	Y2
15:10 – 15:35	Tea and Coffee		Served in the Foyer Poster Area on Ground Floor	
	Invited Lecture		**Session chair: Axel Haase**	
15:35 – 16:15	Michael McCarthy	University of California, USA	Magnetic Resonance Imaging of Food Systems	L7
	Young Investigator 2			
16:15 – 16:45	Alexandre Khrapitchev	Massey University, NZ	NMR as a Tool for the Investigation of Velocity Fluctuation in Porous Media	Y3
16:45 – 17:15	Derek Seeber	Ohio State University, USA	Toward MRI of Single Biological Cells at Micron Resolution	Y4
17:30	Dinner		Served in the Atrium Cafeteria	
18:30 -	**Excursion to Nottingham Castle and Mortimer's hole** www.nottinghamcity.gov.uk/coun/department/leisure_com/castle/castlea.asp **Visit to "Ye Olde Trip to Jerusalem"**. www.triptojerusalem.com/history.htm			

Wednesday September 5th 2001 (Morning)

Time	Presenter	Affiliation	Title	Abstract
	Oral Session 6	**Materials**	**Chair: Peter McDonald**	
9:00 – 9:40	**Ross Mair**	Harvard-Smithsonian Center for Astrophysics, CA, USA	Novel MRI Applications using Laser Polarised Noble Gases	L8
9:40 – 10:20	**Igor Koptyug**	International Tomography Centre, Novosibirsk, RUS	NMR Studies of Hydrocarbon Gas Flow and Dispersion	L9
10:20 – 10:40	**B J Balcom**	University of New Brunswick, NB, CAN	Pure Phase Encode MRI of Materials	C19
10:40 – 11:10	Tea and Coffee		Served in the Foyer Poster Area on Ground Floor	
	Oral Session 7	**Materials**	**Chair: Bernhard Blümich**	
11:10 – 11:30	**A J Sederman**, M D Mantle, L F Gladden *et al*	University of Cambridge UK and others	A new MRI method for measurement of non-steady state two-phase flow: Application to single and multi-channel flow	C20
11:30 – 11:50	S D Beyea, **S Altobelli**	New Mexico Resonance, NM, USA	3-Phase Sedimentation/Flotation	C21
11:50 – 12:10	**R E Botto**, D L VanderHart	Argone National Lab., IL and Inst. of Standards and Technology, MD, USA	Beyond Microscopy: NMR Nanoscopy of Complex Systems	C22
12:10 – 12:30	**D Canet**	Université Henri Poincaré, Nancy, FRA	Carbon-13 Chemical Shift Imaging of rotating solids by Radio-Frequency Field Gradients. Spin Relaxation Filters	C23
12:30 – 13:40	Lunch		Served in the Atrium Cafeteria	

Wednesday September 5th 2001 (Afternoon)

Time	Presenter	Affiliation	Title	Abstract
	Oral Session 8	**Hardware**	**Chair: Eiichi Fukushima**	
13:40 – 14:20	**A. Webb**	University of Würzburg, GER	Biological applications of magnetic resonance microspectroscopy and microimaging	L10
14:20 – 14:40	**R A Wind**, D S Daly, G R Holtom *et al*	Pacific Northwest National Lab. ,WA, USA	Integrated Optical/Magnetic Resonance Microscopy for Cellular Research	C24
14:40 – 15:00	**K Kose**, Y Matsuda, T Haishi *et al*	University of Tsukuba, JPN	Super-Parallel MR Microscope	C25
15:00 – 15:20	**J Leggett**, S Crozier, R W Bowtell	Universities of Nottingham and Brisbane, UK and AUS	Multi-layer Actively Shielded Gradient Coils	C26
15:20 – 16:00	**Y Matsuda**, T Haishi, Y Yamazaki *et al*	University of Tsukuba, JPN and others	Compact MR Microscopes Using Dipole-Ring Permanent Magnets	C27
16:00 – 16:20	Tea and Coffee		Served in the Foyer Poster Area on Ground Floor	
	Oral Session 9	**STRAFI**	**Chair: Teresa Nunes**	
16:20 – 16:40	J Godward, **P J McDonald**	University of Surrey, UK	Orthogonal switched gradients applied in stray field magnetic resonance imaging	C28
16:40 – 17:00	**G Guillot**, T G Nunes, J P Ruaud *et al*	Universities of Paris-Sud and Lisbon, FRA and POR	Photopolymerisation of a commercial dental resin: ^{1}H conventional and stray-field MRI studies	C29
17:00 – 17:20	**K Saito**, Y Saito, J Godward	Nippon Steel Corp., JPN & University of Surrey, UK	A Stray Field Imaging Study of the Drying Process of Precasting Materials used in a Steel Making Converter	C30
			Transport or walk to Main Campus	
			Tour of MR Centre	
19:30			**Reception in Portland Building Ballroom**	
			Conference Dinner and Young Investigator prize-giving	
22:00			Transport back to Jubilee Campus. Late bar in Hall	

Abstracts from:
Invited Speakers
L1 – L10

Abstracts from:
Young Investigators
Y1 – Y4

Aspects of NMR Microscopy

P Mansfield

Magnetic Resonance Centre, School of Physics & Astronomy, University of Nottingham, University Park, Nottingham, UK.

One of the major motivating challenges of NMR microscopy was whether or not the technique could be used to look inside biological cells. The problem is that many animal cells that one might wish to study are relatively small, around 10 μm, or less. Thus, initial work on NMR microscopy was focused on resolution. However, it was apparent from MRI that the pursuit of resolution was made at the expense of imaging time and S/N for a given static magnetic field strength. Early considerations soon showed that very high field strengths are required to approach reasonable imaging times with desired resolution and satisfactory S/N.

To circumvent the cell size problem plant cells which can be much larger than animal cells were studied initially, but it soon became apparent that due to intercellular air spaces, magnetic susceptibility effects at the very high static fields used could vitiate image quality unless steps were taken to overcome this effect.

Other deleterious effects arising from rapid gradient switching led initially in MRI and now in microscopy to active magnetically screened gradient coils.

If resolution and S/N are kept constant and if the sample is inanimate (eg rock) it would appear that time is the only penalty paid for image quality and, therefore, imaging for a very long time ought to produce the desired effect. But this assumes long term equipment stability and no external or internal sources of movement or vibration. The main criterion is that these extraneous sources produce movements which are less than the desired resolution. As resolution is pushed higher and higher, this criterion becomes harder to meet.

L-1

Magnetic Resonance Imaging of Single- and Two-Phase Flow in Packed Bed Reactors

Lynn F Gladden
University of Cambridge
Department of Chemical Engineering
Pembroke Street
Cambridge CB2 3RA
United Kingdom

Over the past five years, the magnetic resonance group in the Department of Chemical Engineering at Cambridge has focussed on the acquisition and analysis of visualisations of flow in various porous media. A motivation for many of these studies was to achieve visualisations of both the inter-particle space and the flow field within it, at relatively high spatial resolution – for the fixed-bed reactor systems considered here, typical spatial resolution was 100 – 200 μm for a packing of beads of diameter 1 – 5 mm. Our initial studies were performed for single-phase flows through these fixed beds. The aim of this work has been two-fold. First, we wish to gain greater insight into the influence of the characteristics of the inter-particle space on the hydrodynamics within the bed. Second, we have become interested in using these high-resolution flow visualisations to validate and develop numerical flow simulation codes. This presentation will review some of this earlier work and then summarise the results of some of our more recent studies on two-phase flow and single-channel flow. In the case of two-phase flow, we have studied an air-water flow within a fixed bed and been able to investigate the effect of gas and liquid superficial velocities on liquid saturation and surface wetting. The studies addressing single-channel flow will be presented more fully, later in the meeting, by Dr A. J. Sederman, but will be highlighted here as an example of how we are using ultra-fast acquisitions to explore flow phenomena in reactor environments at time-scales approaching 'real time'.

Looking Deeper into Vertebrate Development
MicroMRI Applications in Developmental Biology

Russell E. Jacobs

The exquisite sensitivity of MRI to the local physical and chemical environment provides a wide range of mechanisms giving rise to intrinsic contrast in the MR experiment, thus providing images with dramatic differences between different tissue types (*e.g.* white versus gray matter, myelinated versus unmyelinated fibers, and brain parenchyma versus ventricles). The recent advent of MRI contrast agents that are physiologically sensitive opens up new avenues of study, not the least of which is the potential for *in vivo* imaging of gene expression.

Three-dimensional digital atlases of normal development in the mouse

Gene expression patterns, receptor domains, arrays of innervation in the developing nervous system, cell lineage patterns, and a host of other types of biological processes in embryonic and adult animals take place in three spatial and one temporal dimensions. They occur within the context of anatomy of the specific sample being examined. Digital atlases provide a means to put such specific data within the context of normal specimen anatomy, analyze the information in three (or more) dimensions, and examine relationships between different types of information. The atlas discussed here is composed of three different modules: unprocessed μMR images of fixed embryos aged 6.5 to 15.5 days post conception (dpc); an annotated atlas of the anterior portion of a 13.5dpc mouse where anatomical structures in transverse sections of the embryo have been delineated and linked to descriptive files; a three-dimensional model of the 13.5dpc embryo. As an example of how other types of information can be incorporated into this model, we have 'painted' in the gene expression pattern of Dlx5/Dlx6 genes that are involved in the regulation of forebrain development.

Smart contrast agents: selective enhancement of

Geography (what's where when)
Biochemistry (gene expression -> enzyme activity)
Physiology (Ca^{2+} level changes)
Active Neuronal Tracts (Mn^{2+})

SPATIALLY RESOLVED EPR OXIMETRY IN VIVO.

Oleg Y. Grinberg, *Alex I. Smirnov, and Harold M. Swartz.

Dartmouth Medical School, Hanover, New Hampshire 03768 USA
* North Carolina State University, Raleigh, NC 27695, USA

The technique of in vivo EPR has undergone extensive development recently and is becoming a very powerful method for measuring parameters that are difficult to measure by other techniques. It provides information that cannot be obtained as readily by other approaches. The information includes measuring key parameters such as oxygen, redox reactions, pH, and molecular motion. In vivo EPR also has been shown to be able to directly observe free radicals in vivo, a unique and very important capability.

Both spectroscopy and imaging techniques have been developed. Imaging provides the potential to have spatially resolved information, but can be limited by sensitivity. Conventional spectroscopy is inherently more sensitive because the information is not divided over many voxels, but does not provide detailed spatial resolution. Recently, however, techniques have emerged that provide both spectroscopy and spatial resolution. These hybrid techniques range from full spectral-spatial imaging in four dimensions to well localized single voxels. In this presentation the range of techniques will be discussed at a general level. We then will consider in detail results achieved with the technique that we have emphasized: spatially resolved spectroscopy, especially for in vivo oximetry.

During the past several years significant progress in EPR oximetry in vivo has been achieved by technical improvement of L-band (1100 MHz) EPR spectrometers and development of new oxygen sensitive materials. This technique can provide quite accurate and relatively quick reading of actual pO_2 at specific sites non-invasively, after initial placement of the oxygen sensitive material in tissue. The pO_2 measurements can be performed continuously even in awake animals. EPR oximetry now has been used effectively for several specific investigations in the brain: [1] the effects of various anesthetics on brain oxygenation; effects of a hemoglobin shifter on cerebral pO_2 under baseline conditions and [2, 3] after acute hemorrhage; [4] the study of acute cerebral ischemia and reperfusion, induced by selective reversible unilateral occlusion of the middle cerebral artery (MCAO).

Almost all of the experimental uses of in vivo EPR oximetry will benefit from the ability to make spatially resolved measurements at multiple sites. The new method to enhance the spatial resolution of multi-site EPR oximetry will be describe. The method is suitable for any shape (density distribution function) of a solid paramagnetic material implanted in tissue. It corrects for distortions of line shapes caused by the gradient and thus overcomes limitations of previous multi-site EPR oximetry methods that restricted the ratio of the particle size to the distance between sites. The new method is based on consecutive applications of magnetic field gradients with the same direction but with different magnitude and uses a convolution-based fitting algorithm to derive Lorentzian EPR line width of each individual peak of the EPR spectrum. The method is applicable for any particulate EPR oxygen sensitive materials whose EPR spectra can be approximated by a Lorentzian or a superposition of Lorentzian functions. By

incorporating this model of the line shape in the data processing, we are able significantly to decrease the number of parameters needed for the calculations and to recover the oxygen concentration even from quite noisy spectra. The method and the data-processing algorithm will be described, the approach in model and in vivo experiments will be demonstrated, and the limitations will be discussed. The hardware and software for such measurements are under active development and already have been applied effectively to measure cerebral pO_2 at several sites simultaneously, e.g. acute changes of the pO_2 in both the ischemic and control sides of the brain were measured simultaneously over the entire experimental period. Detailed data from these studies will be presented.

References.

1. Taie S, Leichtweis SB, Liu KJ et al, Adv. Exp. Med. Biol. 471 189-198(1999).
2. Grinberg OY, Miyake M, Steffen RP et al, Proc. of the 27th ISOTT meeting. (Dunn, J.F. and H.M. Swartz eds.). Pabst Science Publishers. Lengerich. (2001).
3. Miyake M, Grinberg OY, Hou H, et al, Proc. of the 27th ISOTT meeting. (Dunn, J.F. and H.M. Swartz eds.). Pabst Science Publishers. Lengerich. (2001).
4. Grinberg OY, Hou H, and Swartz HM in "Ischemic Blood Flow in the Brain" Fukuuchi Y, Tomita M, and Koto A (Des), Keio University Symposia for Life Science and Medicine; 6:381-389(2000).

NMR Microimaging in Small Animals and Applications to Cardiovascular Research

A. Haase, J. Ruff, F. Wiesmann, M. Nahrendorf, J. Streif, M. Szimtenings, C. Faber
Physics Institute and University Hospital, University of Wuerzburg, Germany

Mouse models are gaining widespread applications in cardiovascular research. Animal models based on gene overexpression, ablation, or mutation together with cardiac infarct and heart failure models are appearing at a rapid pace. Non-invasive and sequential imaging methods are needed to characterize the anatomy, function, microcirculation and biochemistry of the heart in vivo. NMR imaging has proven to be applicable in the assessment of cardiac morphology and function in animal and clinical studies. In order to perform NMR-experiments on small animals, spatial and time resolution must be taken to the limits. In this presentation, we report on MR experiments at field strengths from 7 T to 17.6 T. Experiments were first performed on a 7 T (horizontal bore, 20 cm diameter) Bruker Biospec equipped with a 870 mT/m maximum gradient coil insert. We have used a quadrature single-tuned transmit/receive birdcage coil adapted to the diameter of a mouse thorax. In all cases, fast gradient echo (FLASH) sequences were used with TE = 1.5 ms, TR = 4.3 ms, in-plane spatial resolution of 70 μm and varying slice thickness of 100 μm to 500 μm. The sequence was ECG-triggered using a ECG-trigger unit (RAPID Biomedical, Würzburg). The mean heart rate varied between 400 and 600 beats/min. Recently, we were able to perform the same experiments on a 17.6 T (Bruker) spectrometer (vertical bore size: 89 mm).

In all experiments ECG-triggered sequences result in multi-slice cine-MRI data. Using the intrinsic inflow contrast between the flowing blood pool in the heart chambers and the myocardium, left ventricular cavity and the myocardium can be segmented. From the heart cycle dependent variation of these image data, the stroke volume, ejection fraction, cardiac output and the myocardial mass can be calculated. In further experiments, we applied additional motion-sensitive gradient pulses and used the phase-contrast to calculate the amount and direction of the flow velocity of the blood inside of large vessels and the velocity of the myocardial motion. The strong inflow-contrast of FLASH images gives also access to the visualization of blood vessels. We were able to reconstruct 3D-coronary angiograms from the beating mouse heart in vivo.

We have used these experiments in a series of animal models, including chronic cardiac infarct and different transgene mouse models. We will also present first results of NMR microimaging of the mouse heart at 17.6 T.

Quantum Information Processing and Nuclear Magnetic Resonance

Timothy F. Havel and David G. Cory
(MIT, Cambridge, U.S.A.)

Introduction. Quantum information processing (QIP) is an emerging field of engineering which is expected to play an important role in bringing nanotechnology to the atomic scale, and which promises spectacular increases in computational speed for certain types of problems. Attempts to attain the very high degree of coherent control needed to realize this potential include: charge and/or flux quantized macroscopic SQUIDs; electrons in mesoscopic systems such as quantum dots; the hyperfine states of atoms in electrostatic traps; and nonlinear optics on polarized photons. At this time, however, none of these approaches have succeeded in performing all the operations needed for general purpose QIP on more than a few qubits (quantum bits) [1].

Surprisingly, the most complex demonstrations of QIP to date have been made using liquid-state NMR on *ensembles* of molecules in which the weakly coupled spin 1/2 nuclei serve as qubits. This talk will introduce the ideas and concepts behind QIP, give an overview of what NMR has contributed to the field, and describe the methodology involved. More detailed accounts may be found in Refs. [2, 3].

Spins as Qubits. A *qubit* is a two-state quantum system, of which spin 1/2 nuclei are a prime example. To store a single bit of information in a spin, one measures its magnetic moment along z, and then rotates the result (if need be) parallel the z-axis to represent 0, or antiparallel to represent 1. The Hilbert space vectors of these states are denoted by $|0\rangle$, $|1\rangle$, resp.

If the spin is placed along the x-axis, its state becomes a *superposition* $|0\rangle + |1\rangle$ over both its z-states. The state of two spins along the x-axis is the product of their superpositions, $(|0\rangle + |1\rangle)(|0\rangle + |1\rangle)$, which expands to a sum over all four longitudinal states: $|00\rangle + |01\rangle + |10\rangle + |11\rangle$. Via their binary expansions, this can also be regarded as a sum over the integers $|\underline{0}\rangle + |\underline{1}\rangle + |\underline{2}\rangle + |\underline{3}\rangle$. Similarly, a set of n distinguishable spins all pointing along the x-axis is in a uniform superposition over all the integers ranging from 0 to $2^n - 1$.

In QIP, one computes by applying unitary transformations (e.g. pulse sequences) to the states. For example, the following unitary matrix swaps the states $|10\rangle$ and $|11\rangle$, and so is equivalent to the fragment of C-code shown to the left of it:

```
bits b1, b2 :
if (b1 == 1) {
    b2 = ~b2 ;
}
```
$$\begin{bmatrix} 1 & 0 & 0 & 0 \\ 0 & 1 & 0 & 0 \\ 0 & 0 & 0 & 1 \\ 0 & 0 & 1 & 0 \end{bmatrix} \begin{matrix} |00\rangle \\ |01\rangle \\ |10\rangle \\ |11\rangle \end{matrix}$$

By the linearity of quantum mechanics, unitary transformations applied to spins in a superposition act on all members of the superposition *in parallel*: $\mathbf{U} \sum_i |\underline{i}\rangle = \sum_i \mathbf{U}|\underline{i}\rangle$. Thus if $\mathbf{U}$ executes a computation on the individual z-states (regarded as the memory in a computer), it executes that same computation on all 2^n states when applied to a uniform superposition. In this way one achieves a degree of parallelism which grows exponentially with the size of the problem to be solved.

There is, of course, a catch to this: Measuring the spins in a superposition yields a random result r, and "collapses" them into the corresponding state $|\underline{r}\rangle$. Hence one cannot read out

more than one result at a time! In several interesting cases, however, additional unitary transformations have been found to extract information on the global properties of a superposition far more efficiently than by sampling it. These include determining its periodicity [4], and the correlation functions implied by the probability distribution it defines [5].

Pseudopure States. NMR pulse sequences which implement the requisite unitaries can be designed in a straightforward fashion. Given two J-coupled spins, for example, the following implements the matrix U shown above (up to phase factors) [6]:

$$\left[\frac{\pi}{2}\right]^2_y - \left[\frac{1}{2J}\right] - \left[\frac{\pi}{2}\right]^2_x - \left[\frac{\pi}{2}\right]_z$$

In implementing QIP concepts by NMR, we are faced with an immediate problem: Most of QIP was developed for pure states, but only mixed states are ordinarily available in NMR. This problem is circumvented by *pseudopure* states [7, 2], which can be thought of as a mixture of a single pure state with density matrix $|\psi\rangle\langle\psi|$ and the random state $I/2^n$ (the identity), i.e.

$$\rho = 2^{-n}(1-p)I + p|\psi\rangle\langle\psi|.$$

It is easily seen that transforming ρ to $U\rho U^\dagger$ also transforms $|\psi\rangle$ to $U|\psi\rangle$, and that the ensemble average of any traceless operator O is proportional to its quantum expectation value:

$$\mathrm{tr}(\rho O) = p\langle\psi|O|\psi\rangle.$$

Thus pseudopure states are logically equivalent to true pure states for the purposes of QIP.

There are nonetheless important physical differences between pseudopure states and true pure states. For example, an ensemble does not collapse into a single state upon being measured — although the lack of signal from multiple quantum coherences

similarly restricts our ability to read superpositions. In addition, the preparation of pseudopure states from high-temperature equilibrium spin states results in a loss of signal which grows exponentially with the number of spins [8]. An example of such a preparation procedure for two spins is given by the pulse / gradient sequence

$$\left[\frac{\pi}{4}\right]_x - \left[\frac{1}{2J}\right] - \left[-\frac{\pi}{6}\right]_y - \left[\nabla\right]_z,$$

where $[\nabla]_z$ is a z-gradient pulse.

We have recently developed more advanced means of creating such spin / space correlations, both for pseudopure state preparation [9], and for simulating the decoherence (aka T_2 relaxation) expected in other QIP implementations [10]. These may also prove useful in NMR imaging and microscopy.

Bibliography

[1] DiVincenzo, D. P., Fort. Phys. **48**, 771 (2000).

[2] Havel, T. F., *et al.*, Applic. Algebra in Eng. Commun. & Comput. **10**, 339 (2000).

[3] Cory, D. G. *et al.*, Fort. Phys. **48**, 875 (2000).

[4] Jozsa, R., IEEE Comput. Sci. Eng. **3**, 34 (2001).

[5] Terhal, B. M., & DiVincenzo, D. P., Phys. Rev. A **61**, 22301 (2000).

[6] Cory, D. G., Price, M. D. & Havel, T. F., Physica D **120**, 82 (1998).

[7] Knill, E., Chuang, I., & Laflamme, R., Phys. Rev. A **57**, 3348 (1998).

[8] Warren, W. S., Science **277**, 1688 (1997).

[9] Sharf, Y., Havel, T. F., & Cory, D. G., Phys. Rev. A **62**, 052314 (2000).

[10] Havel, T. F., *et al.*, Phys. Lett. A **280**, 282 (2001).

Magnetic Resonance Imaging of Food Systems

Michael J. McCarthy
Department of Food Science and Technology
University of California, Davis
One Shields Avenue
Davis, CA 95616-8598 USA
Phone: (530) 752-8921
Fax: (530) 752-4759
e-mail: mjmccarthy@ucdavis.edu

Historically, studies of component migration in foods and related polymeric materials have of necessity been integral experiments. An example would be the characterization of food drying from drying rate data only. These integral experiments are often insufficient to allow the investigation of the underlying physics of component transport, particularly in complex food systems. Magnetic resonance imaging makes it possible to resolve the internal spatial distribution and changes as a function of time in that distribution. This information can then be used to understand the physics of the component transport as well as calculate effective transport coefficients, material structure, physical properties and to control production processes.

Magnetic resonance imaging provides noninvasive data for measuring effective rates of component migration and component self-diffusion coefficients. By comparison between the self-diffusion coefficient and the effective rate of moisture transport, information on the mechanisms of transport may be obtained. These mechanisms of transport are often controlled by the structure of the material, for example the role of capillary forces in drying is related to the development of pore structure of the material. The two most significant components related to quality and stability in foods are oil and water. The state, location and the subsequent migration of these components are critical to quality in most foods. The use of MRI for studying changes in foods after and during processing will be detailed in examples of moisture migration in pasta after cooking and for mixing of a powder into a fluid.

The time dependent internal moisture distributions in lasagna pasta were experimentally evaluated and mathematically modeled as a function of cooking time and holding time. During the holding time, changes in the moisture distribution were followed using a magnetic resonance imaging (MRI) spin-echo based pulse sequence, as shown in Figure 1. Immediately after cooking the moisture distribution was highly non-uniform for all samples. The moisture content was high on the surface of the pasta and low in the central plane. This gradient equilibrated over time as the moisture redistributed. The moisture redistribution was modeled using a one-dimensional Fickian diffusion equation; values of the diffusion coefficient ranged from 1.7 to 3.7 x 10^{-7} cm^2/s. The mathematical model developed can be used to predict the holding time of lasagna pasta containing products in food service applications.

Mixing is a critical processing step. The objective is to combine two or more ingredients and distribute each ingredient uniformly in the food. In many food processes high viscosity and/or shear sensitive materials are mixed under laminar flow conditions. In particular, batch mixing is the leading unit operation for mixing

and many times it is difficult to determine the minimum time necessary for adequate mixing. In addition, structures of different concentration can be established that persist for long periods of time. For example in a mixing vessel with paddle style mixer donut shaped regions are observed that indicate two distinct compositions within the vessel. One of the greatest barriers to improving the understanding of mixing is quantitative experimental data. Here, too, magnetic resonance imaging can be utilized to provide highly quantitative measures of component concentrations. Our objective was to evaluate the extent of mixing in a multi-component batch system, specifically a 10 % carbon black powder suspended in solution. The factors in this study were surfactant type [Neodol 23-5 and Sodium Dodecyl Sulfate (SDS)] at two levels: 1 % and 0.1 %. In addition to surfactant type and level, the third factor was mixing mode: with vortex and without vortex motion. These conditions were displayed at 180 rpm and 60 rpm impeller speed respectively. The type of surfactant did not yield significantly different results in terms of analyzing the MR concentration image center characteristics. The mixing rate, as characterized by the normalized mean value, was enhanced at both impeller speeds. Most notably, there was a statistically significant interaction between impeller speed and surfactant concentration. The incorporation of air and subsequent release played an important role in the mixing process.

Magnetic resonance imaging has been used to directly evaluate internal structure and to determine parameters that characterize the physical and chemical properties of materials. Physical property determination requires quantitative interpretation of the MR information. These new insights are gained through an improved understanding of the structures and dynamics of constituents in the products and are utilized to improve product quality, safety, and processing.

(a)   (b)   (c)   (d)
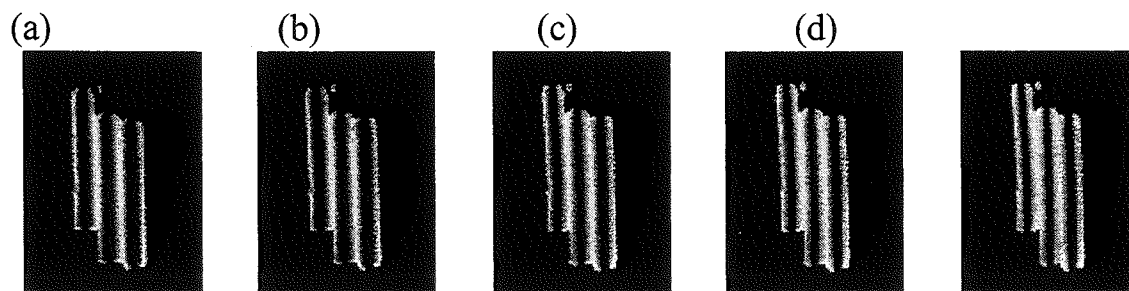
Images of the proton density in the lasagna noodles post cooking, at a cooking time of 9.5 minutes as a function of holding time. Holding time, (a) 15 min, (b) 30 min, (c) 45 min, (d) 60 min, and (e) 80 min.

NOVEL MRI APPLICATIONS USING LASER POLARIZED NOBLE GASES

Ross W. Mair and Ronald L. Walsworth

Harvard-Smithsonian Center for Astrophysics, Cambridge, MA, USA.

Before 1994, gas phase NMR had been a largely neglected field, due to the belief that little useful information could be obtained from a sample whose density was ~ 1000 times lower than water. This view has been changed with the advent of the spin-exchange optical pumping technique which produces large, non-equilibrium spin polarizations (~10%) in samples of the noble gases helium (^{3}He) and xenon (^{129}Xe). This laser-polarization process effectively cancels the spin density deficit, allowing gas phase samples to be created with magnetization density similar to water in magnetic fields ~ 1 T [1]. Such large polarizations enable high-sensitivity gas-phase NMR and MRI, and as a result, the technique has become popular in medical imaging, especially as a non-invasive and high-resolution probe of the human and animal lung space [2].

Our work has focussed on using the peculiar characteristics of the laser-polarized noble gases as NMR-detectable spins to enhance materials and biomedical research with experiments that would not generally be possible using thermally-polarized NMR spins. These include making use of the fact the artificial laser-polarization is created independent of the applied magnetic field, thereby allowing high-sensitivity imaging in fields much lower than those normally associated with MRI [3,4]. The ability to create laser

Figure 1. *Gas-phase imaging at very low fields, showing reduced magnetic susceptibility distortion in comparison to images taken at high field. (A) At 4.7 T an NMR image of a W-shaped water sample is undistorted when no high magnetic susceptibility materials are nearby. (B) The same image is severely distorted when four tubes of paramagnetic salts are placed by the sample. (C-D) At 21 G an NMR image of laser-polarized ^{3}He gas in a triangular glass cell is undistorted both without (C), and with (D), the nearby tubes of paramagnetic salts.*

polarized *liquid* xenon by condensing the laser-polarized gas provides a two-phase system in which both the gas and liquid have extremely high magnetization density, allowing experimental observation of gas-liquid dynamics in a two-phase system [5,6]. The high gas polarization also allows easy observation of xenon exchange into a dissolved state in gas-solid systems such as porous polymers and lung tissue [7]. Finally, the enhanced diffusion coefficient of the gases, at ~ 3 orders of magnitude above water, allow for probing of centimeter length scales in porous media using time-dependent diffusion techniques, an extension of 2 orders of magnitude above what is possible with water diffusion [8,9].

Performing NMR experiments at very low magnetic field is an important new development resulting from the fact the large noble gas polarizations achieved using the spin-exchange optical pumping technique are created without the aid of a high-field magnet. A key feature of operating at very low field strengths (~ 10 - 100 G) is the reduction in background gradients resulting from magnetic susceptibility mismatches, which manifest themselves as severe image distortions. Figure 1 shows water images acquired at 4.7 T and images of laser-polarized ^{3}He taken at 21 G (0.0021 T) in the presence and absence of paramagnetic salts [3]. The ability to avoid such susceptibility effects by operating at low field is a potential benefit not only to human imaging, but also to imaging and diffusion studies of samples rich in paramagnetic impurities or susceptibility mismatches such as reservoir rocks. We are currently constructing a human scale, open, low field imager, which will enable imaging of lung inhalation as a function of gravitational dependence - currently not possible in a conventional high-field MRI scanner with a solenoid superconducting magnet.

At standard pressure, xenon solidifies at 161K and melts at 168K, allowing access to all three phases of xenon at temperatures achieved easily with standard laboratory glassware. Since the xenon liquid NMR resonance is separated by a 250 ppm downfield shift from the gas-phase resonance, one can easily manipulate or observe either phase selectively, and obtain high sensitivity NMR images of the gas or the liquid. Using a sample containing both laser-polarized xenon gas and liquid, we have imaged both a liquid xenon droplet in a glass cell and the xenon gas above it, as is shown in Figure 2. It was also possible to saturate (destroy) the laser-polarized magnetization in the gas phase, and through successive images, watch the gas phase "re-appear" as the laser-polarized signal in that phase is replenished from the evaporating liquid [5]. This phenomenon was studied further by obtaining two-dimensional NMR velocity images of the laser-polarized xenon gas under-

Figure 2: *Magnetic resonance images of laser-polarized liquid (a) and gaseous (b) xenon in a 2.5 cm diameter glass cell acquired sequentially at 4.7 T. The images have a resolution of 195 (a) and 860 (b) micron, and were both acquired in less than 1 min. The arrow in (b) indicates a ghost image of the liquid droplet formed by gas spins exchanging into the liquid during the image acquisition sequence.*

going coherent flow above the droplet of xenon liquid, demonstrating the utility of this technique for studying evaporation, convection, and diffusion in a two-phase system. The high magnetization density in the gas makes such measurements of gas dynamics possible for the first time. We are currently bringing online a larger-scale polarization apparatus which will allow to perform a systematic study of gas flow dynamics in a variety of restricted pathways.

The large electric polarizability of xenon results in significant solubilities and large chemical shifts, especially in lipophilic environments, allowing the dissolved phase signal to be manipulated and observed independently of the gas phase, in a similar manner to that used for liquid xenon above. Using laser-polarized xenon gas imbibed into porous polyethylene granulate, we measured the exchange of xenon between the gas and dissolved phases using a simple saturation recovery sequence. The dissolved phase xenon buildup as a function of exchange time is shown in the spectra in Figure 3. The short-time rate of xenon interphase exchange depends on the surface area of the interface between the dissolved and gas phases, allowing a non-invasive method surface area determination [7]. The porosity and S/V of four different polymer samples were independently obtained by NMR and confocal microscopy.

An important possible application of xenon interphase exchange NMR is mapping the surface area of the lung. The function of the lung is to exchange gases between the bloodstream and the air, and the effectiveness of this process depends critically on the surface area of contact between blood-filled lung tissue and gas in lung alveoli with diameters ~ 100 μm. A non-invasive measure of regional alveolar S/V would provide an early indication of pulmonary failure, as well as fundamental information about normal physiology. Xenon interphase exchange NMR could also be used to measure S/V in a wide variety of non-living, xenon-soluble porous media.
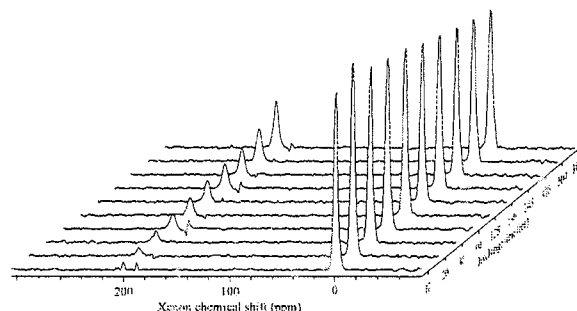
Figure 3: *Xenon interphase exchange spectra as a function of the exchange time. The peaks at 0 ppm arise from the off-center excitation of xenon in the gas phase when the dissolved-phase xenon is pulsed selectively. The dissolved-phase peaks at 200 ppm show recovery as a function of the varying exchange time after the residual magnetization is zeroed by the saturation train.*

One last application of laser-polarized noble gas NMR in materials science has been the study of porous media microstructure by gas diffusion NMR. We have extended the utility of NMR as a technique for probing such structure over length scales of ~ 100 - 2000 μm by using ^{129}Xe gas imbibed into the system's pore space. Such length scales are much greater than can be probed with NMR diffusion studies of water-saturated porous media, the result of (i) gas diffusion coefficients orders of magnitude larger than those of liquids; and (ii) weak noble gas interactions with grain surfaces, allowing inter-pore diffusion without significant surface-induced spin relaxation. In addition, the dependence of the diffusion coefficient on gas pressure allows the gas diffusion coefficient in the porous medium to be controlled in a way that is not possible with water.

We have used NMR to measure the time-dependent diffusion coefficient $D(t)$ of laser- and thermally-polarized ^{129}Xe gas imbibed in various porous media [8,9]. In uniform-size glass bead packs, with bead diameter ranging from 100 μm to 4 mm, $D(t)$ decreased with increasing t, reaching an asymptote of ~ 0.62-$0.65D_0$, consistent with the known tortuosity of random bead packs. Using thermally-polarized ^{129}Xe, we have also obtained the first NMR $D(t)$ measurements that yield the sample tortuosity in large grain (> 50 μm) reservoir rock samples [8]. ^{129}Xe $D(t)$ measurements not only allow the tortuosity limit to be reached, at a diffusion length of ~ 2 mm, but in the approach to this limit the $D(t)$ data shows a number of distinct regions, indicative of the multiple pore length scales present in such complex carbonate rocks.

1. Walker, T., Happer, W., *Rev. Mod. Phys.* 6 9, 629 (1997)
2. Kauczor H., Surkau, R., Roberts, T., *Eur. Radiol.* 8 , 820 (1998)
3. Tseng, C., Wong, G., et al. *Phys. Rev. Lett.*, 8 1, 3785 (1998)
4. Wong, G., Tseng, C., et al, *J. Magn. Reson.*, 1 4 1, 227 (1999)
5. Tseng, C., Mair, R., Wong, G., et al, *Phys. Rev. E* 5 9, 1785 (1999)
6. Mair, R., Tseng, C., Wong, G., et al, *Phys. Rev. E* 6 1, 2741 (2000)
7. Mair, R., Patz. S., Butler, J., et al, 8th ISMRM meeting, 2190 (2000)
8. Mair, R., Wong, G., et al, *Phys. Rev. Lett.* 8 3, 3324 (1999)
9. Mair, R., Hürlimann, M., et al, *Magn. Reson. Imag.*, 1 9, ?? (2001)

L-8

NMR studies of hydrocarbon gas flow and dispersion

Igor V. Koptyug

International Tomography Center, Novosibirsk, Russia

Introduction

It would be hard to overestimate the importance of the flow of gases for modern technologies in chemical engineering and catalysis. Some examples are flow of exhaust gases through catalytic afterburners and gas dehumidification. PFG NMR and NMR imaging are widely employed to characterize diffusion of gases as well as flow and diffusion of liquids. Introduction of NMR of hyperpolarized ^{129}Xe and ^{3}He gave a strong impetus to gas phase NMR imaging, including studies of gas flow. However, gases often exhibit greatly reduced T_1 times when admitted into porous media, and the advantageous signal enhancement may be lost in such applications. Furthermore, it is desirable to utilize a wider range of gases, including gaseous hydro- and fluorocarbons. These have much shorter relaxation times, and even if polarized, would rapidly return to thermal equilibrium. With imaging of a catalytic reaction in mind, hydrocarbons are of particular interest. Therefore, the aim of this work is to extend the scope of gas phase NMR studies by assessing the feasibility of NMR flow imaging and displacement NMR spectroscopy of thermally polarized gases.

Methods

In all experiments, ^{1}H NMR was performed at 300 MHz. The T_2 times of the gases employed are relatively long (590 ms for propane, 750 ms for butane), therefore gas flow imaging and pipe flow PFG NMR studies were carried out using the spin-echo sequence (TE=4.7-5.1 ms). However, the T_2 times are significantly reduced when studies of gas in porous media are performed. Therefore, most of the porous media displacement NMR spectroscopy experiments were based on the stimulated echo pulse sequence, with two 180^0-pulses added to refocus the transverse magnetization in order to eliminate the effect of strong local field gradients caused by magnetic susceptibility mismatch at the numerous gas/solid interfaces in porous media which otherwise lead to severe signal loss due to diffusion-dispersion of molecules in the inhomogeneous magnetic field. The two displacement-encoding gradients were stepped from negative to positive values in the subsequent repetitions of the experiment to allow the detection of pseudo-echo rather than pseudo-FID. Slice selection in the axial direction was used if needed. Comparison with CPMG-type PGSE experiments was done to verify the absence of gross artifacts. Unconsolidated beds of solid glass beads (0.5-3.2 mm in diameter) or porous alumina beads (5.5 mm) packed in a cylinder (22 mm i.d.) were used as model porous media.

Results and discussion

NMR flow imaging of thermally polarized gases in a circular pipe (Fig. 1) and in the channels of monolithic catalysts resulted in 2D flow maps with reasonable S/N [1,2]. For pipe flow, the histogram of the distribution of flow velocities was constructed by counting pixels corresponding to each flow velocity range, and compared to the average propagator measured directly by PFG NMR. The shapes of both propagators were close to rectangular, as expected, since the experiments were performed with a relatively short observation delay (Δ=4.9 ms, diffusion length $l_D=(D_0\times\Delta)^{0.5}$=0.18 mm, pipe i.d. 7.6 mm). However, some differences were apparent. The propagator measured directly exhibited a small decrease toward larger displacements due to the partial loss of faster moving spins from the rf coil during the measurement, and was slightly broadened at the edges due to the fast diffusion of the gas. For gas flow in the monolithic catalysts, a complex flow pattern with recirculating flows has been revealed.

Despite the successful demonstration of the flow imaging of thermally polarized hydrocarbon gases, such applications clearly have significant limitations. Due to limited S/N and fast diffusion, the spatial resolution is low compared to that obtainable with liquids, and it is unlikely that imaging of gas flow in submillimeter channels and pores could be done in any reasonable amount of measurement time. Furthermore, weak as it is, the signal is reduced further by any spatial or temporal flow instability due to intervoxel signal dephasing. Therefore, PFG displacement NMR spectroscopy was chosen for gas flow studies in porous media. If necessary, it can be combined with low spatial resolution MRI to measure average propagators in the well-defined regions of the porous sample. Fig. 2 demonstrates the first observation of the average propagator for the thermally polarized gas (propane) flowing through a cylindrical granular bed comprised of glass beads. Owing to a long observation delay, Δ=300 ms, the displacement of spins exceeded the characteristic pore size of the bed, which resulted in the Gaussian propagator shape. The dispersion coefficient estimated from the width of the propagator, D=0.65 cm^2/s, is an order of magnitude larger than the self-diffusivity of propane at

19 °C and atmospheric pressure, $D_0 = 0.065$ cm^2/s. Further experiments with systematic variation of Δ, porous media structure, and gas properties are in progress. Other studies presently performed at ITC, such as dehumidification of gas by passing it through the adsorbent bed, where mathematical modeling of adsorption fronts is based on the advection-dispersion equation, will benefit from the knowledge of the flow dispersion coefficients.
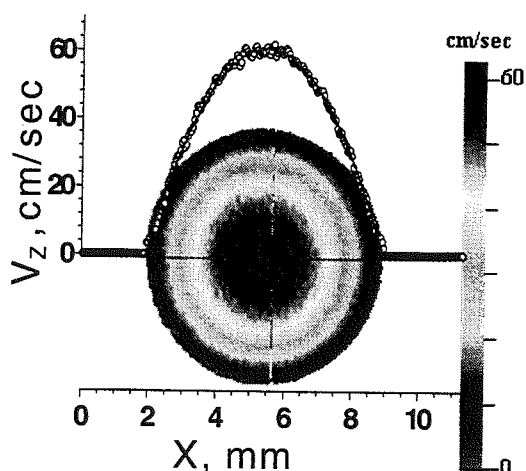
Fig. 1. 2D flow map of the axial velocity of propane flowing in a pipe, and its 1D cross-section along the pipe diameter (circles) with the fitted parabola superimposed (solid line). TE=5.1 ms, slice 4 mm, FOV (24mm)^2, 64×64 matrix zero filled to 256×256, NA=32, acquisition time 2×30 min.
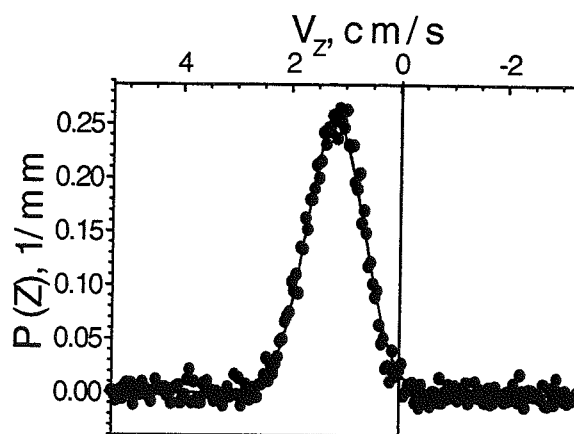
Fig. 2. Distribution of axial displacements for propane flowing in a cylindrical bed of 3 mm glass beads (dots) and the fitted Gaussian curve (solid line). Δ=302 ms, δ=600 µs, 256 steps in g from −7.8 to +7.8 G/cm, NA=8, acquisition time 22 min.

Adsorption of gases and exchange between the bulk gas and the gas adsorbed on a surface or within the porous pellets comprising the bed is yet another promising area of research. Such studies are feasible because strong adsorption of gaseous hydrocarbons on materials such as alumina leads to a dramatic enhancement of the NMR signal. As a preliminary exercise on the way to catalytic reaction imaging in real time, we have imaged the Pt/alumina supported catalyst inside the reactor positioned in the NMR bore by admitting propane into the reactor volume. Contrary to our previous experience with propane adsorbed on alumina, it was found that the T_2 time of propane adsorbed on the actual supported catalyst grain is long enough to make the use of techniques such as SPI unnecessary and to allow the use of conventional SE instead. This is in agreement with the previous results demonstrating the increase of relaxation times of liquids permeating porous alumina pellets upon impregnation with Pt or Pd [3]. Further studies are currently in progress.

Some related results, including flow of liquids and fine granular materials in porous beds will be discussed as well.

Conclusions

It is demonstrated that displacement NMR spectroscopy and NMR imaging of flowing thermally polarized gases is practicable. This may considerably broaden the range of technological processes in chemical engineering and catalysis that can be studied by NMR.

References
1. Koptyug, I.V., Ilyina, L.Yu., Matveev, A.V., et. al., Catal. Today, accepted for publication.
2. Koptyug, I.V., Altobelli, S.A., Fukushima, E., et. al., J. Magn. Reson. 147, 36-42 (2000).
3. Khitrina, L.Yu., Koptyug, I.V., Pakhomov, N.A., et. al., J. Phys. Chem. B 104, 1966-1970 (2000).

Biological applications of magnetic resonance microspectroscopy and microimaging.

Recent developments in small-scale NMR hardware have resulted in considerable progress in both NMR spectroscopic and imaging studies of samples limited in mass or size. One component is the continuing miniaturization of the radiofrequency coil, leading to increases in the intrinsic mass sensitivity of NMR. Concomittant improvements in, and miniaturization of, gradient hardware have also enabled spatial resolution to approach the micron level. Three areas of biological applications of these hardware advances will be highlighted.

At the smallest size scale, high resolution NMR microspectroscopy can be hyphenated with highly efficient microseparation techniques such as capillary liquid chromatograhy, electrophoresis and isotachophoresis for on-line identification of separate components of biological mixtures. The design of multiple-frequency coils can aid in the study of limited amounts of proteins in multi-dimensional NMR spectroscopy. Incorporating multiple coils within a single probehead has been used to increase the throughput and efficiency of NMR detection.

NMR microimaging of single neurons and cells has shown that localized spectra can be acquired from subunits of a single cell, and that detailed multi-exponential diffusion behaviour can also be studied. Examples will be shown from *Aplysia Californica* and *Xenopus Laevis*.

Finally, we have also used NMR diffusion tensor microimaging to investigate the relationship between myelination in white matter and diffusion anisotropy in a myelin deficient rat spinal cord model. Results suggest that, while myelination is not a prerequisite for diffusion anisotropy, it does influence the magnitude of the observed anisotropy.

NMR Imaging of a Falling Drop

Song-I Han, Siegfried Stapf, Bernhard Blümich

*Lehrstuhl für Makromolekulare Chemie, ITMC, RWTH Aachen,
Worringerweg 1, D-52074 Aachen, Germany*

The falling drop is a simple model for studying chemical extraction where two immiscible phases are dynamically blended to promote the transport of solute molecules from one phase to the other [1]. Convective motion inside the drop significantly influences the extraction efficiency. Whereas optical and tracer methods are model bound or invasive [2-3], NMR imaging is noninvasive, direct, and applicable to non-transparent media [4-5]. The first NMR measurements of free falling fluid drops through air are reported and demonstrate, that NMR imaging is able to confirm the presence of large-scale convection rolls and visualize the structure of the inner vortex-dynamics in a falling drop directly.

Water drops with and without surfactant were generated to fall free through air. The setup consisted of a glass pipette plugged vertically inside a 4.7 T magnet and an infrared photo sensor, which triggers the spectrometer each time the drop obstructs its light path. In this work, drops falling with 2 m/s, hence remaining only for about 10 ms within the sensitive volume of the resonator, were studied. As a consequence, any ultra-fast NMR imaging method is incapable of completing the measurement within the residence time of a single drop; using triggered cyclic acquisition was the only possibility for signal accumulation as well as for multi-dimensional experiments. Here, the uniformity in shape of each drop is an indispensable condition, which was proven by various NMR imaging methods. Excellent agreement of 1D projections obtained by the frequency encoding method with different numbers of accumulations and the phase encoding method was found (variance < 1%), thus excluding random variation of the drop formation. 3D spin density images with remarkable quality were obtained, showing different shapes and the reduction in drop size of drops consisting of pure water to those of surfactant solution. Spatial distributions of vertical (z) and transverse (x) velocities within the drop along the cross-section of the drop have been analyzed, revealing small scale variations for surfactant drops and large-scale structures for water drops. In order to directly visualize the internal fluid dynamics, both v_z and v_x components were measured in each pixel of the zx-plane simultaneously within a single experiment to combine these into a vectorial representation. The obtained vector plot unambiguously visualizes the notion of the presence of stable vortices within the water drop. Additionally, an overlapping oscillation was observed, which can be expected under the high Reynolds number of about 400, well outside the regime of stationarity [1-3]. It is confirmed by optical observation of drops under comparable conditions.

References

[1] Brander, B., Brauer, H., "Impuls- und Stofftransport durch die Phasengrenzfläche von kugelförmigen fluiden Partikeln", Reihe 3: Verfahrenstechnik, 326, VDI Verlag, Düsseldorf, 1993.

[2] Edgerton, H.E., Hauser, E.A., Tucker, W.B., "Studies in drop formation as revealed by the high-speed motion camera", *J. Phys.Chem.* **41**, 1017 (1941).

[3] Nijmeijer, M.J.P, Bruin, C., van Woerkom, A.B., Bakker, A.F., "Molecular dynamics of the surface tension of a drop", *J. Chem. Phys.* **96 (1)**, 565, (1992).

[4] Callaghan, P. T., "Principles of NMR Microscopy", Clarendon Press, Oxford, 1991.

[5] Blümich, B., "NMR Imaging of Materials", Oxford Science Publications, Oxford, 2000.

Spatially Resolved Adsorption Isotherms of Thermally Polarized Gases in Mesoporous Solids using NMR Imaging

S.D. Beyea[a], A. Caprihan[a], C.F.M. Clewett[a] and S.J. Glass[b]

[a]New Mexico Resonance and [b]Sandia National Laboratories, Albuquerque, NM, USA

Introduction:

We present NMR imaging of thermally polarized perfluorinated gases in mesoporous solids. Unlike studies of laser-hyperpolarized gases, which have been used to obtain structure parameters such as tortuosity[1], we utilize the ability of gases to interact with the pore walls. MR imaging of nuclear spin density as a function of gas pressure permits space resolved measurements which are analogous to conventional bulk adsorption experiments.

In mesoporous solids, the fine pore structure greatly alters the behaviour of gas molecules, leading to phase transitions and layering. Physical adsorption of gas molecules is caused by attractive forces between adsorbate and adsorbent (such as dispersion and ion-induced dipole), which are similar to those forces that lead to liquefaction of gases in bulk. Therefore, gases with high boiling points (due to strong intermolecular interactions) tend to be strongly adsorbed. In addition, according to Polanyi's potential theory, the adsorbate volume can exist in three different conditions, depending upon the experimental temperature relative to the critical temperature of the gas. Above the critical temperature, the adsorbate can not be liquefied and the gas volume simply becomes more dense at the surface. At temperatures near, but less than the critical temperature, the adsorbate is viewed as a liquid near the surface, and a vapour of decreasing density away from the surface. Substantially below the critical temperature ($T < 0.8\ T_c$), the adsorption volume is considered to contain only liquid.[2]

Discussion:

The use of NMR imaging allows the noninvasive evaluation of macroscopic variations in the underlying microscopic structure. The results obtained from variable temperature and pressure studies can be directly compared to conventional Brunauer, Emmett and Teller (BET) adsorption studies. Space resolved NMR measurements of spin-lattice relaxation time (T_1) and diffusion coefficient provide further information on the underlying pore structure and phase equilibria.[3,4] Studies were performed using hexafluoroethane (C_2F_6) and octofluorocyclobutane (C_4F_8) gases, with bulk critical temperatures of 293 °K and 388 °K respectively. An example 2D image of C_4F_8 at 294 °K in two different ceramics is shown in Figure 1. The image shows both a signal enhancement in the ceramic relative to the bulk gas, due to adsorption, as well as structure within the ceramic itself, caused by spatial differences in mean pore size.

Conclusions:

We have used NMR imaging to spatially measure adsorption isotherms of thermally polarized gases in mesoporous solids, as well as pressure dependent studies of T_1 and diffusion. These results provide information on the spatially varying pore properties of the solid matrix, as well as gas-liquid phase equilibria in mesoporous solids.

1.   Mair, R.W. et al, Phys. Rev. Lett., 83, 3324-3327 (1999).
2.   S. Lowell et al, Powder Surface Area and Porosity 3rd Ed., Chapman & Hall, New York, 1991.
3.   Caprihan, A. et al, Mag. Reson. Imaging, in press.
4.   Lizak, M.J. et al, J. Magn. Reson., 95, 548-557 (1991).
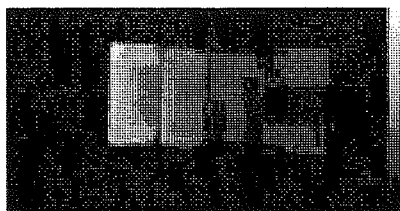
Figure 1. 2D NMR image of C_4F_8 in two ceramic materials (bulk gas region on right). Structure in the ceramic images is due to differences in porosity and gas adsorption.

NMR as a tool for the investigation of velocity fluctuation in porous media.

Alexandre A. Khrapitchev and Paul T. Callaghan

Institute of Fundamental Science – Physics, Massey University
Palmerston North, New Zealand

The study of fluid motion in porous media is of great interest to a variety of industries, such as oil exploration, catalysis, chromatography, dialysis and food quality control. Nuclear Magnetic Resonance (NMR) Velocity Imaging is a unique tool that provides a non-invasive probe of molecular motion in solid media. The simplest model of porous materials is a monodisperse bead pack.

The use of Pulsed Gradient Spin Echo (PGSE) NMR to investigate flow in porous media is well established[1,2]. In particular, the Fourier Transformation (FT) of the spin echo decay yields a displacement propagator (or probability density) whose dependence on encoding time gives information about the transition to asymptotic dispersion. Two crucial parameters are important in describing flow and dispersion in porous media. These are the correlation time τ_c, which describes the time taken for flow across a characteristic length scale (e.g. the pore size) and the Peclet number, which compares the time scales for diffusion and flow across this length scale. Using two pairs of position-encoding pulses in the PGSE experiment gives the possibility of examining velocity fluctuations, by comparing displacements, during the two encoding intervals. In particular Velocity Exchange Spectroscopy (VEXSY)[3] experiments can reveal the gradual transition to asymptotic behavior as the ratio of the exchange time to the correlation time is increased. Furthermore, the off-diagonal of the VEXSY experiment can be used to directly measure the velocity autocorrelation function (VACF)[4]. This can be performed in 1-D mode using compensated double PGSE encoding[5].
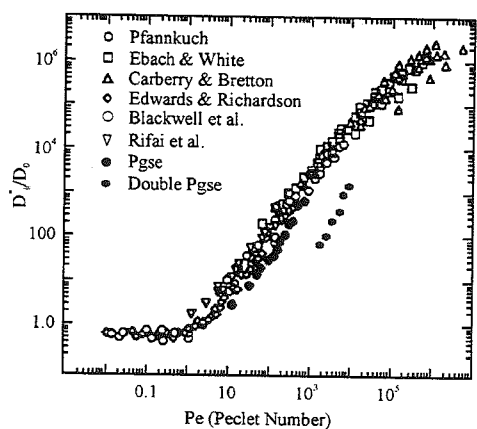
Reduction of Dispersion coefficient due to macroscopic velocity fluctuations in bead pack

Although simple systems can be characterized by their mean velocity, determination of the VACF allows us to obtain additional information for systems undergoing complex flow. By calculating the FT of the VACF we can determine the third fundamental parameter – the dispersion coefficient, as well as the correlation time.

This work will present a detailed investigation of displacement propagators for different liquids, flow rates and in a range of bead packs of differing sizes, so that the Peclet number scaling effects can be seen. We will also show how different variants of the PGSE NMR method can be used to provide new information about flow and dispersion. Measurements of the velocity autocorrelation function for both transverse and longitudinal directions will be presented and compared with the results of recent computer simulations and theory.

[1] P.T. Callaghan, "Principles of NMR Microscopy", Oxford: Clarendon Press, 1991.
[2] B. Blumich, "NMR Imaging for Materials", Oxford Science Publications, 2000.
[3] B. Blumich, P.T. Callaghan, R.A. Damion, S. Han, A.A. Khrapitchev, K.J. Packer, S. Stapf, Submitted to Journal of Magnetic Resonance.
[4] P.T. Callaghan, A.A. Khrapitchev, Magnetic Resonance Imaging (in press).
[5] P.T. Callaghan, A.A. Khrapitchev, Submitted to Journal of Magnetic Resonance.

Toward MRI of single biological cells at micron resolution

D. A. Seeber, L. Ciobanu, and C. H. Pennington
Department of Physics, Ohio State University; Columbus, OH; U.S.

We report development of the major components of a system for proton MRI with attempted resolution of 1-2 microns in all three spatial dimensions, for imaging single biological cells. Major components include micro-receiver coil circuitry with receiver coil diameters typically 100µm or smaller, and strong, rapidly switchable (switching time of a few microseconds) tri-axial magnetic field gradients with strengths exceeding 12 Tesla per meter for each direction. The micro-receiver coil circuitry gives signal to noise equivalent to unity for a single scan (followed by a train of several thousand Carr-Purcell-Meiboom-Gill echoes) applied to 10 cubic microns of water (~10^{12} spins) at room temperature and 9 Tesla magnetic field. We report various phantom images with resolution near 2 µm and preliminary images with biological cells.
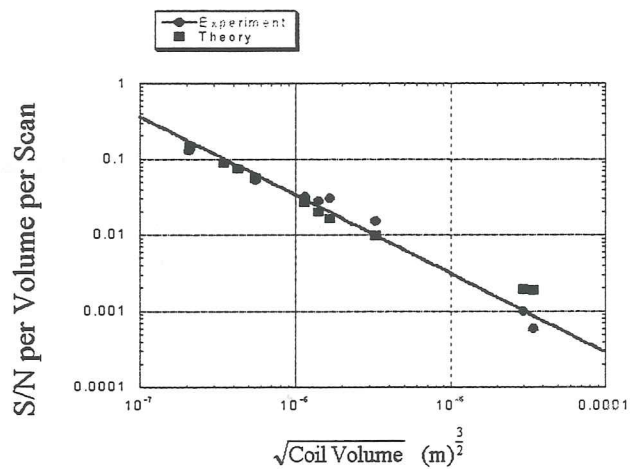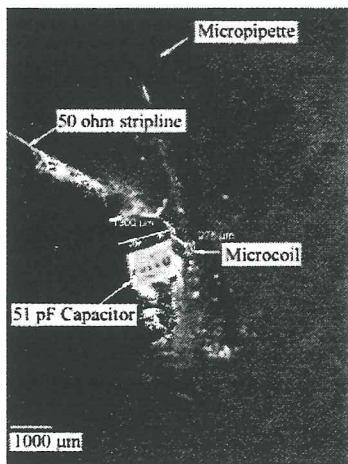
Figure 1. The microcoil used is the experiment is tuned by a capacitor with the circuit designed to minimize stray inductance.

Figure 2. Eleven coils, with diameters from 1 mm to 20 µm were constructed and the SNR was measured. The SNR is normalized per one cubic micron per one scan and is proportional to the square root of the coil volume.
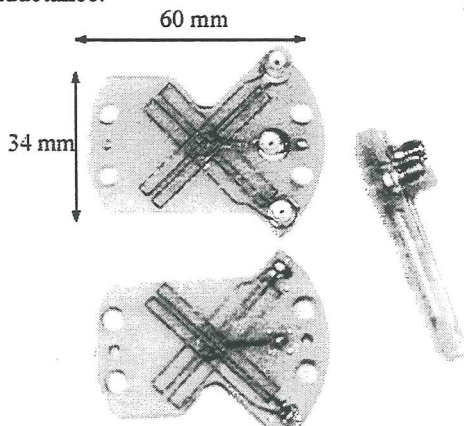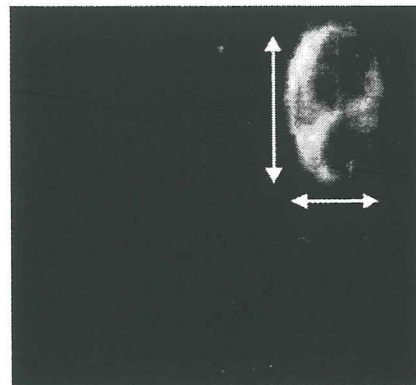
Figure 3. The gradient coils are constructed so the microcoil is in the center of the field. Fields in excess of 12 T/m are possible with our gradient power supply.

Figure 4. This is one of the preliminary images taken; the slice width is 15 µm thick with in-plane estimated resolution (*not* voxel dimensions) of 2 µm by 3.5 µm. The "holes" in the image are from ~20 µm beads.

References:
1. D. A. Seeber *et al.*, Rev. Sci. Instrum. **72**, 2171 (2001)
2. D. A. Seeber *et al.*, Rev. Sci. Instrum **71**, 4263 (2000)
3. D. A. Seeber *et al.*, Rev. Sci. Instrum **71**, 2908 (2000)

Abstracts for:
Contributed Oral Presentations
C1 – C30

MOLECULAR TRANSPORT IN A POROUS MEDIA BY THE PULSE-GRADIENT-SPIN-ECHO SPECTRAL ANALYSIS

Janez Stepišnik, Aleš Mohorič and *Andrej Duh

Physics Department, University of Ljubljana, Slovenia
Institute of Mathematics and Physics, University of Maribor, Slovenia

The measurements of diffusion in the porous media by the modulated gradient spin echo method (MGSE) reveal strong dependence of spin echo attenuation on the velocity self-correlation spectrum of entrapped molecules[1]. This method takes an advantage of the relation between the spectrum of molecular motion and the spectrum of spin phase modulation created by gradient spin echo sequence. We show that for the gradient sequence with the two pulses (PGSE) it brings about, in some other way, known $\sqrt{D\Delta}$ early time dependence of spin echo decay. While at intermediate times, it provides the $D\alpha\Delta + d[1 - \exp(-\Delta/\tau_r)]$ dependence, and leveling into asymptotic time-independent attenuation when displacements are larger than the size of compartments. The measurement of water in the system of packed polydispersed beds (0.1-0.03 mm) clearly shows that the flow-induced turbulences of imbibed water shorten the time-of-flight between boundaries τ_r so that a distinction between these three regimes can be seen. Here the effect of internal gradients due to the susceptibility difference of the heterogeneous structure has been removed by a specially modulated gradient sequence that has identical zero-frequency peak in the dephasing spectrum as the pulse gradient sequence and, consequently, the same evolution of signal decay. This spectral analyses demonstrates that the PGSE with low $q = \gamma D\delta$ can provide information about the parameters of porous structure, like the average pore size d and the tortuosity α, and so reveal the long-range structure of porous media, particularly when used in combination with the methods of modulated gradient spin echo. Figure shows the PGSE attenuation of stationary and trickling water (velocity 1.1 mm/ s) through porous structure. The MGSE attenuation[1] is given for comparison to demonstrate its clear linear rise at same flow velocity.
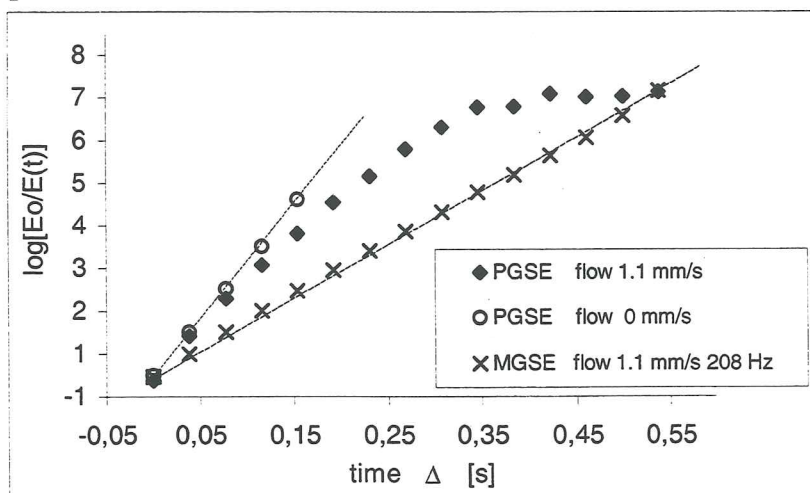
[1]J. Stepišnik and P.T. Callaghan, The long time-tail of molecular velocity correlation in a confined fluid: observation by modulated gradient spin echo NMR. Physica B, 292, 296--301, 2000.

Correlation of Displacements and Relaxation Behaviour of Fluids in Porous Media

Melanie M. Britton[1], Robin, G. Graham[2] and Ken J. Packer[2]

[1] *Department of Chemical Engineering, University of Cambridge, New Museums Site, Pembroke St., Cambridge, CB2 3RA, UK.* [2] *School of Chemistry, University of Nottingham, University Park, Nottingham, NG7 2RD, UK.*

Introduction: Diffusion to an active surface is often the main determining factor in the relaxation behaviour of nuclear spins in fluids contained within porous solids and leads, in general, to multi-exponential relaxation behaviour. The basic theoretical framework describing this comes from the work of Brownstein and Tarr[1]. Transverse relaxation in such systems often has additional contributions arising from diffusion within the internal fields caused by susceptibility contrast between the solid matrix and the pore fluids[2]. Fluid flow through porous solids produces velocity fields such that at any point within the pore space the velocity is related to the local pore structure and hence distance from the pore surface.

Method: In this paper we report a class of experiment which correlates displacements arising from flow and diffusion, determined using PGSE methods, with transverse (T_2) relaxation, determined by a CPMG pulse sequence. The outcome of these experiments is the joint probability density $P\{X(\Delta);T_2\}$, where $X(\Delta)$ is the displacement of the fluid in the time Δ. We have measured $P\{X(\Delta);T_2\}$ for water in random packs of glass beads and calcium alginate beads, both of 1mm diameter, and also in parallel bundles of 1mm id glass capillaries. In each case the fluid was made to flow at various rates through the system. The experiment was repeated for different values of the gradient pulse area, $\mathbf{q}$ ($=\gamma\delta g/2\pi$), giving a signal array $S_\Delta(\mathbf{q},t)$, where $t=2n\tau$ and was the echo sampling times in the CPMG sequence. Fourier transformation of $S_\Delta(\mathbf{q},t)$ with respect to $\mathbf{q}$ gives $S\{X(\Delta),t\}$ and a subsequent regularised Laplace inversion for each $X(\Delta)$ value using CONTIN produces the propagator $P\{X(\Delta); T_2\}$. In addition to the CONTIN analysis, linear least squares fitting has been performed on the signal decays from each $X(\Delta)$ value, with interesting results.

Results: The basic concept in these experiments is that the displacement, to a degree, provides a spatially-resolved view of the diffusion-driven relaxation process. This is clearly seen, for example, in the fact that, for the samples investigated, the bulk relaxation is in the slow diffusion regime and shows several modes. The corresponding $P\{X(\Delta); T_2\}$ shows that differing displacements are associated with different T_2 values within each distinct relaxation mode. The longest relaxation time mode has a displacement distribution, which looks similar to a typical flow propagator, although there seems to be a move to longer T_2 for larger displacements. The shorter T_2 modes seem only to exist over a limited range of displacements and show characteristic variations, which were dependent on the system studied, of T_2 with displacement. However to get a full representation of the correct physics of the process it is necessary to allow amplitudes for the intermediate T_2 modes the possibility of becoming negative. Negative amplitudes have been found both in experimental and simulated data and also in the analytical solution of flow through a cylindrical pipe. This class of experiment provides a considerable challenge to fluid dynamics modelling and also offers possibilities for probing morphologies, within the pore space.

1 Brownstein, K. R. and Tarr, C. E., Physical Review A **19**, 2446 (1979).
2 Le Doussal, P. and Sen, P. N., Physical Review B **46**, 3465 (1992).
3 Britton, M. M., Graham, R. G. and Packer, K. J., Magnetic Resonance Imaging (in press)

MRI of liquid phase and flow distribution and its effect on reactor performance in the film flow monolith reactor

H. Van As[2], A. Heibel[3], T.W.J. Scheenen[2], F.J. Vergeldt[2], J.J. Heiszwolf[1], F. Kapteijn[1] and J.A. Moulijn[1]

[1]*Delft ChemTech, Industrial Catalysis, Delft University of Technology*
Julianalaan 136, 2628 BL Delft, The Netherlands
[2]*Wageningen NMR Centre, Department of Molecular Physics, Wageningen University*
Dreijenlaan 3, 6703 HA Wageningen, The Netherlands
[3]*Corning Inc., Corning, NY, 14831, USA*

Recently, the application of monoliths has been extended to multiphase gas-liquid-solid systems. In the film flow regime the liquid flows down the channel walls, whereas the gas occupies the core of the channel. The separated flow passages of gas and liquid allow both co- and counter-current operation of the film flow monolith reactor.

To understand and describe the fundamental hydrodynamics in the film flow monolith reactor, knowledge about the gas-liquid distribution in the monolith channel is essential. Multi Echo MRI experiments were applied on four monolith channels (hydraulic diameter d_h = 4.11 mm, wall thickness w_{th} = 0.87 mm) at a 0.75 T imager. Quantitative liquid distributions were calculated by mono-exponential decay analysis per pixel (Figure 1). The reproducibility of the measurements was reasonable.
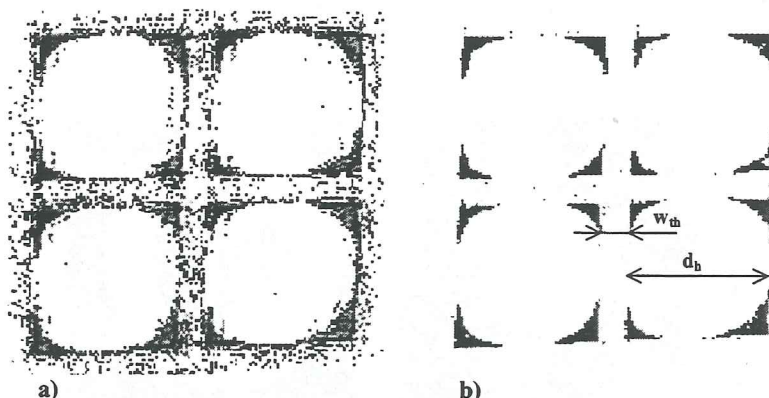
Figure 1: a) Original NMR image, b) Image after post-processing

From a qualitative analysis of the NMR images the following main conclusions can be drawn:
The liquid is accumulated in the corners; The assumption of an arc-shaped G-L interface and complete wetting at the G-L-S contact line can be justified; The liquid hold-up in the individual channel corners can be different, even for a homogeneous liquid distribution over the entire monolith cross-section; The liquid hold-up increases with liquid load, but not linearly.

Extracting the area of the channels occupied by liquid from the MRI results allows a quantitative analysis of the liquid saturation for different superficial liquid velocities. The experimental were compared with a hydrodynamic model for the single channel based on the Navier-Stokes equation, using a pre-set shape of the gas-liquid interface. The **F**inite **E**lement **M**ethod was used to solve this equatuin in the square channel domain. Good agreement between model and experiment was obtained.

The local differences in hold-up over the different corners of the channels are used to investigate the impact on other reactor performance parameters (e.g. **R**esidence **T**ime **D**istribution (RTD) and mass transfer) in comparison to an ideal uniform distribution. The results of these studies show that the impact is significant and they also explain some of the deviations between modeling and experimental results obtained in prior investigations.

Actual liquid film flow distributions were obtained by q-space propagator measurements.

Monitoring Ultraslow Dipolar Correlations in Organised Liquids

F. Grinberg and R. Kimmich

Sektion Kernresonanzspektroskopie, Universität Ulm,

Albert-Einstein-Allee 11, 89069 Ulm, Germany

Ultraslow molecular motions (with correlation times $\gg 10^{-5}$ s) and ordering phenomena in various complex liquids are studied using the frequency dependent measurements of the NMR relaxation rates. Experimental examples are given for bulk and microconfined liquid crystals and polymer elastomers.

The influence of the orienting/adsorbing surface on the low-frequency behavior of the relaxation rates of a confined liquid was investigated using random walk computer simulations. For this purpose, the correlation function of the (residual) dipolar coupling was evaluated during the simulated random walk procedure performed for a spherical and a cylindrical surface. The results clearly reveal two different time scales of the correlation losses. The shorter component characterizes the time necessary for the molecule to leave the oriented layer to the "bulk-like" interior part of the cavity. The longer component of the correlation function is associated with a diffusion process in course of which the molecule changes its preferential orientation as it visits different surface sites. The correlation is (completely) lost in the time scale necessary to probe all possible orientations determined by the surface topology. We discuss the dependence of the correlation times on the pore size, the width of the oriented layer and the molecular diffusivity.

255 a.u.

0

a) Spin density map   b) MSF - map
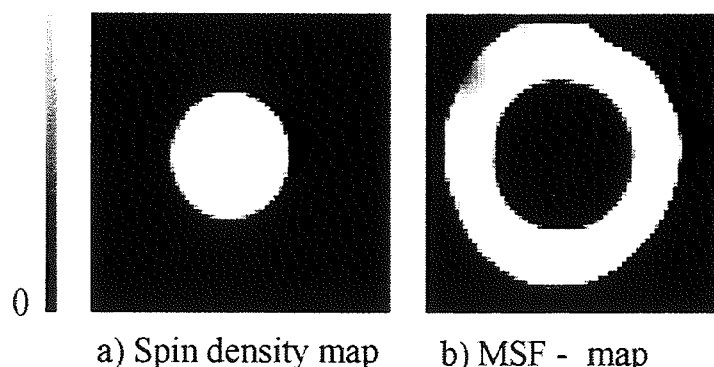
Ultraslow chain relaxation modes of polymer molecules were studied using the dipolar correlation effect [1, 2] on the stimulated echo. The mean squared fluctuation (MSF) of the dipolar coupling constant was shown to strongly depend on the cross-link density of elastomers studied in dry and swollen states [3]. We present maps of the MSF as a new contrast parameter for imaging of polymer objects. The figure above shows the "inverse" contrast of (a) a spin density and (b) a MSF - map measured with a sample consisting of water (middle part) and polyisopren (outer part).

References

1) Kimmich, R. NMR: Tomography, Diffusometry, Relaxometry (Springer-Verlag, Heidelberg, 1997); 2) Grinberg, F. and Kimmich, R., *J. Chem. Phys.* **103**, 365 (1995); 3) Grinberg F., Garbarczyk M., and Kuhn W., *J. Chem. Phys.*, **111**, 11222 (1999).

3D wave analysis in thin falling liquid films - an NMR study

Christian Heine, Siegfried Stapf, and Bernhard Blümich

Institute for Technical Chemistry and Macromolecular Chemistry, Magnetic Resonance Center,

RWTH, 52056 Aachen, Germany

Falling liquid films are very instable hydrodynamical systems that have to our knowledge never been studied by NMR until now. They are widely used in chemical engineering, e. g. in liquid-liquid extraction processes. In the presented approach to investigate such geometries, a thin liquid film is falling down along a strictly vertical plate. It is generated with an average film thickness of $h_0 = 1$ mm. Falling films exhibit instabilities, i. e. waves, the behavior of which depends on the balance of viscous and flow properties of the fluid, characterized by the film Reynolds number Re_f. The surface waves on a falling film are non-linear, their spatial characteristics depend on the average flow velocity. All these properties, in combination with the unfavorable filling factor and signal/noise problems make falling films a challenging system for NMR studies.

As a test system we have chosen silicon oil with viscosities of $\eta = 10$ mPa s and 100 mPa s. Single-stripe tagging experiments, multidimensional NMR-velocimetry measurements using a phase-encoding double spin-echo pulssequence [1,2], and standard PGSE-sequences for the measurement of propagators [3] have been performed. Using these methods we were able to measure the longitudinal velocity component (in direction of the gravity driving the flow) and the velocity components in a plane perpendicular to the longitudinal axis (the transversal velocity components) spatially resolved [4] in the direction across the film thickness.

With increasing Re_f several flow regimes can be distinguished, the limits of which can be derived either empirically [5] or theoretically [6]. Our measurements exhibit laminar, i. e. waveless behavior for a Reynolds number of $Re_f = 0.5$. In this case the Navier-Stokes equations can be solved analytically resulting in a well known half-parabolic profile for the longitudinal velocity component versus the spatial coordinate across the thickness of the film [7].

For an intermediate Reynolds number ($1.0 \leq Re_f \leq 2.5$) the film is in the laminar-wavy flow regime. Here the longitudinal velocity component can be fitted to two parabolas instead of one like in the purely laminar case. The velocity profile is split into a residual film showing laminar behavior and waves measured in a time-averaged fashion. The vertical velocity components are zero within the limits of accuracy through the whole thickness of the film. This indicates that the surface waves behave two-dimensional. This was cross-checked with propagator measurements of the different velocity components for identical Re_f.

We further increased the Reynolds number up to $Re_f = 53$. Under these conditions the film is in the wavy flow regime. The waves behave three-dimensional, as is corroborated by propagator measurements. A residual film cannot be found in this case. A further effect of the three-dimensional waves is the depence of all velocity components on the thickness of the slice excited.

Even if the waves are three-dimensional, it is possible to generate two-dimensional waves by applying a periodic disturbance. In our apparatus this is possible by using sound stimuli generated by a loudspeaker. If stimulated waves are present, it is easily possible to trigger the NMR experiment to the wave, allowing velocimetry measurements without spatial averaging over the thickness of the film.

The experiments presented here are part of an interdisciplinary study of single- and multiphase systems with different geometries. In the long run the design of devices such as the falling film reactor shall be optimized.

References

[1] Fukushima, E., *Annu. Rev. Fluid Mech.* **31**, 95 (1999).

[2] Caprihan, A., Seymour, J. D., *J. Magn. Reson.* **144**, 96 (2000).

[3] Callaghan, P. T., *Principles of Nuclear Magnetic Resonance Microscopy*, Clarendon Press, Oxford (1993).

[4] Blümich, B., *NMR imaging of materials*, Oxford Science Publications, Oxford (2000).

[5] Ishigai, S., Nakanisi, S., Koizumi, T., Oyabi, Z., *Bull., JSME* **15**, 594 (1972).

[6] Kapitza, P. L., *Zhurn. Eksper. Teor. Fiz.* **18**, 3 (1948).

[7] Nußelt, W., *Zeitschrift VDI* **60**, 541 (1916).

Using 3-D MR Microscopy for Morphologic Phenotyping:
Analysis of a Uricase Knockout Mouse

Laurence W. Hedlund[1], Boma Fubara[1], Gary P. Cofer[1], Susan J. Kelly[2], Sally L. Gewalt[1],

Michael S. Hershfield[2], & G. Allan Johnson[1],

[1]Center for In Vivo Microscopy, Departments of Radiology, and [2] Medicine,
Duke University Medical Center, Durham, NC 27710

Introduction. MR microscopy (1) offers a new method for morphologic phenotyping. It is non-destructive, three-dimensional, digital, and offers contrast manipulation (staining) by imaging sequence parameters and exogenous contrast agents. Because the entire body can be examined, additional abnormalities other than those anticipated might be detected. Also, isolated organs can be imaged at higher resolution and processed for optical examination. We have explored the use of MR microscopy of whole body fixed specimens using a uricase knockout model at two ages. Lacking uricase, these mice have pronounced hyperuricemia and hyperuricosuria, and develop obstructive nephropathy from uric acid crystals, resulting in hydronephrosis, renal tubular injury, and cysts (2, 3).

Methods. Eight mice: 4 wild type C57BL/6J (WT) and 4 Uox-/-homozygotes on a hybrid of C57BL/6J-129SV (UKO) were studied. Half of each strain were about 2.5-months old and others were about 24 months old. The animals were anesthetized and prepared for whole body systemic perfusion fixation and staining with MR contrast agents. Catheters were placed the right jugular vein and left carotid artery. After sacrifice by anesthetic overdose, systemic vascular perfusions were performed with a mixture of 10% formalin and Magnevist (gadopentetate dimeglumine, Berlex, Wayne, NJ) in a ratio of 10:1 (V:V). For imaging, the whole body was placed in an acrylic sample holder and imaged in a solenoid coil in 2 T and 7 T systems and excised kidneys in a 9T system using a 3D spin-warp sequence (TR 50 msec, TE 5 msec). At 2 T system, whole body images had a resolution of 110 microns isotropic (array size 256 X 256 X 1024) and at 7 T, the upper abdomen was imaged at 50 microns isotropic (512 X 512 X 512). Isolated kidneys at 9T had resolution of 25 microns (256 X 512 X 512). Data were visualized using VoxelView (Vital Images, MN). Selected organs were processed for H&E histology. Using VoxelView, volumes of the organs were estimated from the whole body images (2T) by tracing the perimeter of each organ on every other axial slice to determine areas. Areas of intervening slices were calculated by interpolation. The correlation between volume estimates and wet weights was 0.99 and on average estimates were within ± 7 % of the wet weights. Volume estimates from images were not corrected for density differences from water.

Results and Discussion. Kidneys of the young UKO tended to be smaller than WT (0.58% vs .73% body wt) and showed signs of hydronephrosis as expansion of the renal sinus. Cortico-medullary cysts were not present in the young UKO kidneys but were numerous in kidneys from old UKO mice. The MR images showed that hydronephrosis was much more severe in the older mice compared to the young UKO mice. The extent of severity was estimated by measuring renal sinus volumes; in the young UKO kidneys sinus was 7.2% of the whole kidney volume while in the older UKO mice it was almost 23% of the kidney volume. In the WT mice the renal sinus within the body of the kidney was too small to measure. Overall kidneys weights were greater for the older mice compared to younger ones (320 mg vs 190 mg). This was also true when renal volume corrected for sinus volume was expressed on a body weight basis. For instance, young WT vs UKO (0.76 % vs 0.61%) compared to the older WT & UKO kidneys were 1.07 % vs 0.79 %. This suggests that the reduced renal mass in the UKO compared to WT is maintained even in advanced age. Other organs were also examined. For instance heart wet weights as percentage of body weight were not clearly different between WT and UKO (young 0.66% vs 0.67%; old 0.91% vs 1.0%). Also, there was no difference in interventricular septal widths between the two strains. The heart weight and wall thickness data suggest a lack of arterial hypertension in the UKO mice. Based on analysis of images and estimates of organ volumes and linear dimensions made from isotropic images, detailed descriptions of differences between strains of mice can be generated. These results show the great value of 3D MR microscopy for morphologic phenotyping. Being able to examine the whole mouse at high resolution using any virtual viewing plane and without destruction should greatly aid characterizing many of these genetic models more completely and rapidly than previously possible.

References
1. Johnson GA et al. Magn Reson Quart 9:1-30, 1993.
2. Wu X. et al. PNAS 91:742-746, 1994.
3. Kelly S. M. Delnomdedieu, M. I. Oliverio, et al. J Am Soc Nephrol 12(5), 1001-1009, 2001.

High resolution T_2^* imaging of the chronic infarcted isolated rat heart at 11.75 T

S. Köhler, K.-H. Hiller, C. Waller[1], C. Heindl, W.R. Bauer[1], A. Haase
Physikalisches Institut, EP5, Universität Würzburg, Am Hubland, 97074 Würzburg, Germany
[1]Medizinische Universitätsklinik Würzburg, 97080 Würzburg, Germany

Introduction:

Tissue changes are known to occur with myocardial infarction. Due to the sensitivity of T_2^* to susceptibility differences between various tissues, the aim of this study is to visualize scar tissue in the chronic infarcted isolated rat heart with T_2^* imaging.

Methods:

NMR imaging was performed on a Bruker AMX-500 microscopy system at 11.75 Tesla. Hearts of male Wistar rats were excised and perfused in the Langendorff mode with Krebs-Henseleit buffer. Chronic myocardial infarcts were induced by ligating the left coronary artery four to eight weeks before the MR examination.

For T_2^* imaging a 2D gradient-recalled multiecho pulse sequence was used (FOV: 20 x 20 mm, matrix: 256 x 256, spatial resolution 78 μm in plane, slice thickness 1 mm). The minimum echo time was 2.05 ms. After each RF excitation 16 echos were acquired with an interecho delay of 3.36 ms. In order to eliminate motion artifacts the data were collected in mid-diastole. Four signal averages were acquired in a total acquisition time of 3.5 minutes. Data were zero-filled before Fourier transformation to 512^2 data points. T_2^* maps were obtained by monoexponential fits.

After MR examination the infarcted hearts were embedded in paraffin and cut in sections of about 4 μm thickness for histologic determination of the infarcted region.

Results and Discussion:

Figure 1 shows a typical T_2^* map of the isolated rat heart. Due to susceptibility-induced reduction of T_2^* in scar tissue, the T_2^* maps of the six isolated rat hearts show excellent visualization of the infarcted region. When compared to histology (Figure 2) the T_2^* map shows excellent spatial correspondence with the scar tissue.

Conclusion:

We have demonstrated, that in correspondence with histology high resolution T_2^* imaging can visualize morphologic alterations of perfused infarcted hearts. In the future the extent of scar

tissue will be quantified by T_2^* imaging in the isolated rat heart.
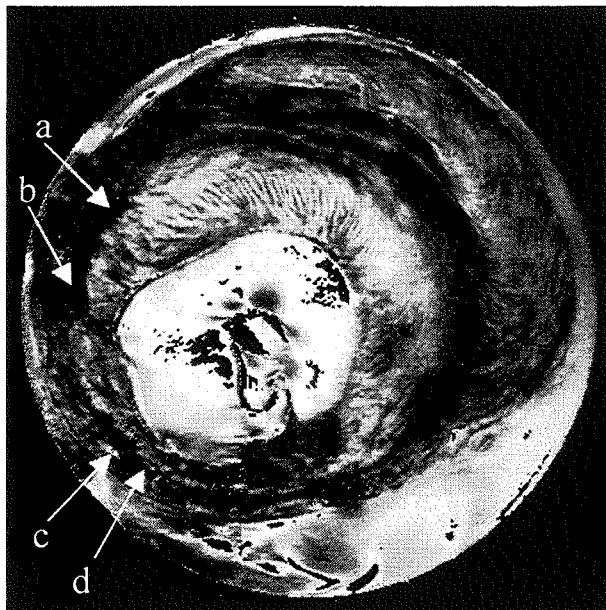
Figure 1: Typical T_2^* map of the isolated rat heart.
a, b, d: scar tissue / c: vessel
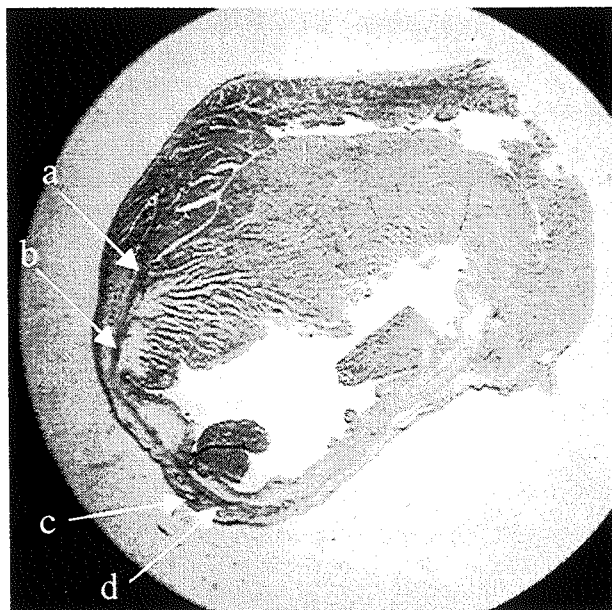
Figure 2: Histology section of the isolated rat heart.
a, b, d: scar tissue / c: vessel

Optimisation of high resolution MR imaging of muscle structure at 4.7 T

J.-M. BONNY, L. MAUNIER AND J.-P. RENOU

SRV / STIM, INRA-Theix, 63122 Saint-Genès-Champanelle, France

Purpose

At high field susceptibility difference is a well-dedicated source of contrast for the study of the connective tissue (CT) network in muscle (1). We address here the optimisation of susceptibility-weighted MR images to facilitate the segmentation step. The objectives were (i) to maximise the contrast between bulk matrix of muscle fibres and CT, (ii) to reduce the macroscopic inhomogeneities of the images.

Methods

Bovine *Biceps Femoris* (BF) samples were positioned so that the best spatial resolution was obtained perpendicular to the CT layers. Experiments were performed on a Biospec 4.7 T MRI system (Bruker) with fast gradient hardware (max. amplitude 50 mT/m, rise time 260 µs) and an Helmoltz coil ($\varnothing$ = 35 mm) used both for excitation and reception. R2* maps were reconstructed for different in-plane resolution and at constant slice thickness (0.5 mm) using a multiple GE sequence (1). Moreover, subslice averaging method called SSAVE (2) has been tested to reduce the effect of static field inhomogeneities. It consists of magnitude averaging over thin subslices (0.5- and 0.25-mm thick) to form the final 1-mm thick slice. To select slices, Shinnar-Leroux (SLR) linear-phase pulses (3) were tested with passband and stopband ripples of 1 %, duration of 8192 µs, and bandwidth of 1 kHz and 0.5 kHz.

Results

Fig.1 shows the same ROI extracted from the R2* maps at four different in-plane spatial resolution (in mm^2 A: 0.55 x 0.55, B: 0.27 x 0.27, C: 0.18 x 0.18, D: 0.14 x 0.14). Fig.2 and Fig.3 plot the coefficient of variation (a gauge of image homogeneity) and the average S/N of muscle signal using SSAVE, for five different 1-mm thick slices.
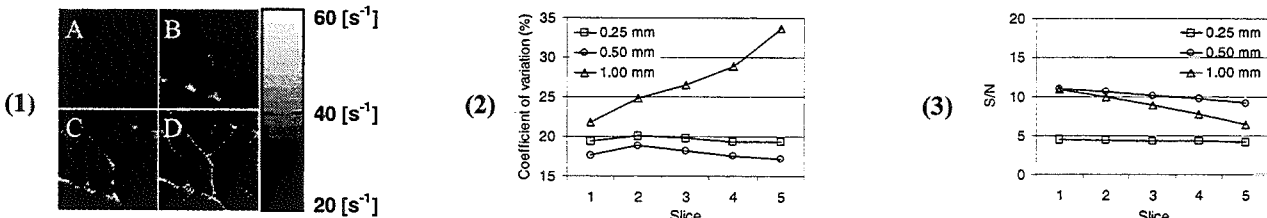
Discussion

Fig.1 demonstrates that R2* increases with the in-plane spatial resolution when a voxel intercepts CT. This dependence is explained by the size of the CT causing the local magnetic field inhomogeneities, which is larger than the voxel dimensions (continuous layers of $\approx$ 0.1 mm thick) (4).

SSAVE improves dramatically the image homogeneity. It is expressed by both reduction of coefficient of variation inside the muscle area and stabilisation of its value for the different selected slices (*cf.* Fig. 2). SSAVE improves the image S/N only when 0.5-mm thick slice are selected, whereas averaging of thinner slices generates S/N losses (*cf.* Fig. 3). Even if the good slice definition of SLR pulses restricts the signal loss when selecting thin slices, 0.5 kHz bandwidth was required instead of 1kHz to select a 0.25-mm thick slice. This lower duration-bandwidth product induces a degradation of pulse performance (4) which explains the decrease of S/N when four 0.25-mm thick slices were averaged instead of two 0.5-mm thick slices.

Fig.4 shows an example of high resolution (0.14 x 0.14 x 1 mm^3) MR image obtained using SSAVE (2 slices of 0.5 mm), low bandwidth (39 Hz/pixel) and susceptibility-weighted GE sequence (TR/TE = 5000/30 ms). A high correspondence is observed between images obtained using a non-destructive MR approach and histology (10-µm thick frozen section stained using red sirius, *cf.* Fig.5).

Conclusion

Our results demonstrate quantitatively that an increase in spatial resolution perpendicular to CT layers is a key-factor to improve susceptibility-contrast between CT and muscle fibres. SSAVE is then a solution to compensate the S/N decrease, without increasing the sensitivity to macroscopic inhomogeneities of magnetic field.

References

(1) Bonny, J.-M., et al., Magn. Reson. Imaging 18, 1125-1128 (2000)
(2) Wadghiri, Y. Z., et al., Magn. Reson. Med. 45, 470-476 (2001)
(3) Pauly, J., et al., IEEE Transactions on Medical Imaging 10, 53-65 (1991)
(4) Reichenbach, J. R., et al., J. Magn. Reson. Imaging 7, 266-279 (1997)

Application of diffusion tensor microscopy to study spinal cord nervous tracts in a rat model of spinal cord injury

A.T. Krzyżak, A. Jasiński, D. Adamek*, P. Brzegowy*, J. Pindel, Z. Sułek, W.P. Węglarz

H. Niewodniczański Institute of Nuclear Physics, 31-344 Kraków, Poland, *Jagiellonian University Medical College, 31-503 Kraków, Poland

Introduction: Water diffusion is regarded as the most important and non-invasive contrast mechanisms in MRI of brain and spinal cord tissues because it changes very quickly after the injury. Early quantification of the presence and extend of damages induced by the injury is very important for proper medical diagnosis and treatment.

A diffusion tensor microscopy (DTM) experiment determines water diffusion tensor in the laboratory. Diagonalizing the tensor one can find principle directions of diffusivities in every voxel. Since they reflect the local order of nerve fibers, in this way one can visualize the orientation of nervous tissue tracts [1,2].

The aim of this work was to map the directions of nervous tissue tracts and its changes after the injury using principal directions of water diffusion tensor in the spinal cord of a rat.

Subjects and Methods: Well characterized "dynamic load" rat spinal cord injury model [3] with minor modifications was used to induce injury. Male Wistar rats of 250 g to 300 g were used for all experiments.

For *in vitro* experiments laminectomy was performed at the Th13 level under general anesthesia. Animals were sacrificed 10 min. to 4 hrs after the injury. Spinal cords were fixed *in situ* by formaline perfusion. After excision they were placed in 4% formaline solution. Before measurements the samples were washed in physiological solution and placed in sample tubes filled with the same solution. The control group consisted of spinal cords with laminectomy but without any injury.

Samples were measured in a home-build 8,5T MR microscope using Multislice SE diffusion sequence. MR images (512x256) were acquired at room temperature with an in-plane resolution 20x20µm, a slice thickness of 300 µm, a slice separation of 200 µm, FOV of 10 mm and a gradient factor b-factor up to 2000 s/mm^2. Diffusion tensor components (DTCs) were evaluated for each voxel of the image. After diagonalization of the diffusion tensor directions of principal axes and values of principal diffusivities were determined for each voxel. The direction corresponding to the largest diffusivity was used to determine the direction of largest diffusion. To reconstruct a fiber the direction of largest diffusion was followed through all slices of the 3D data set [2]. To visualize the fiber RGB images were composed for each voxel along its tract using principal diffusivities for colour coding as proposed by Inglis et al. [4], i.e. R-red color corresponding to Dzz component, G-green and B-blue corresponding to two perpendicular directions Dxx and Dyy.

Results and Conclusions: Good quality MR micro-images of water diffusion tensor components from the excised spinal cord of the rat were obtained, showing a very good contrast between the white matter and the gray matter. DTC measured before diagonalization are dominated by diagonal components, reflecting nearly cylindrical symmetry of the spinal cord. The region of injury is clearly seen, especially on saggital images of Dzz of longitudinal diffusion component along the spinal cord. These images correspond well to histopathological images of the injury region of the spinal cord. After diagonalization principal diffusivities were combined in color-coded RGB images, reflecting the relative ratios of diffusivities. In transverse images of the control spinal cord, the white matter is predominantly red, indicating dominating diffusion along the longitudinal direction. The gray matter is green and blue, indicating more isotropic diffusion, but also local differences in diffusion. In the injured spinal cord the region of dorsal column of white matter, close to the center of impact, shows disappearance of redness, which becomes greenish, corresponding to a decrease of longitudinal diffusion due to traumatic changes in the white matter. In this way 3D reconstruction using this RGB color-coding visualizes the traumatic region very clearly.

Individual fiber tracts were determined in the white matter as in [2]. The fiber tracts in the control spinal cord run mostly parallel to its axis. In the injured spinal cord the fiber tracts change direction or in some cases are disrupted near the center of the trauma. Our voxel of 20µm by 20µm, 300 µm long, contains around 20 individual axons [5]. For selected fiber tracts RGB color-coding was used to visualize the diffusion changes along the tract. For the fiber tract running through the pyramidal tract of the dorsal column, near to the center of injury, color changes from red to almost gray reflect damage to the axons and corresponding changes in the diffusion tensor.

RGB color-coding may be a useful way of visualizing water diffusion changes in the traumatic spinal cord and especially along the fiber tracts.

References:
[1]. Lori N.F. *et al*, Proc. Intl.Soc. Magn. Reson. Med., 7, 324, 1999. [2]. Vedeen V.J. *et al* Proc. Intl. Soc. Magn. Reson.Med., 8, 82, 2000. [3]. Ford J.C. et al, Magn. Reson. Med., 31, 218(1994). [4]. Inglis B.A. *et al*, Magn.Reson.Imag., 15, 441, 1997. [5]. Ford J.C. et al, JMRI, 8, 775, 1998.

Spatially Selective NMR Observation with a High Spectral and Spatial Resolution

Igor Serša[1] and Slobodan Macura[2]

[1]Jožef Stefan Institute, Ljubljana, Slovenia, [2]Mayo Clinic, Rochester MN, USA

Introduction

Often it is desirable to observe the NMR signal from a well-defined region within a sample. This region however, may be in general quite complex which is especially true if we want it to correspond to anatomical structures within a human body or other biological structures. In that case simple techniques for a volume selective excitation, which allow NMR excitation only within simple shapes (cube, sphere, cylinder), do not offer enough flexibility for designing excitation profiles. In 1996 we proposed a technique CARVE [1] for volume selective excitations of arbitrary shapes, which overcomes this problem. However, the main drawback of CARVE is that is prone to off-resonance artifacts and can therefore not be used for volume selective spectroscopy.

In CARVE the targeted profile is excited by the use of a long excitation sequence consisting of a synchronized train of RF and gradient pulses in which during one event (a pair of an RF pulse followed by a gradient pulse) one spatial harmonic is excited. Resulting profile is then a weighted sum of these harmonics with weights proportional to RF pulse amplitudes and phases. CARVE is prone to off-resonance artifacts due to a long excitation sequence. By reducing the number of events in CARVE off-resonance artifacts may be significantly reduced, however, spatial resolution is then reduced too. To keep the spatial resolution unchanged the profile must consist of the same harmonics. This can be achieved by splitting the original excitation sequence into several shorter excitation sequences with less events, each of which does not excite the targeted profile, however, the sum of their signals corresponds to the signal from the targeted region. In an extreme, a high resolution spatially selective observation may be designed by a sum of CARVE sequences consisting of one event only [2,3]. Since CARVE with one event has no off-resonance artifacts such observation method can be used for a spatially selective high-resolution spectroscopy.

Methods

Feasibilities of the above-proposed method for volume selective observation were studied on a phantom sample consisting of an acetone filled inner tube (4 mm diameter) inside a larger cylindrical tube filled with water (15 mm diameter). First, micro MR image of the phantom was acquired (Fig. 1a) with a field of view 25 mm and a slice thickness 2 mm. From this image excitation profiles for water (Fig. 1b) and acetone (Fig. 1c) were segmented and corresponding 250 single event excitation sequences were calculated for each profile, i.e., each profile was represented by 250 most significant harmonics. This was followed by signal acquisition with repletion rate 10 s. Experiments were performed on a 300 MHz Bruker Avance high-resolution spectrometer equipped with a 50 G/cm micro-imaging gradients.

Results

In Fig. 1 (bottom row) corresponding spectra from different sample compartments are shown: a) nonselective excitation, b) spectrum from only water compartment and c) spectrum from only acetone compartment. The efficiency of the method may be well seen from the spectra where residual peaks arising from signals from unselected compartments are practically negligible.
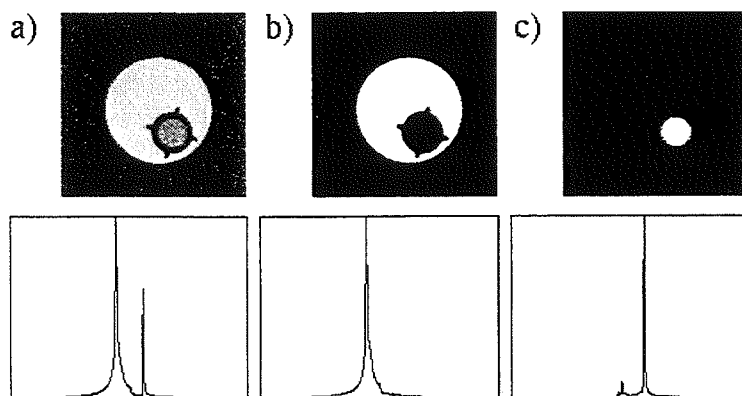
Discussion

Volume selective observation method presented here has advantage over the standard volume selective excitation methods because of its superior flexibility for designing excitation profiles and good spectral properties. Its drawback is maybe need for larger experimental time for signal observation from more complex profiles. Namely, these may be well described only by large number of harmonics (up to several thousands) and since for each harmonic corresponds to one excitation sequence this prolongs also the experimental time.

References

1. Sersa I, Macura S, *J.Magn.Reson., Ser.B* **111**, 186-188 (1996).
2. Mareci TH, *J.Magn.Reson.* **57**, 157-163 (1984).
3. Sersa I, Macura S, *J.Magn.Reson.*, **143**, 208-212 (2000).

Microscopic Susceptibility Contrast in the CRAZED Experiment

Sarah Gutteridge, Chandrasekhar Ramanathan, Richard Bowtell,
University of Nottingham, MR Centre, School of Physics and Astronomy, Nottingham, U.K.

Introduction The nuclear magnetic dipolar field is usually neglected in liquid state NMR experiments as isotropic molecular tumbling successfully decouples its interaction at short distances. However, in highly polarised samples, residual long-range components have a significant effect on the evolution of the magnetisation giving rise to multiple spin echoes[1,2] and unexpected multiple quantum coherences[3]. Warren and co–workers have explored the utilization of the zero and double quantum(ZQ and DQ respectively) CRAZED experiments to selectively probe local susceptibility variations on small length scales[4,5]. They have also suggested that changing the distance over which the dipolar field acts, by varying the modulating gradients, could provide a unique contrast in functional magnetic resonance imaging[6,7]. This abstract describes an investigation of the signal changes produced in the DQ–CRAZED experiment due to susceptibility variations generated by a range of perturber sizes from 5.4 to 102 µm as a function of gradient modulation and compare this to the standard spin echo experiment.

Theory and Methods For the DQ-CRAZED pulse sequence shown in Figure 1, if $t_2 \langle\langle \tau_d = (\gamma\mu_0 M_0)^{-1}$, the measured signal is given by Eqn.1 ; $S = \dfrac{iM_0 \sin\theta \cos^2(\theta/2)}{\tau_d} e^{-(2t_1+t_2)T_2}\left[\dfrac{1-e^{(2k_m^2 D - 1/T_1)t_2}}{2k_m^2 D + 1/T_1}\right]$. Where $k_m = \gamma G \tau$, D is the bulk diffusion coefficient and all other symbols have the their usual meanings. Experiments were performed with a 2.4T horizontal bore magnet. Polystyrene microspheres with diameters of 5.4, 10.8, 15.8, 24.9, 51.5 and 102µm were used. The samples were prepared at 2% volume fraction of microspheres, with a trace quantity (0.05%) of Triton X-100 to prevent agglomeration of the spheres. The susceptibility difference between the microspheres and the solvent was modified by adding Dysprosium Chloride. Solutions were prepared with susceptibility differences of $\Delta = 5.6 \times 10^{-8}$ cgs units (0.7ppm) and 1.1×10^{-7} cgs (1.4 ppm). The solutions were placed into 1.2cm diameter, 6cm long tubes and were oriented perpendicular to the main magnetic field. The samples were cooled to reduce the diffusion coefficient of water, and placed in a styrofoam holder. Echo planar imaging was used to minimise the imaging time and therefore limit the effects of sphere settling during the experiment. 64 x 64 SE images were acquired using a slice thickness of 2cm with TE of 20 to 200ms. The TR was set to optimise the SNR of the DQ-CRAZED experiment and remove the effects of stimulated echoes. A 120^0 pulse was used for the second pulse to maximise the signal amplitude. To eliminate any unwanted phase accumulation $t_2 = 2t_1$. The DQ-CRAZED experiments were performed with a slice thickness of 2.5cm and t_2 = 68ms. 12 different values of modulation gradient were used (k_m= 16 to 161mm^{-1}) corresponding to helix pitches in the range 39 to 390µm. Four tubes were imaged at a time, 3 containing spheres and one without. The tube without spheres allowed us to eliminate effects due to bulk relaxivity and diffusional attenuation due to the applied field gradients. 32 averages were acquired over a total time of a minute. In between experiments the tubes were removed and gently rolled in order to redisperse the spheres.

Results R_2 values were obtained by fitting the SE data to an exponential decay and the relaxation due to the bulk solvent subtracted (Figure 2a). The circles and the crosses represent the smaller (0.77ppm) and larger (1.4ppm) susceptibility differences, respectively. The DQ-CRAZED data from the tube without spheres was fit to Eqn. 1 as a function of gradient amplitude. This fit was then divided out of the data for the remaining tubes containing the spheres in order to obtain the signal changes purely due to the microscopic susceptibility variations. These data are displayed as pseudo-relaxivity $-\ln(S_c)/t$, where S_c is the signal after correcting for diffusion and t = $2t_1+t_2$, the effective signal evolution time. Figure 2b shows an example of this data at k_m=24mm^{-1} and Figure 2c at 80mm^{-1}.

Discussion The relaxation changes in the SE data show the behaviour expected from previous studies[8]. Increasing the susceptibility difference increases the peak relaxivity and shifts it to smaller perturber sizes. The apparent relaxation in the DQ-CRAZED signal is stronger than that in the SE experiment. This is in agreement with the results of Richter *et al.*[6] who observed larger changes in FMRI experiments compared to the SE experiment. While there is a slight change in relaxation rate with gradient strength the modulation length does not appear to have a strong effect under our experimental conditions. We are currently investigating this further, along with a broader range of $\Delta\chi$ and evolution times.
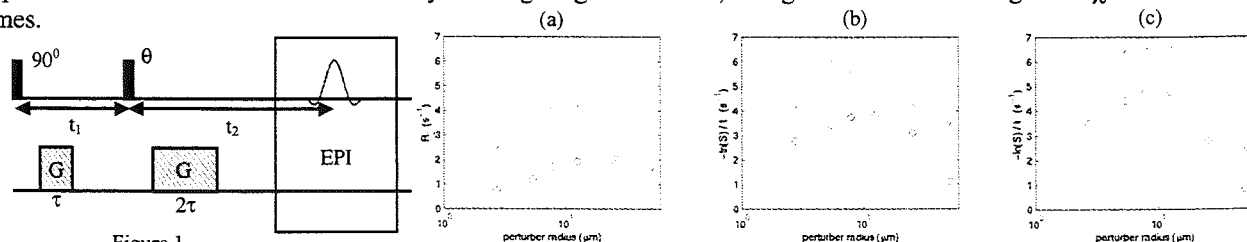
Figure 1.

Figure 2.

References
1. Deville *et al. Phys. Rev. B*, **19** 5666 (1979). 2. Bowtell *et al,. J. Mag. Reson.*, **88**, 642 (1990), 3. Warren *et al., Science*, **262**, 2005 (1993), 4. Warren *et al., Science*, **281**, 245 (1998), 5. Garret –Roe *et al., J. Mag. Reson,* **146**, 1 (2000). 6. Richter *et al., Proc.* ISMRM, **8**, 504 (2000), 7. Li *et al. Proc.* ISMRM, **8**, 267 (2000) 8. Weisskoff *et al.,Magn. Reson. Med.,* **31**, 601, (1994).

Electric Current Density Imaging of a Tablet Dissolution

Ursa Mikac[1], Alojz Demsar[2], Igor Sersa[1], Franci Demsar[1]

[1]"Jozef Stefan" Institute, Jamova 39, Ljubljana, Slovenia;
[2]Faculty of Chemistry and Chemistry Technology, University of Ljubljana, Ljubljana, Slovenia;

Introduction

Electric current density imaging (CDI) is a magnetic resonance imaging technique that images induced current density and conductivity distribution within a sample [1, 2]. Electric currents that flow through the sample change the magnetic field in the sample. The changed magnetic field B_C is added to the static magnetic field and causes a shift in the Larmor frequency $\Delta\omega = \gamma B_c$. The frequency shift is obtained by measuring the phase shift $\varphi_c = \Delta\omega T_c$, where T_c is total duration of applied electric currents. Once the magnetic field change B_c is known electric current density can be calculated using the Amper's law $j = 1 / \mu_0 \nabla \times B_c$. In this study this technique is used for imaging the spatial variation of the ionic concentration during dissolving of a tablet [3]. Ion migration was modeled using the diffusion equation. For different acids diffusion constants were calculated by fitting experimental data to the theoretical model.

Methods

CDI experiments were performed on 100 MHz Bruker Biospec system equipped with micro-imaging accessories. Experiments were carried out in plexi-glass cell filled with 1% agar-agar gel. The cell contained two concentric cylinders. The inner cylinder with a diameter of 10 mm and 12 mm in length had electrodes on both ends, so that electric currents were flowing along the cylinder axis. The electrodes were connected to an amplifier with 220 V output voltage. The outer cylinder with a larger diameter (16 mm) was used as a reference and was also filled with 1% agar-agar gel, but no current was flowing through it. A cylindrical tablet with dimensions: diameter, $2r = 3$ mm and height, $h = 12$ mm was placed in the center of the inner cylinder. The dissolving processe followed by ion migration was monitored by CDI at regular time intervals of approximately 4 minutes until the tablet was completely dissolved and the current density was uniform through the inner cylinder.

Results

Once the acid tablet was inserted into the 1% agar-agar gel, positive and negative ions started to separate and migrate away from the tablet. The concentration of mobile ions changes gel conductivity and therefore reflects in CDI images. Current density images thus show a progression of tablet dissolution and ion migration, while no difference (except for the position of the tablet at the beginning of the experiment) is observed on conventional MRI images. The intensity of the CDI represents the concentration of positive and negative ions (black: no electric current, white: maximum electric current).

Discussion

CDI technique enables monitoring of spatial and temporal changes of conductivity. The potential use of this technique is for monitoring migration of ions through liquids and membranes. Thus, it can be used in pharmaceutical sciences where the dissolution of drugs from tablets, powders, and granules and distribution of drug molecules in tissues is important. These processes cannot be monitored by conventional MRI, since it can only show changes in the size of the tablet during dissolving, whereas CDI can detect also ion distribution around the tablet. CDI may be therefore important for better understanding of the transport of drug molecules in tissues.

References

1. Joy MLG, Scott G, and Henkelman RM, Magn. Reson. Imaging 7, 89 (1989)
2. Scott GC, Joy MLG, Armstrong RL, and Henkelman RM, Magn. Reson. Med. 28, 186 (1992)
3. Beravs K, Demsar A, and Demsar F, J. Magn. Reson. 137, 253 (1999)
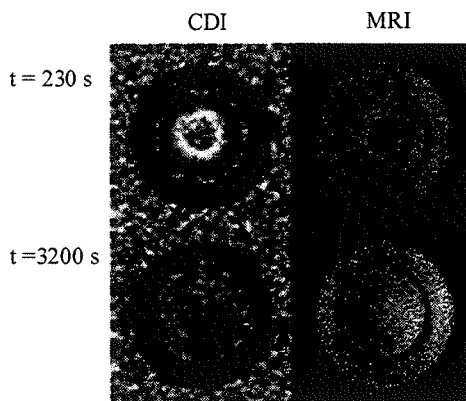
Liquid-liquid phase separation in porous systems as seen by NMR cryoporometry

R. Valiullin and I. Furó
Royal Institute of Technology, Stockholm, Sweden

The behaviour of binary liquids in porous materials is important for both fundamental and applied research. Differences in liquid-surface interaction between components of the mixture as well as the structure of the porous host lead to a rich variation in phase separation and equilibrium behaviour [1,2]. One of both experimentally and theoretically established phenomena is the slow kinetics of phase separation as compared to that of bulk mixture. Since the presence of the matrix complicates the data analysis of widely used experimental methods, such as light and neutron scattering, some of the features of the liquid-liquid distribution may remain hidden. In this work, we show that the NMR cryoporometry [3] applied to the mixture with one frozen component in a random solid environment can be used to probe directly of the structural properties of the liquid domains [4].

Uncoated controlled porous glasses (CPG) with pore sizes 24 nm (G24) and 73 nm (G73) were used as porous matrix. Nitrobenzene-hexane mixture with the critical composition $\phi = 0.36$ nitrobenzene volume fraction and upper critical solution temperature $T_{cr} = 293.2$ K was imbibed into the CPGs at $T > T_{cr}$. The freezing temperatures of the bulk components are $T_{NB} = 278.9$ K and $T_{HX} = 178.2$ K. Starting at temperatures above T_{cr}, the samples were cooled until the nitrobenzene phase froze and then the spin-echo signal recorded by a Bruker DMX-200 spectrometer using the $90°-\tau-180°$ pulse sequence with $\tau = 5$ ms was measured with increasing temperature. Fourier transformation was used to distinguish the NMR signals from the nitrobenzene and hexane molecules that have a large difference of chemical shift.

On cooling the bulk mixture below T_{cr}, nitrobenzene-rich lower and hexane-rich upper phases form and at $T \approx 250$ K the nitrobenzene part freezes, while the hexane signal remains unchanged. With subsequent heating, the frozen nitrobenzene phase melts at a well-defined temperature. For the nitrobenzene component in pores the melting region is broadened and depends on the pore size of CPG. From this melting point suppression, the size distribution functions of the frozen nitrobenzene domains were derived using the Gibbs-Thompson equation [5], and the results are shown in the figure. The dashed lines show the pore-size distributions of the CPGs obtained by the same method using pure nitrobenzene.

The domain distribution has a well-defined bimodal character for the mixture in G73, whereas it is unimodal in G24. The mode that contains the bigger domain sizes in G73 coincides in size range with the pore-size distribution function of G73. One of the features of both samples is the existence of a mode that contains domains smaller than the dimension of the pores. These modes are characterized by mean crystal diameters d_m, which are less than the pore sizes, and equal to about 15 and 30 nm for the G24 and G73 glasses, respectively. This experimental result reveals that the hexane-rich phase surrounds the droplets of the nitrobenzene-rich phase located in the middle of pores or pore junctions. This feature is in agreement with the stronger affinity of hexane to the walls [6].

For the small nitrobenzene droplets the major coarsening mechanism is the coalescence of diffusing droplets. We suggest, that the observed dependence of the size distribution on the pore size is caused by the suppression of such coalescence. As the droplet size d_0 reaches the pore dimension, the diffusion of droplets slows down,

Nitrobenzene domain dimension (nm) deduced from NMR cryoporometry.

and the local concentration of the droplets and the random structure of the matrix determine the kinetics of the further domain growth. If d_0 is in the order of 10-20 nm, coalescence in G24 is suppressed. In G73 some of the droplets may coarse until the dimension of the pore is reached, while other droplets remain trapped in some pores because of the tortuosity of the porous space and bottlenecks. The validity of the proposed model was also tested by diffusion measurements in a wide temperature range using pulsed-field-gradient NMR, and the results are in agreement with the conclusions obtained above by NMR cryoporometry.
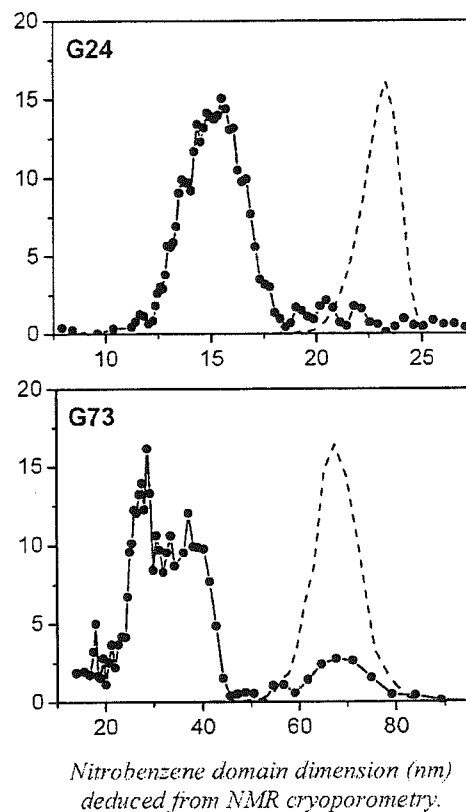
1. Gelb L. D., Gubbins K. E., Radhakrishnan R., Sliwinska-Bartkowiak M., Rep. Prog. Phys. 62, 1573 (1999).
2. Binder K., J. Non-Equilib. Thermodyn. 23, 1 (1998).
3. Strange J. H., Rahman M., Smith E. G., Phys. Rev. Lett. 71, 3589 (1993).
4. Valiullin R., Furó I., submitted.
5. Jackson C. L., McKenna G. B., J. Chem. Phys. 93, 9002 (1990).
6. Sliwinska-Bartkowiak M., Sowers S. L., Gubbins K. E., Langmuir 13, 1182 (1997).

Double Quantum Filtered and Quadrupolar Echo MRI Microscopy of Cartilage

Hadassah Shinar[1], Keren Keinan- Adamsky[1], Uzi Eliav[1], Yoshiteru Seo[2] and **Gil Navon**[1]

[1]School of Chemistry, Tel Aviv University, Tel Aviv, Israel; [2]Department of Physiology, Kyoto Prefectural University of Medicine, Kyoto, Japan

Articular cartilage is a dense connective tissue whose main biological function is to absorb and dissipate load. The main constituents of cartilage are collagen fibers, proteoglycans (PG) and water. The collagen fibers induce motional anisotropy to the water molecules and sodium ions interacting with them. Thus dipolar and quadrupolar interactions are not averaged to zero, leaving some residual splittings. The splitting is related to the order of the fibers and the degree of their interaction with the small molecules.

For ^{1}H and ^{2}H nuclei double quantum filtered (DQF) NMR is specially suited for the investigation of connective tissues, since, it filters out the large signal of the isotropic water molecules. One dimensional ^{2}H DQF spectroscopic MRI gives the distribution of the quadrupolar splitting, and thus the orientation of the collagen fibers along the depth of the cartilage. This is exemplified in Fig. 1 for a cartilage and bone plug equilibrated with deuterated saline, both at rest (1a) and under a load of 0.97 MPa (1b). As can be seen from the spectral traces for the cartilage without load the splitting is much larger in the calcified zone than in the radial zone. After the application of the load, the splitting at the calcified zone is almost lost while the splitting at the

surface is dramatically increased. After releasing the load and re-equilibrating the plug in deuterated saline, the image reverted to its original indicating that the effect of pressure is fully reversible. After removal of the cartilage from the bone above the calcified zone, the image of the latter was obtained at rest (Fig. 2a) and under load (Fig. 2b). This time, the splitting in the calcified zone is almost unaffected by the load. A plausible explanation is that in the bone-cartilage plug, due to the crimping of the collagen fibers in response to load, the collagen fibers penetrate into the calcified zone.

One of the early signs of osteoarthritis is a decrease in the PG content of the cartilage. The concentration of sodium is known to be related to the amount of the negatively charged PG. We have found that the splitting of the sodium resonance is also sensitive to the amount of PG. Thus ^{23}Na spectroscopic image gives information about the status of the PG within the cartilage. Quadrupolar echo spectroscopic image gave us the distribution of the ^{23}Na quadrupolar splitting. The splitting was found to double following the depletion of PG by trypsin digestion.
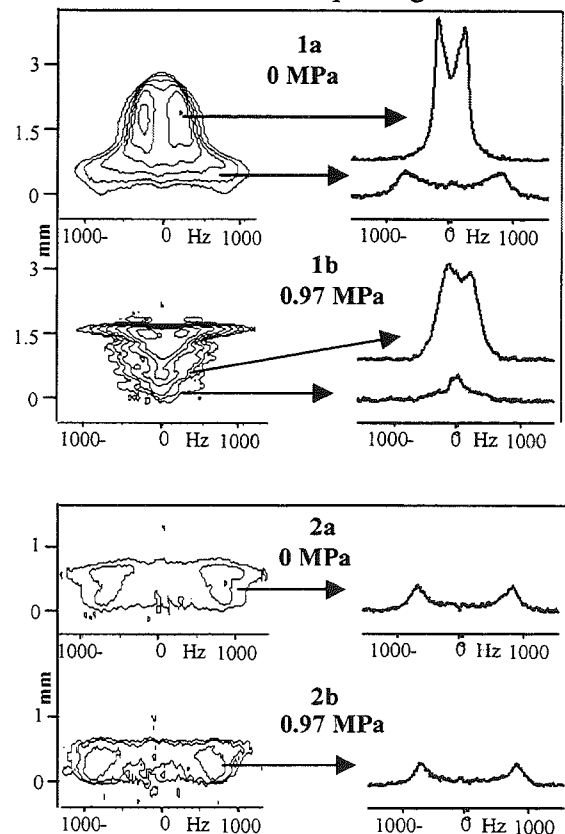
Degeneration of Neurofilament of Rat Sciatic Nerve Detected by ^{2}H Double Quantum Filtered NMR Spectroscopy and Microscopy

Yoshiteru Seo[1], Hadassah Shinar[5], Yasushi Morita[2], Kazuya Ikoma [1,2], Yoshiaki Kusaka[3], Masataka Murakami[4] and Gil Navon[5]

[1]Dept of Physiology and [2]Dept of Orthopedic Surgery,
Kyoto Prefectural University of Medicine, Kyoto
[3]Dept of Orthopaedic Surgery, Murakami Memorial Hospital, Asahi University, Gifu
[4]Dept of Molecular Physiology, National Institute for Physiological Sciences, Okazaki,
Japan
[5]School of Chemistry, Tel Aviv University, Tel Aviv, Israel

The signals of water in the epineurium, endoneurium, and axon of peripheral nerve can be resolved by the ^{2}H double quantum filtered (DQF) NMR spectroscopy, due to their different quadrupolar splittings (v_Q) and the dependence of the DQF signal intensity of each of the signals on the creation time of the DQ coherences. While in the epineurium and the endoneurium the quadrupolar splitting is a result of the interaction of the water with the oriented collagen fibers, in the axon the neurofilaments and microtubules may cause the ordering. Histological and biochemical studies have reported that degeneration of neurofilaments occur in the first 72 hours of the Wallerian degeneration. We observed the Wallerian degeneration of rat sciatic nerve for 4 days, and measured the ^{2}H DQF signal intensity of the intraaxonal water. ^{2}H DQF spectroscopic images were also obtained for the intact and degenerated nerves.

The right sciatic nerve of Wistar rats was severed, and the nerve was isolated 1, 2, 3, and 4 days after the incision. The isolated nerve was equilibrated in deuterated saline, and was placed in a 100 uL capillary tube. NMR measurements were carried out Bruker ARX500 and AMX300wb spectrometers at 24^0 C. ^{2}H DQF spectra were measured as a function of the creation time, τ. Spectroscopic imaging (micro5 and micro2.5 Bruker imaging probes) was performed with a 1D version of a pulse sequence with the phase encoding gradient applied during the DQF relaxation period. In ^{2}H DQF the DQ evolution time is relatively long. Applying the gradients during this period, doubles their effective strength, thus improving the spatial resolution.

The intraaxonal signal (v_Q = 9 Hz) This peak, is already decreased 24 hours after the incision, and the signal almost disappeared after 4 days. In addition, as the degeneration progresses, the maximum intensity of the ^{2}H DQF intraaxonal signal is obtained at longer creation times. This time-course well agrees with biochemical studies of three neurofilaments proteins (NF). The TEM image obtained by Jeol JEM-1200EX also confirmed the degeneration process of the neurofilaments. Preliminary result of ^{2}H DQF spectroscopic imaging suggests that the technique is well suited for following the heterogeneous spatial degeneration of the nerve.

From these results, we can conclude that ^{2}H DQF NMR can be quantify the degeneration process of the neurofilaments in the axon, and it might be possible to monitor the regeneration process of the peripheral nerve.

Bone Formation Studied by Proton NMR Microscopy

Kimberlee POTTER[1], Richard D. LEAPMAN[2], Peter J. BASSER[2], William J. LANDIS[3],

[1]Armed Forces Institute of Pathology, Rockville, Maryland, USA; [2]National Institutes of Health, Bethesda, Maryland, USA; [3]Northeastern Ohio Universities College of Medicine, Rootstown, Ohio, USA.

Introduction: Bone yields very little signal in proton NMR images, but trabecular architecture and hence strength and fracture risk of cancellous bone can be assessed because of the high intensity signal from the intervening bone marrow (1). A few investigators have applied solid state imaging techniques to detect phosphorus-31 nuclei immobilized in the inorganic matrix of bone with some encouraging results (2). In this work, proton NMR imaging has been used to investigate bone formation *de novo* in a mineralizing cell culture system. Small mineral deposits in the cultures do not result in a complete loss of signal and thereby provide a unique opportunity to relate water proton NMR properties to mineral quantity and quality.

Methods: To study the earliest stages of the endochondral ossification process, a three-dimensional mineralizing cell culture system, based on a hollow fiber bioreactor, was developed (3). All NMR microscopy experiments were performed on a Varian Inova spectrometer (Varian, Palo Alto, CA) coupled to a 4.7 T magnet (200.6 MHz for 1H). The radio-frequency probe consisted of a three-turn solenoid coil wrapped around individual bioreactors. The probe was inserted into a radio-frequency resonant circuit. A field-of-view of 8 mm, a slice thickness of 2 mm, and a matrix size of 128 x 128, yielding a nominal in-plane resolution of 62 μm, were used. Throughout data acquisition, bioreactors were maintained under incubator-like conditions (37°C, 5% CO2). Measurements were made of the water proton longitudinal (T1) and transverse (T2) relaxation times, the magnetization transfer rate (km) constant, and the water diffusion coefficient (D), at 4, 5, and 6 weeks after inoculation of bioreactors with hypertrophic chondrocytes isolated from the cephalic half of 17-day-old chick embryo sterna.

The spatial distribution of developing mineral deposits in the cultures was detected with von Kossa and Alizarin Red stains, which gave the locations of phosphate and calcium, respectively. To verify that the mineral deposits in the bioreactor-derived cartilage were hydroxyapatite (HA), tissue sections were prepared using anhydrous techniques and the mineral crystals, detected by transmission electron microscopy, were subjected to selected area electron diffraction and x-ray microanalysis (4).

Results and Discussion: The earliest evidence of mineral formation was apparent in water proton diffusion maps of cartilage 4-weeks post-inoculation. The cartilage tissue was relatively homogeneous ($2.04 \pm 0.22 \times 10^{-5}$ cm^2/s) except for a dark pre-mineralized zone ($1.72 \pm 0.30 \times 10^{-5}$ cm^2/s), which appeared prior to a detectable change in both the water proton T1 and T2 values for the same zone. This result confirms that the water in this cartilage zone is rapidly tumbling but has reduced diffusivity. At week 4 the km values of the pre-mineralized zone (0.73 ± 0.09 s^{-1}) were slightly higher than for cartilage zones that did not mineralize (0.63 ± 0.15 s^{-1}), data suggesting collagen enrichment prior to mineralization. By week 5 mineral deposits had formed in the collagen-rich zones, reducing water proton T1, T2, and D values and increasing km values. These results support the hypothesis that mineralization proceeds by means of a collagen template. In non-calcifying zones, after 6 weeks of growth, water proton T2 values decreased by 13% and water diffusion values increased by 7% compared to the same tissue one week earlier. These changes could be attributed to the formation of small mineral inclusions possibly associated with matrix vesicles which are thought to play a role in the endochondral ossification process.

In summary, NMR images acquired before and after the onset of mineralization of cartilage tissue grown in a bioreactor can provide novel information concerning compositional changes of a cartilage organic matrix as it undergoes mineralization as well as mineralization events themselves.

References
1. Majumdar S, Kothari M, Augat P, et al. Bone 1998; 22: 445-454.
2. Wu Y, Ackerman JL, Chesler DA, et al. Calcif Tissue Int 1998; 62: 512-518.
3. Potter K, Butler JJ, Adams C, et al. Matrix Biol 1998; 17: 513-523.
4. Landis WJ, Glimcher MJ. J Ultrastruct Res 1978; 63: 188-223.

NMR Imaging as a Tool in Podocarp Taxonomy

Sheila M. Glidewell[1], Diane Masson[1*], Brian Williamson[1], Michael Möller[2] & Robert R. Mill[2]

[1] Scottish Crop Research Institute, Invergowrie, Dundee, DD2 5DA, UK
[2] Royal Botanic Garden, Edinburgh, 20A Inverleith Row, Edinburgh EH9 3JH, UK
* Current address: Department of Chemistry, University of Durham, Durham DH1 3LE, UK

Introduction

The Podocarpaceae are a family of rare southern hemisphere conifers, some of which are of conservation interest. The paucity of specimens and the intractable nature of the fruits for conventional histological analysis means that investigation by NMR imaging can reveal aspects of their internal morphology which are otherwise difficult or impossible to obtain.[1-2]

Methods

Specimens of fully developed green fruits of *Afrocarpus falcatus* and *Prumnopitys ferruginea* were obtained from St Helena and New Zealand respectively. NMR images were acquired on a Bruker AMX300 using a microimaging probe. For investigation of internal anatomy, 2D spin echo and gradient echo, and 3D spin echo images were acquired with a variety of weightings. Chemical shift imaging was carried out on single slices. Conventional sectioning and microscopic techniques and low temperature SEM were used where possible to aid the interpretation of the NMR images.

Results

Interwoven branching systems of canals and vascular traces were clearly visible in both species. Careful examination of sequential slices allowed the vascular traces to be followed in *P. ferruginea*. Maximum intensity projections revealed the patchy distribution of resin in the canals whose 3D morphology was visualised by surface rendering of the strong signal from the cells surrounding the canals. Chemical shift imaging demonstrated the presence of peaks commensurate with terpenes known to occur in these species. In contrast, no resin was found in the canals of *A. falcatus* and the embryo had a higher lipid content than the prothallus (endosperm), the reverse of the situation in *P. ferruginea*.

Discussion

The use of NMR imaging allowed a variety of studies to be carried out on single specimens. Traditional sectioning would have required many more specimens and been well nigh impossible because of the fleshy sarcotesta (pericarp) of the fruit surrounding an extremely hard sclerotesta. The application of NMR microscopy to preserved herbarium specimens[3] opens up the possibility of investigation of historic or possibly extinct species.

References

1. Glidewell, S.M. *et al., International Journal of Plant Sciences,* submitted January 2001.
2. Mill,R.R. *et al., Annals of Botany,* In press
3. Masson, D. *et al., Edinburgh Journal of Botany,* **58**, 1-14, 2001

Interpretation of relaxation and diffusion parameters of plants during osmotic stress

L. van der Weerd, F.J. Vergeldt, S.M. Melnikov, H. Van As
Wageningen University, Laboratory of Biophysics, Wageningen, The Netherlands

The water balance in plants is of great interest for the understanding of differences in drought sensitivity and drought tolerance between various species. To investigate the effect of osmotic stress on the water status in the plant stem, maize (drought-sensitive) and pearl millet (drought-tolerant) are compared by means of in vivo NMR imaging. The obtained parameters spin-spin relaxation time T_2, proton density and Apparent Diffusion Coefficient are interpreted using a model for vacuolised plant cells based on the diffusion model of Brownstein and Tarr (1). This model assumes the spins to be confined in a volume (the vacuole) with known geometry with radii R_x, R_y and R_z. Within this volume the magnetisation decays with a certain $T_{2,bulk}$. In addition to this bulk relaxation, relaxation occurs at the boundaries, i.e. the tonoplast membrane. The observed T_2 of the vacuole can be described by a single exponential, which is dependent on the cell dimensions (R, m), the T_2 value of the vacuole solution ($T_{2,bulk}$, s) and a sink strength parameter for the tonoplast (H, m.s^{-1}):

$$1/T_{2,obs} = H(1/R_x + 1/R_y + 1/R_z) + 1/T_{2,bulk}$$

This equation holds for situations when exchange of protons over the tonoplast between the vacuole and the cytoplasm is the rate limiting step (RH<<D).

Under non-stress conditions the T_2 of the stem internodial tissue varied as a function of the cell dimensions. The H parameter can be calculated from the measured T_2 when the cell dimensions are known, and appeared to be constant for cell volumes ranging from 2.10^4 to 2.10^6 μm^3 within the plant stem. Between the two species, however, there are differences in H. The fitted values for H are 2.8 10^{-5} and 4.0 10^{-5} m.s^{-1} for maize and pearl millet respectively, assuming that $T_{2,bulk}$ is 2 s for both plants.

During osmotic stress maize showed neither changes in T_2 in the full-grown internodes nor in the shoot apical parts of the stem, though the leaves wilted and growth of the shoot apex stopped almost completely. The T_2 values in pearl millet stem tissue on the contrary decreased about 30% within 48 hours of stress. During recovery, the T_2 returned to the initial values.

To interpret this decrease in T_2 during stress, a number of additional parameters were checked. First the stem water content and stem diameter were calculated from the amplitude images, and appeared to be constant during the entire stress period. Optical microscopy for both stressed and non-stressed millet stem tissue yielded identical cell dimensions, and cryo electron microscopy showed that the vacuole dimensions did not change during stress either. All together these results prompt the conclusion that the cell size and water content in the millet apical tissue did not change during osmotic stress.

According to Clark *et al.* (2), the T_2 of the bulk solution does not change as a function of significantly increasing concentration of osmotic solutes such as sugars. This, in combination with the unchanging cell dimensions lead to the conclusion that a change of H is the cause of the observed decrease in T_2. As H represents both the exchange of protons between the vacuole and the cytoplasm over the tonoplast membrane and the effectiveness of the relaxation sink, the observed change must be caused by either an increased membrane permeability for protons, most likely water and/or by an change in cytoplasmic relaxation sink properties. Theoretically this sink effectiveness is determined by the cytoplasmic $T_{2,bulk}$, the compartment width, the cytoplasmic diffusion coefficient and the plasmalemma permeability.

To obtain some insight in the possible influence of all these parameters in the observed T_2 decrease in millet, the multi-compartment simulation models of Melnikov *et al.* (3) and Hluskou *et al.* (4) were used to evaluate the possible influence of these parameters on relaxation and diffusion behaviour. Thus, the experimental NMR results are linked to theoretical calculations of relaxation and diffusion for these complex multi-compartment geometries.

references
1. Brownstein, K.R. et al., *Physical Review A* **19 (6)**, 2446-2453 (1979).
2. Clark, C.J. et al., *Journal of the science of food and agriculture* **78 (3)**, 349-358 (1998).
3. Melnikov, S.M. et al., in prep.
4. Hluskou et al., in prep.

Pure Phase Encode MRI of Materials

B.J. Balcom

MRI Research Centre, Department of Physics, University of New Brunswick, Fredericton, NB, Canada

A wide variety of physical systems which one may wish to visualize with MRI are difficult or impossible to image with traditional techniques due to very short transverse spin-spin relaxation times. The SPRITE technique, introduced more than 5 years ago, and reviewed at the last Heidelberg meeting (1) has proven to be a very robust and general method to examine a very wide range of physical systems including, gases, porous media and polymeric materials. Recent work with SPRITE and related pure phase encode methods has been directed at: (i) Increasing their fundamental sensitivity to permit better and more rapid image acquisition. (ii) Developing new acquisition strategies to simplify the image contrast. (iii) Exploiting the narrow pure phase encode diffusion point spread function, and the lack of a line width restriction on resolution, for high resolution imaging in heterogeneous materials. These ideas will be illustrated through application to a range of materials systems, including metal-polymer composites.

1. Balcom, B.J. SPRITE Imaging of Short Relaxation Time Nuclei , in "Spatially Resolved Magnetic Resonance: Methods. Materials, Medicine, Biology, Rheology, Geology, Ecology, Hardware Wiley/VCH, Weinheim, Germany, 1998.

A new MRI method for measurement of non-steady state two-phase flow: Application to single and multi-channel flow

A.J. Sederman[1], M.D. Mantle[1], L.F. Gladden[1]
S. Raymahasay[2], J.M. Winterbottom[2], E.H. Stitt[3]

1. Department of Chemical Engineering, University of Cambridge, U.K.
2. School of Chemical Engineering, University of Birmingham, U.K.
3. Synetix, P.O. Box 1, Billingham, Cleveland U.K.

Introduction: The unstable nature of many two-phase gas-liquid flowing systems presents a challenge for MR imaging and velocimetry techniques (Sederman *et al.*, 2001). This is principally because of the very fast imaging times required (while the system is in pseudo-steady state) in the presence of high susceptibility and short T_2^*. Of particular interest in the chemical industry is two-phase flow in regular and irregular packings, used for promoting mass transfer and chemical reaction between gas and liquid. Recently, structured supports are increasingly considered because of the several potential improvements they offer. Monoliths, consisting of a collection of parallel channels, are an example of such structured supports and their use for single-phase chemical reactions is well established; e.g. the monolithic exhaust converter used throughout the automotive industry. In contrast, the application of monoliths to gas-liquid reactions is not well advanced or understood (Nijhuis *et al.*, 2001). Undoubtedly, such efforts would be aided significantly if it were possible to develop an *in-situ* probe of multi-phase transport, mass transfer and reaction within these porous structures. Here we report on the development and application of a magnetic resonance imaging technique which provides information on bubble sizes, velocities and phase volume fractions in gas-liquid flow in single and multi-channel systems.

Methods: Two-phase gas-liquid flow visualisations within single capillary and multi-channel ceramic monoliths (more commonly referred to as Taylor flow or bubble-train flow) were performed on Bruker DMX 200 MHz and 300 MHz spectrometers. The new method implemented here is based on the RARE sequence (Hennig *et al.*, 1986) but extended to acquiring multiple images from a single excitation pulse (Mantle *et al.*, 2001). In this way spins are all 'tagged' at the same point in time and successive images display the subsequent motion of the fluid.

Results: In general, single and multi-channel capillary systems under conditions of gas-liquid flow do not exhibit steady state behaviour. Each of the images acquired from the initial excitation have been analysed to obtain bubble-size distributions, gas/liquid velocities, phase volume fractions and bubble-velocity distributions. Figure 1(a) shows a typical processed MR data set showing the location of gas, liquid and solid matrix displayed as black, white and grey respectively. Corresponding bubble size and velocity distributions are shown in figure 1(b) & (c).
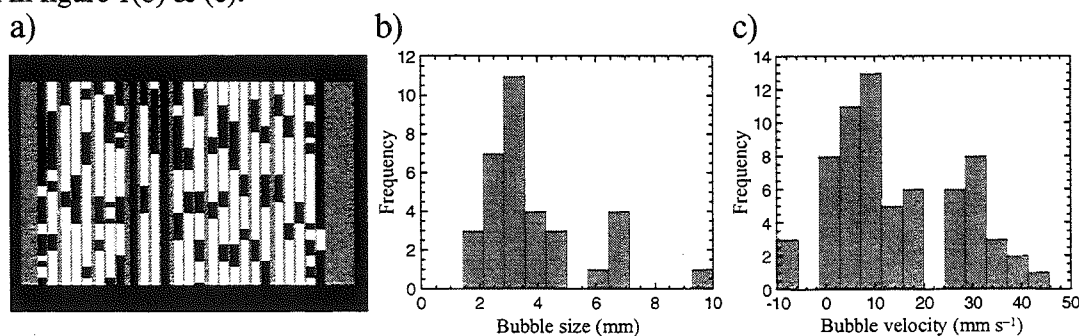
Figure 1

References
Hennig, J. *et al.*, *Magn. Reson. Med.*, **3**, 823-833 (1986)
Mantle, M.D. *et al.*, *AIChE J.*, submitted
Nijhuis, T.A. *et al.*, *Chem. Engng Sci.*, **56**, 823-829 (2001)
Sederman, A. J., and L.F. Gladden, *Chem. Eng. Sci.*, In Press

3-Phase Sedimentation/Flotation

Steven D. Beyea and Stephen Altobelli
New Mexico Resonance, Albuquerque, New Mexico, USA

Introduction

Since many suspensions of practical use separate due to density differences, there is a wide and lengthy literature on the process of sedimentation. In an initially uniform suspension of mono-disperse, non-colloidal spheres in a Newtonian liquid, for instance, a particle free layer and a densely packed layer grow linearly in time at the expense of a layer which remains at the initial concentration. The speed of the sharp boundary between the clear and middle layers, divided by the speed of an isolated particle, depends only on the initial concentration of the mixture. We recently developed a simple NMR method for measuring this dependence, which is termed the hindered settling function.[1] In this communication we describe two ways we are developing which allow us to study suspensions which have both sinking and floating solid phases.

Methods

In suspensions of oil-filled 1-mm pills and 40 μm glass micro-bubbles in silicon oil, we used inversion nulling to alternately measure the oil and pills (sinking phase). We used simple ^1H spin-echo techniques to measure vertical profiles of the concentration of the two phases we could observe and deduced the micro-bubble concentration profiles by subtraction.

In suspensions of polyethylene and glass spheres in perfluoropolyether oil, we alternately measured vertical profiles of polyethylene (^1H, using SPRITE[2,3], floating phase), and the fluorinated oil (^{19}F, spin-echo) and deduced the profiles for the sinking glass phase by subtraction.

Results

Currently, we obtain profiles at intervals of approximately 10 s with both of these methods, limited in the first by the long T_1 of the silicon oil and in the second by the duty cycle of our gradient set. This sampling rate is sufficient to allow calculation of the desired hindered settling functions for mixtures in which the rates of sinking and flotation are not too disparate.

Conclusion

We have developed two experiments that allow measurement of mixtures of two solid phases in a liquid. The experiments were evaluated in terms of an effective fluid theory that combines the silicon oil and micro-bubbles. In our experiments, using Krieger's viscosity correlation, the effective fluid picture seems to be inadequate.

References

1. S. Altobelli, et al, Journal of Rheology, submitted, (2001).
2. B. J. Balcom et al, J. Magn. Reson. A, **123**, 131-134 (1996).
3. S. D. Beyea et al, J. Magn. Reson., **135**, 156-168 (1998).

Beyond Microscopy: NMR Nanoscopy of Complex Systems*

Robert E. Botto[1] and David L. VanderHart[2]

[1]Chemistry Division, Argonne National Laboratory, Argonne, IL 60439 and [2]Polymer Division, National Institutes of Standards and Technology, Gaithersburg, MD 20899

Introduction

Recent work in our laboratories has focused on identifying the variation of chemistry on the nanometer scale. One question that we would like to answer is: "At what length scale does the chemical heterogeneity persist in complex carbonaceous solids?" While MRI has inherent resolution limits that are difficult to overcome, some earlier experiments have provided some insight into this question. Previous MRI and x-ray microscopy studies provided images showing some details of the chemical variation in these systems. While the images obtained were impressive, showing a definitive separation in chemistry along phase boundaries, the maximum pixel image resolution achievable was well above the nanometer scale.

NMR spin-diffusion provides an alternate approach that allows an investigation of chemical heterogeneity on the nanometer length scale, 2-50 nm. The concept behind the experiment is to set up a magnetization gradient between chemically different (via CRAMPS) protons that reside in different domains, and then to allow the magnetization to 'diffuse' between domains. From the time dependence of magnetization transfer, one can estimate the size of the domains. The challenge has been to apply the method to very complex substances.

Results and Discussion

Proton NMR experiments, both inversion-recovery and spin-diffusion types, employing CRAMPS methods were performed on a solid carbonaceous sample containing largely aliphatic and largely aromatic domains of unknown dimensions. The T_1^H decays of the two domains were distinct. Nevertheless, the fact that the T_1^H decays were separable and, in particular, that the aliphatic component, representing about 10% of the total protons, had an upward rather than a downward deviation from exponentiality, implied that most of these domains exceed 100 nm in size.

We were also interested in the possibility that there might be some aliphatic domains, which were significantly smaller and within spin diffusion (SD) distances. A slightly accelerated decay was found for the resinite polarization along with a hardly perceptible rise in the aliphatic polarization in the 4-ms to 12-ms range. Thus, a maximum of 20% of the aliphatic protons were in domains small enough (< 6nm) to undergo SD on the time scale of 12 ms or less, which suggests that there is little or no chemical heterogeneity at length scales between 6 and 100 nm. The SD results were consistent with aliphatic domains that are mainly large with clear phase separation, akin to domains found in slowly formed, thermodynamically incompatible polymer blends. The remaining 20% of the aliphatic protons were found within microdomains. The findings suggested that low molecular weight aliphatic materials had percolated through the microporous structure prior to polymerization.

Toward NMR Nanoscopy

Current work is being directed toward implementing CRAMPS methods during the NMR imaging experiment. To this end, we have designed and constructed three robust, rapid-switching gradient power supplies and low-inductance gradient coil system capable of producing intense, short duration (2-3 μs) gradient pulses in excess of 100G/cm. This capability will allow intense gradient pulses to be placed within CRAMPS cycles, facilitating greatly enhanced image resolution in solid samples (10 μm may be achievable). The further possibility of incorporating NMR spin diffusion protocol into a spatially-resolved experiment will be considered.

Carbon-13 Chemical Shift Imaging of rotating solids by Radio-Frequency Field Gradients. Spin Relaxation Filters.

Daniel Canet

Université Henri Poincaré, Nancy I, France

NMR imaging (and microscopy) has become a major tool in material science[1]. Concerning polymeric materials, the method can be dealt with in two different ways, either indirectly by imaging a solvent embedded in the material or directly by imaging the solid material itself. The former relies on the mobile components within the object under investigation and makes use of liquid state imaging techniques. The latter is much more demanding with regard to spectroscopic methodology as, in that case, one is faced with the problem of lines broadened by internal anisotropic interactions, with however the benefit of obtaining genuine information devoid of any additional effect related to solvent uptake (swelling or more generally any kind of interaction between the solvent and the polymer). As we are trying to detect possible heterogeneities which could be modified by solvent swelling, we shall resort to solid state methods. The first task is obviously to choose a procedure, compatible with imaging techniques, for getting rid of line broadening due to dipolar couplings or other anisotropic interactions. Basically, two approaches can be thought of. The first one makes use of large amplitude gradients capable of overcoming this line broadening[2] while the second one employs spectroscopic techniques[3] for removing (or attenuating) dipolar coupling effects. Even if proton NMR affords the best sensitivity, line narrowing is difficult and, in spite of a lower sensitivity, an interesting alternative is natural abundance carbon-13 spectroscopy provided that the following techniques are employed : i) proton dipolar decoupling (DD) for removing dipolar couplings affecting the rare spin (carbon-13), ii) magic angle spinning (MAS) for removing chemical shift anisotropy (CSA) effects and iii) cross-polarization (CP) for improving sensitivity. In order to carry out an NMR imaging experiment, field gradients are needed and severe difficulties are encountered for synchronizing the gradient direction with sample rotation even though relatively slow spinning is employed[4]. Nevertheless the only direction which is fixed is obviously the rotation axis, thus making it relatively easy to perform one-dimensional imaging. It turns out that, by contrast with static field gradient techniques[4,5], radio-frequency (rf) field gradient techniques can be readily implemented for achieving such a goal[6]. They just require a flat coil, the axis of which coincides with the rotation axis whereas the coil system needed in the case of static field gradients is somewhat more complicated[7]. Moreover, advantages of rf field gradients are well known[8] in terms of very short rise and fall times and for their immunity to magnetic susceptibility variation effects. As a disadvantage of this approach, one must however note the necessity of minimizing the leakage between the gradient coil and the coil dedicated to normal spectroscopy operations. With respect to a previous report[6], we have used a probe which has been considerably improved regarding sensitivity and dipolar decoupling so that the method has become operational for attacking truly solid state problems. In this respect, it must be stressed that NMR microscopy provides not only spin density images but also images contrasted by spectroscopic parameters[1] (relaxation times, chemical shifts, self-diffusion coefficients...); maps of these parameters can eventually be obtained. The technique will be precisely devoted to the separation (in terms of images) of the different components in heterogeneous polymeric samples. Several types of discriminating procedures, prior the imaging procedure itself, have been considered in order to assess the spatial distribution corresponding to these components. They include cross-polarization and depolarization experiments and an approach based on carbon-13 longitudinal relaxation times. The latter will be shown to be especially efficient for spatially resolving three phases (crystalline, amorphous, intermediate), further characterized by different chemical shifts, in "anisotropic" High-Density PolyEthylene.

References

(1) Blümich, B. *NMR Imaging of Materials*; Clarendon Press : Oxford, 2000
(2) Demco, D.E.; Blümich, B. *Concepts Magn. Reson.* 2000, *12*, 188.
(3) Demco, D.E.; Blümich, B. *Concepts Magn. Reson.* 2000, *12*, 269.
(4) Scheler, U.; Schauss, G.; Blümich, B.; Spiess, H.W. *Solid State NMR* 1996, *6*, 375
(5) Nonaka, M.; Matsui, S.; Inouye, T. *J. Magn. Reson.* 2000, *145*, 315
(6) Malveau, C.; Diter, B.; Tekely, P.; Canet, D. *J. Magn. Reson.* 1998, *134*, 171
(7) Maas, W.E.; Bielecki, A.; Ziliox, M.; Laukien, F.H.; Cory, D.G. *J. Magn. Reson.* 1999, *141*, 29
(8) Canet, D. *Prog. NMR Spectrosc.* 1997, *30*, 101

Integrated Optical/Magnetic Resonance Microscopy for Cellular Research

Robert A. Wind, Don S. Daly, Gary R. Holtom, Paul D. Majors, Kevin R. Minard, and Brian D. Thrall.

Pacific Northwest National Laboratory, P.O. Box 999, Richland, WA 99352, USA

A combined optical (confocal) and magnetic resonance microscope (OM/MRM) is being developed, which makes it possible to look at live cells and follow cellular events such as cell transformation or therapy response simultaneously with both techniques and in real time (1). It is anticipated that this microscope will significantly enhance the capabilities of both techniques for cellular research. Two versions of a combined microscope are approaching completion. The first version will be used to investigate large single cells and small three-dimensional cell agglomerates, whereas the second version is capable of examining single layers of heterogeneously populated live mammalian cells.

In this presentation the design of the instrument will be discussed and the first results, obtained with the combined microscope, will be shown. Specifically, the following issues will be addressed:

1. *The layout of the instrument.* The instrument utilizes an 89-mm diameter, vertical-bore Oxford magnet, operating at 11.7 Tesla, into which a bottom-loading OM probe and a top-loading MRM probe are inserted. Proton magnetic resonance images and spectra are acquired using a Varian, Unity-Plus imaging spectrometer.

2. *The sample compartment.* In both versions the sample chamber is part of a perfusion system, and has VT capabilities in the temperature the range 10-45 °C. In the first version the sample chamber is a horizontally-aligned silica capillary sample tube (1mm OD, 0.8 mm ID, 6-mm length), whereas for the second microscope the chamber is a short cylinder, into which a horizontal cover slip, onto which cells are plated, can be inserted.

3. *The confocal microscope.* The objective is custom-made of non-magnetic materials. The field-of-view has a diameter of 2 mm, and the confocal microscope has an in-plane resolution of maximal 1 micron and a vertical resolution of about 33 microns.

4. *The MR microscope.* The MR microscope consists of two parts, an outer probe containing a gradient system, capable of producing gradients of 150-250 G/cm in a volume of about 200 mm^3, and an inner RF probe. The RF probe contains the sample chamber and the components of the NMR RF circuitry. In the first microscope the NMR coil is a solenoid, wound around the capillary sample tube. In the second microscope the NMR coil is a butterfly coil, mounted on top of the sample chamber. With both setups MR images of intracellular water can be obtained with an isotropic resolution of 20-30 microns after about 4000-8000 acquisitions, and proton NMR cellular metabolite spectra can be observed after as little as 500 scans on a volume of 0.008 mm^3, corresponding to about 6,000 mammalian cells.

5. *The image registration.* Registration and calibration of the confocal and MR image spaces is obtained by inserting fiduciary markers into the sample compartment. In the first microscope polystyrene beads are used, whereas in the second microscope a 100-μm thick Kapton layer is placed near the top of the chamber, into which a micro-pattern is laser-etched.

6. *First results.* First combined images will be shown of the fiduciary markers, large and small single *Xenopus laevis* oocytes, JB6 mouse cell model tumor spheroids, and a monolayer of Cho cells. MR metabolite spectra of these cells will be shown as well.

7. *First applications.* A method will be discussed to use the *a priori* knowledge provided by the high-resolution confocal images to improve the boundary resolution and the contrast in the MR images. Also, first results will be shown of the use of the combined microscope to monitor death in Cho cells during energy deprivation occurring when the perfusion medium is replaced by phosphate buffered saline.

8. *Current and future research.* Initially the combined microscopes will be used to study stress in *Xenopus* oocytes, growth/regression in model tumor spheroids, and programmed death or apoptosis induced in cancer cells. Other potential applications of combined OM/MRM for cellular studies other than apoptosis will be discussed as well.

Reference:
1). Wind RA, Minard KR, *et al*, J. Magn. Reson. 147, 371-377 (2000).

Super-Parallel MR Microscope

Katsumi KOSE, Yoshimasa MATSUDA, Tomoyuki HAISHI(*), Shin UTSUZAWA(*)
Yukako YAMAZAKI, Izumi ANNO(**)
Institute of Applied Physics, (**) Institute of Clinical Medicine, University of Tsukuba,
Tsukuba 305-8573, (*) MR Technology Inc. Tsukuba 300-2642, JAPAN

MR microscope applications for a large number of samples (1,000 or more) are expected to increase in biological sciences (gene expression in mice etc.). For these applications, the processing speed of existing MR microscopes has a limitation. To overcome this problem, parallel image acquisition is required.

Three approaches can be considered for the parallel MR microscopy. The first is to use a large-diameter RF coil for multiple samples. However, the RF coil gives poor SNR images because the RF coil is not optimized for each sample. The second is to use small RF coils optimized for each sample with a single gradient coil. This approach is good only for a relatively small number of samples because the electric power required to drive the gradient coil increases 5th power of the size (diameter) of the gradient coil. We thus propose the third approach which uses small RF coils optimized for each sample together with multiple gradient coils attached to each RF coil (Fig.1). By using this approach, the electric power for the gradient coil can be drastically reduced. Since this approach enables us to take MR microscope images of about 100 samples at the same time by using a whole body MRI magnet (50 cm dsv homogeneous region), we call this system "super-parallel MR microscope".

The key units for the system are the gradient probe array and multiple receiver system, because the RF transmitters supply the same RF pulses to the RF coils at the same time. The details for the gradient probe and receiver system will be given in other presentations.

To confirm the system concept, we developed an eight-channel gradient probe array and imaged two fixed mouse samples at the same time using two compact MRI consoles. Figure 2 shows images of two mice simultaneously acquired at two sample zones. These images show a great promise for the super-parallel MR microscope.

Fig.2 Cross-sectional images selected from 3D data sets of two mice simultaneously acquired. 200 microns cube voxel, 28 min, acquisition time.

Fig.1 Concept of super-parallel MR microscope.

Multi-layer Actively Shielded Gradient Coils

J. Leggett[1], S. Crozier[2], R.W. Bowtell[1]

[1] University of Nottingham, Nottingham, England; [2] University of Queensland, Brisbane, Australia

Introduction

Large field gradients are desirable in MRI since the spatial resolution is directly proportional to the gradient strength. The gradient should also be as homogeneous as possible over the imaging region of interest (ROI) in order to obtain a spatially accurate representation of the spin system. The gradient can be increased for a given current by increasing the number of wires in the coil, thus increasing the efficiency. A limit is reached once the conductors are spaced such that they are touching. For a single layer coil, the only way to insert more turns is to reduce the conductor diameter, thus rapidly increasing the coil's resistance and ohmic power losses. The increase in power dissipation can be reduced by allowing the wire distribution to spread out radially, thus dispensing with the necessity of decreasing the conductor diameter.

A further important issue to consider is that of the eddy currents which a temporally varying gradient field will induce in any conducting material near the coil. These in turn give rise to magnetic fields which distort the gradient field produced by the coil.

As a development of previous work [1, 2] on multi-layer gradient coils, active magnetic screening has been incorporated into the design of axial and transverse multi-layer coils in a cylindrical geometry.

Method

The design method that was used was an extension of Turner's "Target Field Approach" [3]. An ideal field is specified over a volume ROI represented by a grid of points. A current distribution is defined over a number of equally spaced layers, and comprises a weighted set of axial fourier harmonics [4] which are only non-zero over the extent of the coil. A weighted combination of the power dissipation, inductance, deviation of the field from linearity within the gradient ROI, and deviation of the field from zero within a ROI outside the shield, is minimised in order to determine the weightings for each harmonic in each layer. Having thus calculated the optimum continuous current distribution required to satisfy any constraints imposed on the coil, a set of wire paths must be derived that approximate to the current density. This is achieved in the usual manner using the stream-function of the current density [3]. The variables in the system were the weightings in the minimisation, which were varied to maintain the gradient homogeneity within 5%, and the number of wires in the layers, which were varied in order to obtain a coil of resistance 1Ω.

Results

The following results were obtained using a Biot-Savart calculation performed on the discretised current densities. The axial coils consisted of eight layers spaced 0.36mm apart. All layers had a half-length equal to twice the radius of the innermost layer (ρ_i=4.5mm). The ROI was of radius and half-length $0.5\rho_i$, and ten axial harmonics were used. For one particular coil, the layers contained 14, 9, 6, 3, 0, 2, 4 and 6 turns, working outwards from the innermost layer. The coil had an efficiency of $0.707 \text{Tm}^{-1}\text{A}^{-1}$, an inductance of $12\mu\text{H}$, and a resistance of 1.043Ω using $254\mu\text{m}$ copper wire. An unshielded eight layer coil designed to the same criteria had an efficiency of $1.778 \text{Tm}^{-1}\text{A}^{-1}$, an inductance of $76\mu\text{H}$, and a resistance of 1.108Ω using $315\mu\text{m}$ wire. The number of turns per layer was 14, 12, 10, 9, 8, 7, 6, and 5. An average of the ratio of the shielded to unshielded fields over a grid of test-points outside the shield was less than 4%.

The transverse coils consisted of eight layers spaced 0.6mm apart. The half-lengths of all coils were four times the radius of the innermost layer (ρ_i=5.65mm). Again, the ROI was of radius and half-length $0.5\rho_i$. Ten axial current harmonics were used, and for a particular coil the layers contained 12, 8, 5, 4, 0, 1, 3 and 5 turns (see Figure 1). The coil had an efficiency of $0.324 \text{Tm}^{-1}\text{A}^{-1}$, an inductance of $10\mu\text{H}$, and a resistance of 0.8Ω using $376\mu\text{m}$ wire. The equivalent unshielded coil had an efficiency of $0.604 \text{Tm}^{-1}\text{A}^{-1}$, an inductance of $64\mu\text{H}$, and a resistance of 1.07Ω using $376\mu\text{m}$ wire. The number of turns per layer was 9, 7, 6, 5, 4, 4, 3 and 3. The averaged value for the shielding was just under 2%.

(a) Layer 1   (b) Layer 3

(c) Layer 6   (d) Layer 8
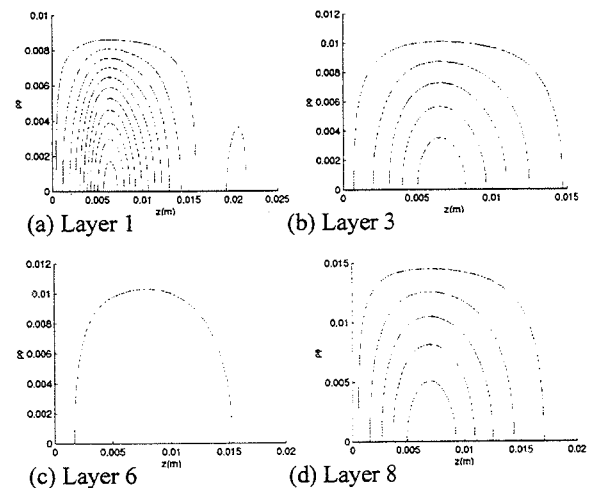
Figure 1: Wire distributions for one octant of selected layers of an eight layer transverse gradient coil.

Conclusion

A multi-layer approach allows the design of coils exhibiting larger gradient strengths than single layer coils. These shielded multi-layer coils have yet to be constructed and tested experimentally, although unshielded multi-layer coils have previously been constructed and shown to work [1, 2]. Future work includes the development of a design formalism capable of interleaving x, y and z coils to enable the construction of an integrated multi-layer, screened three-axis coil.

References

1. Bowtell, R.W., *et al.*, J. Magn. Reson. **131**, 286-294 (1998)
2. Bowtell, R.W., *et al.*, Proc. 7th Annual Meeting ISMRM, P468
3. Turner, R., Magn. Reson, Imag. **11**, 903-920 (1993)
4. Carlson, J.W., *et al.*, Magn. Res. Med. **26**, 191-206 (1992)

Compact MR Microscopes Using Dipole-Ring Permanent Magnets

Yoshimasa MATSUDA, Tomoyuki HAISHI(*), Yukako YAMAZAKI, Katsumi KOSE

Akio NAKANISHI(**), Sigemasu OKADA(**), Masaaki AOKI (**), Tuyoshi TSUZAKI(**)

Institute of Applied Physics, University of Tsukuba, Tsukuba 305-8573,

(*) MR Technology Inc. Tsukuba, 300-2642
(**) Sumitomo Special Metals Co. LTD, Osaka, JAPAN

Recent developments of electronic devices and systems have enabled us to make compact MRI consoles. Thus if a small magnet for MR microscopy could be developed, a desktop MR microscope can be constructed. For such a compact magnet, permanent magnets are the first choice because they require no cryostat and the stray fields are usually much smaller than that of superconducting magnets. Yokeless permanent magnets composed of segmented high-performance magnetic materials (e.g. FeNdB magnets) have been expected to present drastically compact magnets. However, as far as we know, no practical yokeless permanent magnet for MR microscopy with a high magnetic field (~1 T) has been reported, mainly because of technical difficulties.

In the present study, we have successfully developed compact yokeless permanent magnets with the field strength of about 1.0 T and constructed compact MR microscopes.

For the compact MR microscopes, we used two kinds of dipole-ring magnets: (a) gap size; 60 mm, weight; 210 kg, size; 36 cm x 32 cm x 28 cm, (b) gap size; 41 mm, weight; 85 kg, size; 27 cm x 24 cm x 18 cm. Figure 1 shows the overview of the one of the compact MR microscopes. The most serious problem for the system operation was large temperature drift of the magnetic field. Figure 2 shows temperature and resonance-frequency changes for the magnets measured through a whole day. On the basis of these data, we acquired 3D MR microscope images using an NMR lock technique operated in a time-sharing mode. Figure 3 shows a surface rendered 3D image of a fixed mouse fetus acquired at the 70 microns cube voxel dimension. This image shows a great promise of this type MR microscope.

Fig.2 24 hours' change of room temperature (lower) and resonance frequencies (upper) for the magnets.

Fig.1 System overview. Total weight is about 300 kg.
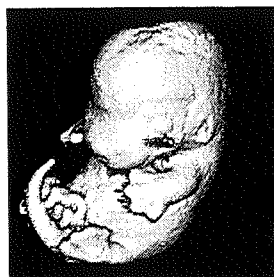
Fig.3 Surface rendered image of a fixed mouse fetus.

Orthogonal switched gradients applied in stray field magnetic resonance imaging.

J. Godward[1], **P. J. McDonald**.

Department of Physics, University of Surrey, Guildford, Surrey GU2 7XH

Stray field imaging exploits the large magnetic field gradient surrounding a high field NMR spectroscopy magnet for the high spatial resolution NMR imaging of broad line systems[2,3]. In the large gradient, a radio frequency pulse only excites nuclei of the sample in a thin slice orthogonal to the gradient. The sample is translated through this slice in order to build up a MR profile in the gradient direction. Spatial resolution of the order of 50 μm is routinely obtained using echo times of the order of 100 μs. Multi-dimensional data may be acquired by additional sample rotation. It is our experience, however, that more than one-dimensional profiling is usually impractical. There are two primary reasons. First, whereas one-dimensional profiles are acquired in tens to hundreds of seconds, full three-dimensional data acquisition can take ten hours or more. In many instances, mapped features of the sample change on the shorter timescale. Second, many samples are significantly influenced by gravity and so rotation is not practical.

Much of our own imaging now focuses on profiling through planar samples such as emulsion and latex coatings[4]. There are situations where some degree of additional in-plane spatial resolution would be desirable. A good example is the study of lateral drying fronts where lateral variation in composition and microstructure arises from uniform evaporation across as sample of non-uniform thickness[5]. This has prompted us to consider alternate means of generating orthogonal spatial resolution in stray field experiments. This we have done by adding additional pulsed gradients to a stray field experiment. Our ideas build on work using switched gradients attached to the so-called NMR mouse[6].

We show preliminary results of experiments in which we frequency encode with high spatial resolution across the slice of a planar sample in the static gradient (z) direction and phase encode the in-plane (x and y) directions using switched gradients. The experiments have been performed in the fringe field of a 9.4 T magnet using a ^{13}C (100 MHz) probe operating at the ^{1}H fringe field resonance position and a commercial iso-centre gradient set suspended below the magnet. The distortions of the images due to field curvature have been considered. We believe the real future of this development lies as an addition to our GARField magnet. GARField is a small permanent magnet with an inbuilt, large static gradient[7]. This magnet is designed for planar samples and is used for most of our current coatings work. It has a magnetic field of constant magnitude in the horizontal plane and a strong vertical gradient. With GARField, curvature distortion is expected to be less significant.

---

1 Current address, Department of Chemistry, University of Nottingham
2 Samoilenko A A., Artemov D. Y., Sibel'dina A L., *JETP Lett.* **47** (1988) 348.
3 McDonald P. J., Newling B. *Rep. Prog. Phys.* **61** (1998) 1441.
4 Wallin M., Glover P. M., Hellgren A-C., Keddie J. L., McDonald P. J., *Macromol.* **33** (2000) 8443.
5 Salamanca J. M. et al. *Langmuir* accepted.
6 Prado P. J., Blumich B., Schmitz U., *J. Magn. Reson.* **144** (2000) 200.
7 Glover P. M., Aptaker P. S. Bowler J. R. Ciampi E., McDonald P. J. *J. Magn. Reson.*, **139** (1999) 90.

PHOTOPOLYMERISATION OF A COMMERCIAL DENTAL RESIN: [1]H CONVENTIONAL AND STRAY-FIELD MRI STUDIES

Geneviève Guillot [1], Teresa G. Nunes [2], Jean Pierre Ruaud [1], Sónia G. Pereira[2], Ricardo Pires[2]
1 U2R2M CNRS ESA 8081 Bât. 220 Université Paris-Sud 91405 Orsay CEDEX France
2 Departamento de Engenharia de Materiais/IST-Universidade Técnica de Lisboa , Av. Rovisco Pais, Lisboa, Portugal

INTRODUCTION

Dental resins include, in general, visible light-cured dimethacrylate monomers, which should ensure efficient bonding to both enamel and dentin. The photopolymerisation reaction, highly anisotropic, is a diffusion-controlled process and can be monitored by MRI. Recent results[1] obtained by 1D and 3D stray-field (STRAFI)-MRI show that for a new generation adhesive (All Bond 2, Bisco, Itasca IL USA) (AB2), the degree of conversion is affected by the presence of oxygen. This study presents a novel approach to monitor the photopolymerisation of AB2, in order to obtain information about the depth of cure (DC), the mobility map evolution and the variation of the bulk mobility in the kHz range with curing time, and, in particular, to study the resin-tooth interface, using complementary MRI methods, in conditions that mimic the oral environment (conventional MRI at low- and high- magnetic fields, for the observation of liquids and soft tissues, and one-slice STRAFI MRI which also enables the study of hard materials).

RESULTS

With low-field MRI (0.1 T) it was checked that DC is about 1 cm in the light-irradiation conditions used (44.5 mW/cm^2). 3D images were acquired in a 8.5 T MRI prototype (360 MHz for ^{1}H), after different light-curing periods, using a standard 3DFT spin-echo sequence (TE/TR 5.5/300 ms), from class I cavities opened in freshly extracted molar teeth, and totally filled with resin. Each 3D data set was acquired over 25 min as a 128x128x10 matrix (Figure). After a 30 s light curing period, mobile protons were still present at both air/resin interface and resin/tooth interface (Fig b). One-slice STRAFI-MRI was used to study the variation of the bulk mobility with curing time, at 2.9 T in a 37.5 T/m stray-field gradient, with Long Echo Train acquisitions:[2] the first echoes refocus magnetisation from all the protons in the resin, and only signals from mobile domains contribute to the last echoes. Double-exponential functions were used to fit the data. The long time was in the range 8-18 ms, while the short time was always much shorter (0.23-0.48 ms). The relative amplitude of the long time component (interpreted as the mobile fraction) was decaying from 80% (liquid resin) to 0% (after more than 40 s curing time).

resin
tooth (hard tissue)
tooth (soft tissue)
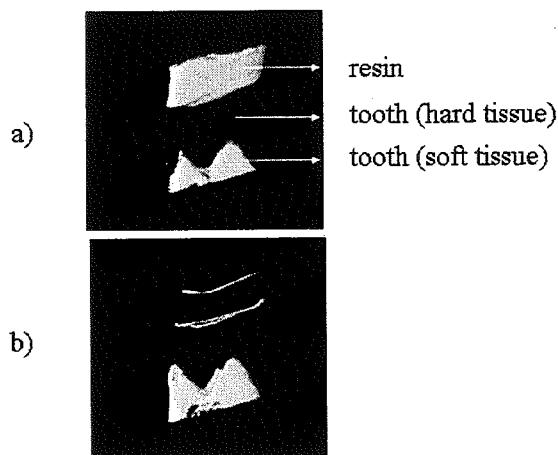
Figure: Human molar with a cavity totally filled with a resin, at a resolution of 80x80x800 μm^3, a) before any light irradiation, b) after 30 s curing time (470 nm, 44.5 mW/cm^2). The resin thickness (a), and the distance between the visible layers (b) is about 2 mm.

CONCLUSION

Mobile domains visualised in the resin/tooth interface (fig. b) have deleterious effects in adhesion to dentin and may explain adhesive failures. NMR and MRI are powerful techniques for the quantitative study of resin curing in conditions comparable to oral environment.

ACKNOWLEDGEMENTS

REFERENCES

1. Nunes, T.G., Pires, R., Perdigão, J., Amorim, A., Polido, M. *Polymer* (in press)
2. Randall, E.W., Nunes, T.G., Guillot, G., Bodart, P., *Solid State NMR* 14, 165 (1999).

A Stray Field Imaging Study of the Drying Process
of Precasting Materials used in a Steel Making Converter

Koji Saito [1], Yoshitoshi Saito [1], John Godward [2]
1) Nippon Steel Corporation, Advanced Technology Research Laboratory.
20-1 Shintomi, Futtsu City, 293-8511, JAPAN,
e-mail;saito@re.nsc.co.jp, Fax;+81-439-80-2746
2) Department of Physics, University of Surrey

Optimisation of the drying process conditions in a steel making converter in a steel works is very critical since the process is basically off-line and very time-consuming. However, it is very difficult to optimize drying process conditions (temperature, surface active agents, etc.), as steam explosion can readily occur with insufficient drying-time. To help understanding, we have demonstrated that we can monitor the drying of real refractory mortar using Stray Field Imaging. We choose this method because of the possibility of detecting short T_2 components.

Fig.1 shows representative STRAFI profiles recorded from a sample of refractory mortar at 50 °C with an initial water content of 5%. "Each profile consists of 200 separate NMR echo decay trains recorded 60microns apart along the sample length. The total profile (sample) length is thus 12.0 mm. Each train consists of 32 echoes with a pulse gap, 2*tau of 70 microseconds. It is evident that the water content decreases with time from the drying surface. T_2 information was extracted from the echo decay trains by fitting the equation $M = M_0 \exp(-2i\tau/T_2)+c$ (c = constant, i = echo number) to the decays as a function of time and position.

Fig.2 shows that the relaxation time is shortening from drying surface as drying proceeds because of the loss of free water. In this presentation, I will show the effect of varying water content, of different materials of adding surface active agents on the drying rate. In particular, we find that the free water loss rate is relatively independent of these parameters. However the bound water loss rate is more affected. It is clear that imaging gives useful information to optimize drying conditions. Using this data, we can adjust and optimize the drying process and time in steel works.
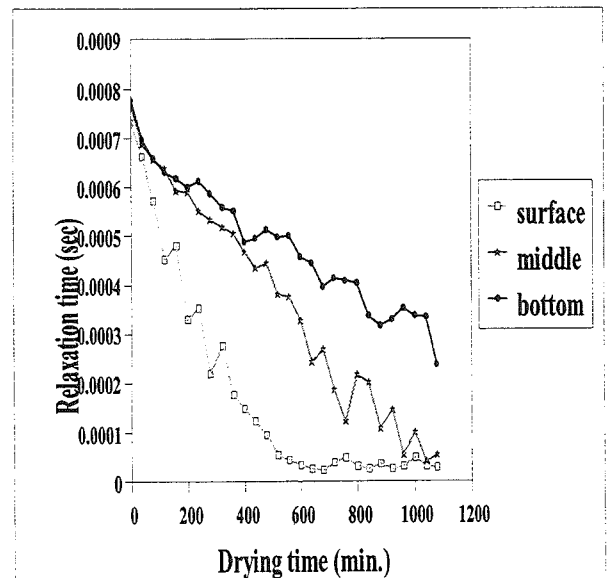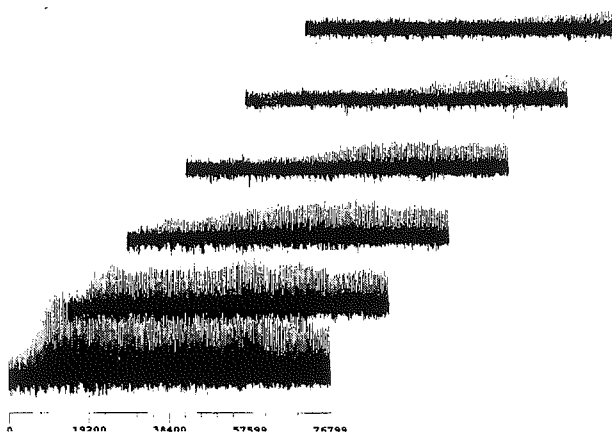
Fig.1 Representative STRAFI echo train profiles recorded at 50 °C every 40 min from a sample of drying refractory mortar. Fig.2 The relaxation time behavior of the same sample.

Abstracts for:
Poster Presentations

P1 – P59

New *In vivo* Visualization Techniques of Moisture Content in the Human Epidermis by NMR Microscopy

Joszef C. Szeles*, Markus Klarhöfer[+], Andrea Weber-Mußmann°, Lothar Motitschke°, Ewald Moser[+], Peter Polterauer*, Winfried Kuhn[#]

* Dept. of Vascular Surgery, University of Vienna, Vienna, Austria
[+] Institute of Medical Physics, University of Vienna, Vienna, Austria
° Marbert AG, Düsseldorf
[#] *IIC* Innovative Imaging Corp. KG, Blieskastel, Germany

Abstract

The aim of this study was the development of new visualization techniques in high resolution magnetic resonance imaging (HR-MRI) as a tool for in vivo quality tests of cosmetic creams and topical pharmaceutical formulations based on emulsions and gels. A screening of one cosmetic cream on three female volunteers in the age between 41 and 48 years was performed. In addition to the well known high resolution MR images, spatially resolved signal intensity plots and histogram analysis of the hydrated regions of the epidermis have been used to visualize and measure the changes of the thickness and properties of the epidermis. The results demonstrate not only the uptake of moisture by the epidermis of about 40%, but also a swelling of the epidermis by about 50%, depending of the cream applied. The thickness of the forearm epidermis of the untreated skin was about 400µm, while the moisturized epidermis was swollen to a thickness of 625µm and 986µm. Moreover, a very detailed picture of the moisture distribution within the epidermis could be obtained. Furthermore, high-resolution images acquired on a clinical whole body imager without any additional accessory except a surface detection coil show structures inside the epidermis at a depth resolution of 38 µm.

Corresponding Author:

Dr. Winfried Kuhn

IIC Innovative Imaging Corp. KG

Langental 18

D-66440 Blieskastel/Germany

Phone: ++49 6842 3448

Fax: ++49 6842 3449

Email: wpk01@iic-nmr.com

Applying the NMR MOUSE to in-vivo analysis of human skin.

N. Routley, K.J. Carlton,
Science Department, Canterbury Christ Church University College,
North Holmes Road, Canterbury, Kent CT1 1QU, U.K.

M.J.D. Mallett,
School of Physical Science, University of Kent at Canterbury,
Canterbury CT2 7NR, U.K.

P. Blümler
Max-Planck Institute for Polymer Research, Mainz, Germany

Abstract:

The NMR MOUSE (*MO*bile *U*niversal *S*urface *E*xplorer) is a palm sized probe, which provides the B_0 static field as well as the B_1 RF field. The RF pulse is generated using a MARAN spectrometer which is controlled by a PC. Due to the inhomogeneity of both magnetic fields, applications of the MOUSE are limited to soft matter samples. In such samples the molecular mobility is sufficient to provide long transverse relaxation times yet diffusion can be ignored. The open geometry of the MOUSE places few restrictions on the sample size or shape[1,2].

The current application that is being developed centres upon in vivo investigation of human skin. A variation in the depth of excitation should be possible by varying the RF frequency. Preliminary investigations have shown variations in transverse relaxation as a function of depth within skin. The aim is to produce a 1D depth profile of human skin. The resolution of this profile will be determined by the thickness of the excited region, which is inversely proportional to pulse length. It is expected that at least half-millimeter resolution can be achieved.

Reference:

1.   See for instance: http://www.nmr-mouse.com/

2.   B. BLÜMICH: *"NMR Imaging of Materials"* Oxford Science Publications, Clarendon Press, Oxford, 2000.

Magnetic Field Inhomogeneity Effects on Intermolecular Multiple Quantum Coherences

R. Bowtell, S. Gutteridge, C. Ramanathan,
School of Physics and Astronomy, University of Nottingham, Nottingham, NG7 2RD

Introduction

Although the dipolar field, $\underline{B}_d$, is generally neglected in NMR experiments on liquid-state samples, the long range component of this field can give rise to significant effects, particularly when the magnetisation is spatially modulated by the application of gradients. Such effects include the generation of inter-molecular multiple quantum coherences (iMQC's) (1) and the formation of multiple spin echoes (2). Recently, it has been suggested that these effects are sensitive to local magnetic field inhomogeneities occurring on a controllable length scale, set by the degree of spatial modulation of the magnetisation (3). This sensitivity could be exploited in fMRI to allow the tuning of contrast to field inhomogeneity effects produced by changes in blood oxygenation occuring at different levels of the vascalature. However, although the detection of brain activation using iMQC's has been reported (4), the sensitivity of iMQC signals from macroscopic samples to the spatial form and magnitude of field inhomogeneity, fundamental to understanding how these signals may be exploited in fMRI, has not been characterised. Here, we therefore describe an investigation of the iMQC signal dependence on field inhomogeneity in two model systems. These were studied via computer simulation and imaging experiments carried out at 3.0 T.

Methods
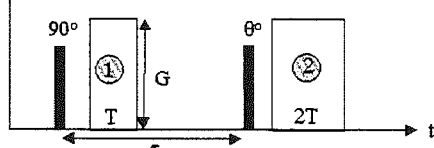
We consider the basic double-quantum CRAZED sequence shown in Fig. 1. Despite the unequal gradient pulse areas, a signal is formed as a result of the action of the dipolar field, $\underline{B}_d$ generated by the nuclear magnetisation. In the presence of field inhomogeneities described by $\Delta\omega(\underline{r})/\gamma$ this takes the form of an echo refocussing at time, 2τ, after the θ^0 RF pulse.

Two sources of field pertubation were considered: (a) a long wire running in the y-direction, located at z=x=0 and carrying current, I, so that $\Delta\omega\tau=\alpha\sin\varphi/r$ where $\alpha=\mu_0\gamma\tau/2\pi$, $r^2=x^2+z^2$, and $\varphi=\tan^{-1}(x/z)$; (b) a long cylinder of radius, a, running in the y-direction and located at z=x=0, differing in magnetic susceptibility from the surrounding fluid by an amount, $\Delta\chi$, so that $\Delta\omega\tau=\beta\cos2\varphi/r^2$, where $\beta=-0.5\gamma\tau\Delta\chi a^2 B_0$. With the field modulation in the y-direction, calculation of the signal then reduces to a two-dimensional problem. Simulations were carried out for varying values of k_m and α or β.

Experiments were carried out at 3 T, using a specially constructed phantom, consisting of a water-filled box, containing a rectangular wire loop, with the short side oriented in the vertical, y-direction. A vertical glass rod of 6 mm diameter, was also included in the phantom. Coronal images with resolution of 1 x 1 x 30 mm^3, were acquired by making the 2nd RF pulse slice selective, and adding phase encode and read gradients, such that the centre of k-space was acquired at time ($2\tau=88ms$) after the 2nd RF pulse.

Results and Discussion

Figures 2a and b, show simulations of the spatial variation of signal, with x (horizontal) and z (vertical) for the wire ($\alpha=1450mm$), and the cylinder (a = 3mm, $\beta=163mm^2$) both with $k_m = \gamma GT = 4.7$ mm^{-1} and a FOV of 64 x 64 mm^2. Figure 2c shows an experimentally acquired image of the phantom, where similar values of α and β obtain (corresponding to I = 60 mA and $\Delta\chi \sim 1$ ppm), but the FOV is 128 x 128 mm^2. The simulated and experimental data show similar patterns of signal loss. Data gathered at varying values of k_m and α or β, indicate that for the wire, the pattern scales in size with the square root of (α/k_m) and as the cube root of (β/k_m) for the case of the cylinder. This behaviour implies that for this geometry, the signal variation follows the pattern of the z-gradient of $\Delta\omega\tau$, which varies as $\alpha\sin2\varphi/r^2$ in the case of the wire and $-\beta\cos3\varphi/r^3$ for the cylinder. A further inference is that there is significant signal loss in regions where $d(\Delta\omega\tau)/dz \geq k_m$. This can be explained as being a consequence of the significant perturbation of the angle between B_0 and the effective direction of modulation of magnetisation in regions where this inequality obtains. Using this information we can estimate the size of the region around a blood vessel where iMQC signal would be lost as a consequence of field inhomogeneity. Considering a venule of 25 μm radius, with a blood-tissue susceptibility difference of 0.3 ppm (SI units) (6), the extent of this region would be approximately 50 μm, for $k_m = 50$ mm^{-1} and $\tau = 50$ ms.
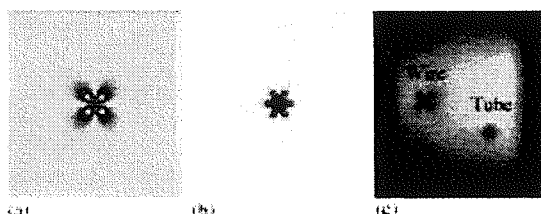
References

1) Warren WS *et al., Science,* **262**, 2005, 1993.
2) Bowtell R *et al.* P, *J. Magn. Res.,* **88**, 643, 1990.
3) Warren WS. *et al., Science,* **281**, 247, 1998.
4) Richter W, *et al., J. Magn. Imag.,* **18**, 489, 2000.
5) Deville G *et al., Phys. Rev. B,* **19**, 5666, 1979.
6) Weisskoff RM *et al. Magn. Res. Med.,* **24**, 375, 1992.

Application of Single Point Imaging in Restorative Dentistry

JA Chudek[1], G Hunter[1], CH Lloyd[2] and **SN Scrimgeour**[1,2]
[1]Division of Physical and Inorganic Chemistry, and [2]Dental School, University of Dundee, Dundee DD1 4HN, Scotland, UK

Introduction Conventional 'liquid' magnetic resonance microimaging is limited when studying mineralised tissues such as enamel and dentine in teeth due to the very short T_2 values (of the order of 10^2 μs) for the nuclei in these tissues. 'Liquid' MRM can image root canals and caries [1,2]. Imaging of the anatomy of the mineralised tissue is possible using three dimensional STRAFI [3]. The advent of SPI/SPRITE [4], however, has made it possible to produce much more detailed images of teeth in which both soft and mineralised tissues are present in the image [5]. SPI would appear to be an optimum nmr technique with the potential to study teeth which are both diseased and restored. The progress of disease in extracted teeth in artificial caries-inducing environments could be studied. Healthy tooth tissue (soft/mineralised), primary and recurrent disease, and restorations might be imaged together.

Method Single Point Image data for a number of extracted teeth were acquired using a three-dimensional SPI pulse sequence and a microimager attached to a Bruker AVANCE DPX 300 nuclear magnetic resonance spectrometer. Data processing was carried out on a Silicon Graphics O2 workstation with ParaVision software.

Results Encouraging results have been obtained for restored teeth that contain both healthy and diseased tissue. Metallic restorations are still widely used in restorative dentistry, therefore, it is important that the images are not distorted by the presence of the metal. This was found to be the case. The use of SPI has also allowed us to make direct cavity volume measurements, applying the technique to endodontics as well as repair of hard tissue.

Discussion and Conclusions If MRM is to be used to its full potential in restorative dentistry, imaging of the critical interfacial area between the prosthetic material and natural tissues must be achieved. Recurrence of disease in this area is the primary reason for failure of treatment [6]. For MRM this is complicated by the composition of the dental materials. SPI offers the best solution to this dilemma, to date.

References

[1] Lloyd, CH, Scrimgeour, SN, Chudek, JA, Hunter, G and MacKay, RL, 1997. Magnetic resonance imaging of carious teeth. Quintessence Int **28**; 349-355.

[2] Lloyd, CH, Scrimgeour, SN, Chudek JA, Hunter, G and MacKay, RL, 2000. Application of magnetic resonance imaging to the study of dental caries. Caries Res **34**; 53-58.

[3] Baumann, MA, Doll, GM and Zick, K, 1993. Strayfield imaging of teeth. Oral Surg Oral Med Oral Pathol **75**; 517-522

[4] (a) Gravina, S and Cory, DG, 1994. Sensitivity and resolution of constant-time imaging. J Magn Reson B **104**; 53-61. (b) Balcom, BJ, 1998. SPRITE imaging of short relaxation time nuclei, in Spatially Resolved Magnetic Resonance: Methods, Materials, Medicine, Biology, Rheology, Geology, Ecology, Hardware. Eds. P Blumler, B Blumich, R Botto, E Fukushima, Wiley-VCH, Weinheim, Chapter 5, p75-86.

[5] Seo, Y, Takamiya, H, Ishikawa, H, Nakashima, T, Sharfand, Y and G Navon, 1998. NMR imaging of rigid biological tissues, in Spatially Resolved Magnetic Resonance: Methods, Materials, Medicine, Biology, Rheology, Geology, Ecology, Hardware. Eds. P Blumler, B Blumich, R Botto, E Fukushima, Wiley-VCH, Weinheim, Chapter 42, p 445-457.

[6] Burke, FJT, Cheung, SW, Mjor, IA and Wilson, NH, 1999. Reasons for the placement and replacement of restorations in vocational training practices. Primary Dental Care **1**: 17-20.

Evaluation of the Internal Structure of Articular Cartilage in terms of ^{1}H-NMR Relaxation Behavior and ^{1}H DQF MRI

Kazuya Ikoma[1,2], Takeshi Matsuo[2], Yoshiaki Kusaka[3], Yoshiteru Seo[1]

Department of Physiology[1] and Orthopaedic Surgery[2],
Kyoto Prefectural University of Medicine, Kyoto, Japan
Department of Orthopaedic Surgery[3],
Murakami Memorial Hospital, Asahi University, Gifu, Japan

Introduction: In conventional MR images, articular cartilage has a laminated appearance. The number of the laminae, their thickness and intensity varies from sample to sample and from study to study, and strongly depend on the orientation of the tissue in the magnetic field (1-3). This effect has been shown to be a consequence of the transverse relaxation rate that is dominated by the residual dipolar interaction and depends on the orientation of the collagen fibers relative to the magnetic field. In the present study, we measured the NMR parameter and ^{1}H DQF MRI of weight bearing and non-weight bearing regions of articular cartilage, and examined the distinction of the non-weight bearing part and the weight bearing part of articular cartilage.

Materials and Methods: Cartilage and cancellous bone plugs, 7 mm in diameter, were obtained from every 5 regions into which fresh bovine femoral medial condyle was divided from anterior to posterior of articular surface. The plugs were placed in an NMR tube so that the surface of the cartilage was perpendicular or parallel to the static magnetic field. The ^{1}H longitudinal (T_1) and transverse (T_2) relaxation times were measured by fast-inversion-recovery method and multi-spin-echo method, respectively. The ^{1}H DQF MR images were measured by changing the creation time (τ) from 0.3 ms to 10.0 ms. NMR measurements were recorded on an AMX-300 WB Bruker NMR spectrometers. All experiments were conducted at room temperature (about 25^0C).

Results and Discussions: The T_1 of the cartilage showed a maximum value at, or just beneath, the articular surface and this value decreased gradually towards the deeper zones. The T_2 of the same cartilage showed a maximum value at, or beneath, the articular surface, decreased rapidly towards the intermediate zone yet increased again in the deepest zone. The increase of T_2 in the deepest zone was more greatly pronounced in the weight bearing region than in the non-weight bearing region. On the ^{1}H DQF MR images of the articular cartilage, when the articular surface was setting perpendicular to the static magnetic field, the signal intensity showed maximum value at the deep zone, decreased gradually towards the intermediate zone, and disappeared at surface zone at τ value of 0.3 ms. The signal intensity of the deep zone was getting more decrease and that of the intermediate zone was getting more increase at the longer τ value. When the articular surface was setting parallel to the static magnetic field, the signal intensity of the whole articular cartilage decreased, and this tendency was remarkable in the deep zone. The ^{1}H DQF MR images have revealed that the orientation of collagen fibers is vertical at the deep zone, widely separated at the intermediate zone, and the surface zone is very thin. These layer-dependent differences in the T_1, T_2, and the ^{1}H DQF MRI could account for the laminar appearance of the articular cartilage in the MR images.

References:
1. Lehner KB, Rechl HP, Gwenwieser JK et al., Radiology 170, 495-499 (1989).
2. Mlynarik V, Degrassi A, Toffanin R et al., Magn Reson Imaging 14, 592-601 (1996)
3. Xia Y, Magn Reson Med 39, 941-949 (1998)

Mandibular bone microarchitecture by MRI combined with DEXA measurements

Last David[1], Choel L.[2], Lissac M.[2], Briguet A.[3], Duboeuf F.[4], Boivin G.[4] and Guillot G.[1]
GDR 2237: [1] U2R2M CNRS ESA 8081, ORSAY, FRANCE, [2] LEIBO CNRS EA 637, LYON, FRANCE, [3] LRMN CNRS UMR 5012, LYON, FRANCE, [4] INSERM U403, LYON FRANCE.

INTRODUCTION

Primary osseointegration of endosteal dental implant is dependent on biomechanical properties (1). Dual Energy X-ray Absorptiometry (DEXA) measures Bone Mineral Density (BMD), but does not give any information on trabecular microarchitecture. It has been shown (2) that different trabecular bone structures having the same BMD, can present different mechanical strengths. As it is a non invasive method, MRI is of great help for the analysis of bone microarchitecture (3). Prior to histomorphometric parameter evaluation, MR images must be first binarized. This is often a difficult task due to the histogram complex shape; the simple case of a two peak histogram, the lower Gray Level (GL) peak corresponding to noise (bone), and the upper GL peak, corresponding to signal (marrow), is rarely encountered in practice. Simple thresholding (choosing for instance the threshold σ as the midpoint between the two peaks) can be applied with negligible partial volume effect and high enough Signal to Noise Ratio (SNR) (4). However, a compromise has often to be made for optimum resolution and SNR (5). The purpose of this work is to suggest an unambiguous method to binarize MR images using DEXA measurements, thus to compare different anatomical sites (with or without tooth) from standard histomorphometric parameters.

METHODS

14 mandibular bone specimens (8 mm thickness) were cut from 10 cadavers. The faces of each specimen were cut as close to parallel as possible to the teeth axis if teeth were present, and perpendicular to the alveolar ridge, if not. Non-defatted specimens were taken from non-formoled cadavers. MR images were obtained at 2 T using a multislice 2D spin-echo sequence (TE/TR 21/550 ms, FOV 25-30×15 mm^2, 8-10 slices), always perpendicularly to the mandibular arch. This yields to a spatial in-plane resolution better than 110 μm (600 μm slice thickness) with a SNR higher than 20, within less than 50 min. For each sample, two DEXA (Hologic 4500A) images were acquired so as to obtain two BMD evaluations (BMD$_1$ and BMD$_2$). The same Regions Of Interest (ROIs) were defined manually on the MR slices and the DEXA projection image, in the alveolar bone excluding nerves. Only one ROI could be defined for 9 samples, whereas two ROIs (ROIa, ROIb) could be distinguished for the 5 others, giving a total of 19 ROIs. Given the mean degree of mineralization of cancellous bone, 1.09 g.cm^{-3} (6), the Bone Volume Fraction (BVF) could be computed from the BMD. By thresholding the MR image, BVF$_{MR}$ can be easily calculated, choosing the threshold as leading to the smallest BVF deviation Δ between MR and DEXA. Two threshold values, σ_1 and σ_2, were then determined for each ROI: σ_1 (resp. σ_2) using BMD$_1$ (resp. BMD$_2$) with a minimum deviation Δ_1 (resp. Δ_2). The optimal threshold value, σ_{OPT}, was the one associated with the smaller deviation Δ_{OPT}: $\Delta_{OPT} = \min\{\Delta_1, \Delta_2\}$. For the samples with two ROIs, σ_{OPT} was defined as $\sigma_{OPT} = (\sigma_{ROIa} + \sigma_{ROIb})/2$, where σ_{ROIa} (resp. σ_{ROIb}) is the optimal threshold value associated to ROIa (resp. ROIb). Trabecular thickness (Tb.Th), trabecular spacing (Tb.Sp), and the angle (α) between trabeculae and tooth axis were then computed on the previously defined ROIs.

RESULTS

For the 19 ROIs, BVF$_{DEXA}$ varies in the range 18.4 - 68.9%. For all MR images, it was possible to find a threshold σ_{OPT} leading to a low deviation Δ_{OPT} (mean value 0.13%, SD = 0.1%). The deviation between σ_1 and σ_2 did not exceed 3 GL, indeed BMD$_1$ and BMD$_2$ were very close (mean deviation for all ROIs 1.6%). The MR images could be classified into two groups depending on their histogram: i) histogram with two peaks (11 images, including 4 images with partial volume effect); ii) histogram with a single low GL peak (3 images). For the first group, σ_{OPT} was roughly 30% higher than the midpoint between the two peaks. For the samples with two ROIs, the mean deviation between σ_{ROIa} and σ_{ROIb} never exceeded 10 GL. Tb.Th was 291±148 μm (mean±SD) and Tb.Sp 425±147 μm. On mid-tooth slices (18), α was 98°±29, 22°±64 on nearby ones (10) and 23°±37 on the furthest ones (10).

DISCUSSION

BVF$_{DEXA}$ evaluations were consistent with known values, the high values corresponding to ROIs with large trabeculae or/and with some cortical bone. DEXA measurements were highly reproducible. The small difference between σ_{ROIa} and σ_{ROIb} showed the method robustness. The selected ROI must be without soft tissues: indeed as they usually appear as intermediate GL pixels in the image, they could introduce an error in the determination of σ_{OPT}. σ_{OPT} is used to binarize the whole image: thus, histomorphometric parameters could be easily calculated on other ROIs than those used to determine σ_{OPT}. The evaluations of Tb.Th and Tb.Sp were consistent with known values but no significant difference was observed between mid-tooth locations and other locations. The trabeculae were perpendicular to the tooth axis on mid-tooth slices, more disorganized on nearby ones and recovered a privileged parallel orientation on the furthest ones.

CONCLUSIONS

Even when the MR histogram could not be used to determine σ, DEXA enabled MR image binarization. The technique is as well applicable to 2D multislice or 3D images. 3D isotropic acquisition of the same samples and calculation of topological parameters are currently in progress.

REFERENCES
1: Misch, C.E., et al., J Oral Maxillofac Surg., 57, 700-706 (1999); 2: Kleerekoper, M., et al., Calcif. Tissue Int., 37, 594-597 (1985); 3: Genant H.K., et al., J. Bone Mineral Res., 11, 707-729 (1996); 4: Antoniadis, T., et al., Medical Image Analysis, 3, 119-128 (1998); 5: Guillot, G., et al.,Proc. ISMRM, (2001); 6: Boivin, G., et al., Bone, 27, 687-694 (2000)

Projection reconstruction MR microscopy
for the quantitative analysis of trabecular bone

Renato Toffanin[1,2], Agostino Accardo[3], Giulia Candido[3], Vladimír Jellúš[4] and Franco Vittur[1]

[1] Dept. BBCM, University of Trieste, Trieste, Italy; [2] PROTOS Research Institute, Trieste, Italy; [3] DEEI, University of Trieste, Trieste, Italy; [4] Institute of Measurement Science, Slovak Academy of Sciences, Bratislava, Slovakia

Introduction

The skeleton comprises two different forms of bone: cortical bone and trabecular bone. Cortical bone serves primarily mechanical and protective functions and also provides skeletal strength. Trabecular bone, in addition to providing mechanical and skeletal strength, plays an important metabolic function. Bone disorders such as osteoporosis lead to alterations in the trabecular bone. These alterations are characterised by a reduction of bone mass and by structural changes in trabecular bone architecture. MRI has recently been applied to the study of osteoporosis as a non-invasive technique with the potential to provide information on the trabecular bone architecture (1). However, as the high difference in diamagnetic susceptibility between bone and marrow causes intravoxel signal dephasing, the trabecular thickness derived from conventional MR images is generally overestimated. This artefact can be minimised if the echo time (TE) or the voxel size are reduced. The aim of this study was to assess the potential of short-TE projection reconstruction (PR) MR microscopy in the quantitative evaluation of trabecular bone morphology. The conventional FT-based method was used to compare the derived structural data.

Materials and methods

Cylindrical bone plugs ($\varnothing$=4 mm) were obtained from weight-bearing and not weight-bearing porcine humeral heads. The bone explants were examined at 7.05 T on a Bruker AM300 WB instrument, equipped with a standard microimaging accessory. 3D spin-echo images (TE = 3.0 ms) were acquired according to the PR method with constant gradient step (2). The final voxel resolution of the PR images was $41 \times 41 \times 41$ μm^3. 3D spin-echo images (TE = 6.2 ms) obtained on the same explants by the standard FTI method were also acquired for comparison. Image analysis was performed using specific programs written for MATLAB. Standard morphologic parameters such as trabecular bone volume (TBV), trabecular thickness (Tb.Th) and trabecular separation (Tb.Sp) were computed from the binary images using a modified version of the *t3m* software (3).

Results and discussion

In this work, we demonstrate that the PR method can be used to obtain architectural information from isolated intact specimens of trabecular bone. In the analysis of the best threshold for image segmentation, a better separation between bone and marrow peaks was evident in the histograms of the PR spin-echo images. Due to the high spatial resolution, the PR approach provided values, for the derived morphologic parameters, comparable to those calculated by the conventional FT imaging approach. However, the PR derived structural data appear to be more accurate as their SD resulted lower than those calculated for the FT derived values. In addition, since the amplification of the trabecular dimensions also depends on the echo time (TE), the advantage of using the short-TE PR method should be more evident at lower resolution. *In vivo* projection reconstruction MRI could be applied to assess bone architecture and evaluate skeletal changes related to age and osteoporosis.

References

1. Majumdar S., Kothari M., Augat P. et al., *Bone* 22, 445-454 (1998). 2. Toffanin R., Szomolányi P., Jellúš V. et al., in El-Genk M.S. (Ed.): *Space Technology and Applications International Forum-2000* (American Institute of Physics), pp. 295-299 (2000). 3. Hipp J.A., Jansujwicz A., Simmons C.A. et al., *J. Bone Min. Res.* 11, 286-292 (1996).

Secretion Rate of Cerebrospinal Fluid of Rat Measured by Gd-DTPA Enhanced T_1-weighted MRI

Yoshiteru Seo[1], Akira Takamata[1], Takashi Ogino[2], Hironobu Morita[3],
Masataka Murakami[4]

[1] Department of Physiology, Kyoto Prefectural University of Medicine, Kyoto

[2] Department of Biochemistry and Cellular Biology, National Institute of Neuroscience, National Center of Neurology and Psychiatry, Kodaira, Tokyo

[3] Department of Physiology, School of Medicine, Gifu University, Gifu

[4] Department of Molecular Physiology, National Institute for Physiological Sciences, Okazaki, Japan

Cerebrospinal fluid (CSF) secretion rate of rat was measured by longitudinal relaxation time-weighted magnetic resonance imaging (T_1-weighted MRI) in combination with cerebroventricular infusion of gadolinium-diethylene triamine-N,N,N',N'',N''-pentaacetic acid (Gd-DTPA).

Rats were placed in the prone position on a custom-built Plexiglas sledge, and position of the head was fixed by a pair of ear plug and a bite bar. ^{1}H MR images were obtained by a Biospec spectrometer (ABX-4.7/40, Bruker) with an active shielded gradient (BGA-120), a home-built ^{1}H RF surface coil (18 mm in diameter) and a ParaVison 2.1 software. A cannula was inserted in the left lateral ventricle, and 5 ul of 8.5 mM Gd-DTPA saline was injected as a T_1-relaxation reagent. Using a T_1-weighted GE image sequence (TR/TE = 100 ms / 4.2 ms, FOV = 2.56 x 2.56 cm, slice thickness = 1 mm, data matrix 128 x 128), changes in intensities of CSF were measured every 30 sec, and the turnover rate (k) of CSF was obtained by a linear fitting on an assumption of a single compartment model. Reliability of fitting procedure was confirmed by computer simulations.

In the control intact rat, k was 0.158 ± 0.011 min^{-1} at arterial CO_2 tension (pCO_2) of 40.5 ± 2.1 mmHg (n=8). In the dead rat, very small k value (ca. 0.02 min^{-1}) was observed which confirmed that the secretion of CSF is essential for dilution of Gd-DTPA and also suggested a low pearmeability of the ventricule-brain-barrier of rat brain. The k value was decreased (0.081 ± 0.011 min^{-1}, n=4) by a carbonic-anhydrase inhibitor (acetazolamide). The turnover rate decreased by hypocapnia (0.094 ± 0.019 min^{-1}, pCO_2 = 24.7 ± 2.9 mmHg, n=4), and increased gradually and reached at plateau level at hypercapnia (0.182 ± 0.008 min^{-1}, pCO_2 = 95.0 ± 7.8 mmHg, n=8).

These results demonstrate feasibility of the Gd-DTPA enhanced T_1-weighted MRI technique, and also suggested that CO_2 upregulates the secretion of CSF in the rat.

MANY COMPARTMENTS OR RESTRICTIONS ? MR DIFFUSION MICROSCOPY OF THE RAT SPINAL CORD *IN VITRO.*

Wladyslaw P. Weglarz, Dariusz Adamek[1], Joanna Pindel, Piotr Kulinowski, Andrzej Jasinski
Institute of Nuclear Physics, [1]Collegium Medicum, Jagiellonian University, Kraków, Poland

Introduction. Recently, growing attention was focused on the non-exponential anisotropic diffusion in nervous tissue [1-7], opening discussion on its origin. Spinal cord represents useful model system to study anisotropic diffusion as it contains two distinct type of tissue: in outer part highly anisotropic white matter (WM) contains axons (long cells oriented approximately along the spinal cord axis) and inside much more isotropic gray matter (GM). The aim of this work was to use MR Microscopy for detection and quantification of the non-exponential anisotropic diffusion in excised rat spinal cord and to correlate results with structure of the nervous tissue dominating in spinal cord.

Methods. Experiments on the excised rat spinal cord were done on a 8.4 T MR Microscope using DWSE imaging sequence. Diffusion gradients in slice and phase directions (longitudinal and transversal diffusion components respectively) were used. Slice thickness was 0.4 mm. MR images (128x128) were acquired with TE = 65 ms, Δ = 26 ms, and δ = 7 ms. The gradient amplitudes were incremented to give b-value up to 4000 s/mm^2.

Results. The transversal diffusion in the spinal cord white matter (WM) is non-exponential and may be described by two components: fast one with D^f_{trans} = (1.1+/- 0.1)10^{-3} mm^2/s comprising 70% of the total signal and the slow one D^s_{trans} = (1.0+/-0.4)10^{-4} mm^2/s with relative abundance equal to 30 %. The longitudinal (mono-exponential) diffusion component is equal to D_{long} = (1.04 +/- 0.03)10^{-3} mm^2/s. In contrast in the gray matter (GM) the slow diffusion component is present in both directions.
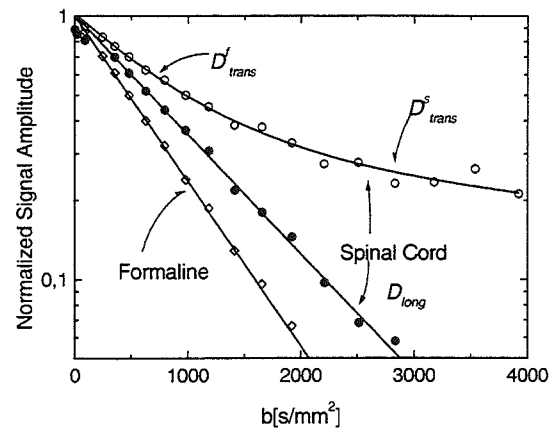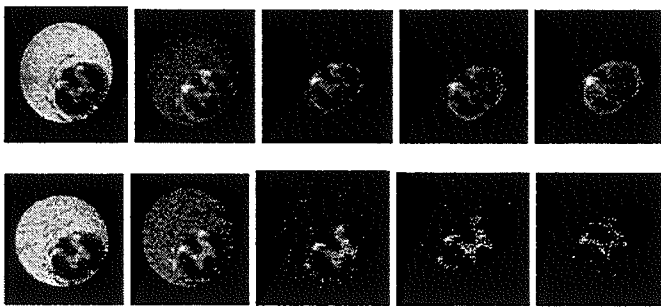
Fig. 1. a)The set of diffusion weighted MR images of the excised rat spinal cord. Diffusion gradients oriented in transversal (upper row) and longitudinal (lower row) direction, with b-values equal to: 360, 810, 1440, 2250 and 3240 s/mm^2 respectively. b) The corresponding dependence of the signal amplitude on b-value for spinal cord WM.

Discussion and Conclusions. The fact that fast transversal and the longitudinal components in the WM has essentially the same values suggests that they come from water experiencing isotropic diffusion within a distance of ~7μm. This value is comparable to typical axon's diameter and is much smaller than axon's length [8]. Therefore, in direction perpendicular to the spinal cord axis water diffusion is restricted to much higher extent than in longitudinal direction, resulting in the "slow component" observed in transversal diffusion. In the WM lack of the dominant long cells structures causes restriction in water diffusion in both directions. This result is in line with conclusions drawn from the investigations of the bovine optic nerve [1]. In the view of difficulties with binding diffusion components to different water compartments within nervous tissue [2-7] seems reasonable to conclude that the observed diffusion anisotropy in the spinal cord WM may be explained entirely by the restrictions in the direction perpendicular to the spinal cord axis.

[1] Stanisz GJ, et al., *MRM* 37, 103-111(1997).
[2] Mulkern RV, et al. , *NMR Biomed.,* 12, 51-62(1999).
[3] Mulkern RV, et al. , *MRM,* 44, 292-300(2000).
[4] Assaf Y, Cohen Y , *MRM,* 43, 191-199(2000).
[5] Assaf Y, Mayk A, Cohen Y, *MRM,* 44, 713-722(2000).
[6] Clark CA, Le Bihan D, *MRM,* 44, 852-859(2000).
[7] Inglis BA, et al., *MRM,* 45, 580-587(2001).
[8] Chetley Ford J, et al., *JMRI,* 8, 775-782(1998).

In vivo observation of magnetically labeled cells in rat brain: A high-resolution magnetic resonance microscopy investigation

Ekkehard Küstermann, Stefan Wecker, Torsten Trapp, Melanie Föcking, Mathias Hoehn

Max-Planck-Institute for Neurological Research, Cologne, Germany

Introduction:

With the progress in understanding the biology of stem cells, application to cerebral disease models with the aim for regeneration are now being considered. For this purpose, it is highly desirable to observe, non-invasively, their location and/or migration after implantation into a host brain.

Methods:

Neurons of a murine hippocampal cell line were labeled with magnetic iron-oxide nanoparticles (MIONs; SINEREM®; Guerbet) by lipofection. These MIONs produce high contrast in MR images, and thus are expected to demarcate the treated cells within the host tissue. The lipofection efficiency was 70% or better, leading to a high concentration of MIONs in the cells. Even at concentrations 4 times higher than used in our studies, acute toxicity of the MR-contrast agent was not observed.

MR sensitivity was validated by implanting defined numbers of cells either *in vitro* into gelatine phantoms or *in vivo* into the brain of Sprague-Dawley rats. For the *in vitro* experiments, labeled cells were titrated between 8×10^4 down to 4 cells and injected into a tissue phantom consisting of 1% gelatine. For *in vivo* experiments, variable numbers of labeled cells were stereotactically injected into the striatum of Sprague-Dawley rats.

MR microscopy was performed on a 7Tesla animal scanner (BioSpec®, Bruker) equipped with home-built rf-electronics for the optimization of sensitivity and actively shielded gradient coils (200mT/m). RF-pulses were applied by a 12 cm diameter Helmholtz coil actively decoupled from the reciever surface coil. High resolution multislice images with a matrix size of 256^2 to 512^2 were recorded with a gradient-echo sequence (TE = 30-70ms, TR = 0.56-0.74s). The nominal inplane spatial resolution was 55x55 or 110x110μm, slice thickness was between 300 and 700 μm.

Results:

In the phantom experiments it was possible to differentiate, against the background, cell nests consisting of 40 cells or less. In the rat brain - as demonstrated in the figures below - 8×10^4 labeled cells showed an easily detectable area of decreased signal intensity while the same amount of unlabeled cells, implanted in the contralateral hemisphere, were completely invisible on the MR images. A cell dilution series of implantation demonstrated that small clusters of less than 500 cells were reliably demarcated against the host tissue background.

Conclusion:

We conclude that regeneration processes with stem cells can be studied non-invasively with MR microscopy using magnetically labeled cells. Thus, localization of cells and their potential migration can be followed over time within individual animals. Ongoing studies with GFP expressing neural stem cells will provide further independent proof of the MRM sensitivity and accuracy, and will demonstrate the cell mobility in vivo.

Figures:

Figure 1:
Coronal slice through rat brain after implantation of ca. 8×10^4 cells on both sides of the striatum. Only the MION-labeled cells on the right side are visible.
TR=560ms, TE=30ms, 55x55x700μm
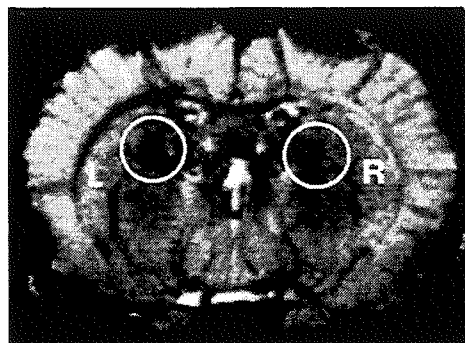
Figure 2:
Dilution series of implantated cells:
RIGHT: 500 cells (**R**); LEFT: ca. 8000 cells (**L**).
TR=740ms, TE=70ms, 110x110x700μm

3D-NMR Imaging of Dolphin Embryos and Fetuses

D. Haddad, V. Behr, H.H.A. Oelschläger*, A. Haase

Physikalisches Institut EP5, Universität Würzburg, Germany

*Dr. Senckenbergische Anatomie (III), Johann Wolfgang Goethe-Universität, Frankfurt a.M., Germany

INTRODUCTION:

Dolphins always attract our attention when we happen to encounter them. They are not only elegant and playful swimmers and perfectly adapted to their aquatic environment, but also warm-blooded and air-breathing mammals. Moreover, they possess large and complex brains with striking morphological features. Using a 3D-Spin-Echo MRI sequence, it was possible to acquire non-invasively 3D images of formalin and ethanol fixed dolphin embryos and fetuses. These images show in great detail internal organs (Figure 1), the nose and jaw (beak) regions. By using NMR, all the images were acquired without damaging the specimens.

MATERIALS AND METHODS:

Two very young stages of the spotted dolphin (*Stenella attenuata*), one late embryo and one early fetus were investigated. The embryo, an ethanol-fixed specimen of 14 mm crown-rump length (CRL) still shows small rudiments of pelvic limbs (not shown). The fetus of 45 mm CRL is formalin-fixed. Both specimens were collected and preserved 26 and 28 years ago, respectively, by the U.S. government. The NMR experiments were performed on a Bruker AMX500 spectrometer at 11.75 T. The maximum gradient strength of the system is 0.66 T/m. For the embryo a birdcage coil with 20 mm in diameter and a length of 30 mm was used. The fetus was scanned in a birdcage coil with 28 mm in diameter and a length of 42 mm. A temperature of 11°C was maintained during the whole experiment. First, two-dimensional Spin-Echo images were acquired to select a sagittal slice through the fetus. The in plane resolution of these images was $175 \times 156 \ \mu m^2$ (256×128 pixels) for the fetus and $78 \times 78 \ \mu m^2$ (256×128 pixels) for the embryo. In both cases slice thicknesses of 100 and 200 μm were used. After choosing a suitable orientation three-dimensional Spin-Echo images were acquired. The embryo was scanned with a $256 \times 256 \times 128$ matrix and a spatial resolution of $58.5 \times 58.5 \times 117.2 \ \mu m^3$. For the fetus a $256 \times 128 \times 128$ matrix was used with a resolution of $175 \times 156 \times 156 \ \mu m^3$. For all experiments a repetition time TR of 1.5 s and an echo time TE of 14.4 ms were chosen. Zero filling by a factor of two was applied in each dimension after the acquisition.
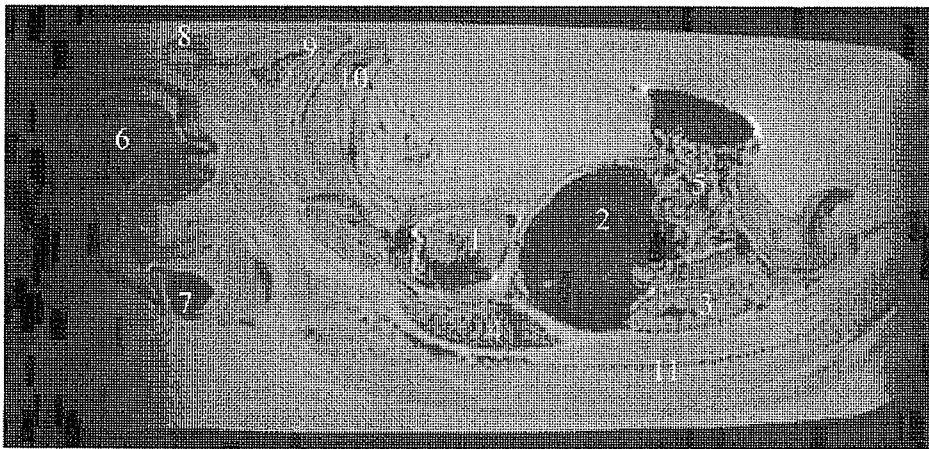
Figure 1: Sagittal slice through the dolphin fetus:
1) heart
2) liver
3) kidney
4) lung
5) intestine
6) diencephalon
7) cerebellum
8) blowhole area
9) upper jaw
10) lower jaw
11) spine

RESULTS:

The NMR images show the anatomy of the dolphin fetuses in great detail. The achieved resolution was sufficient to visualize various organs like the heart and liver as well as the kidney and lung (Figure 1: 1-4). In these prenatal dolphins even substructures of the heart are distinguishable. Parts of the intestine (5) are protruded into the umbilical cord (physiological umbilical hernia) and the genital region is clearly visible (not labeled). In the head, the skull base (not labeled) bears the brain (diencephalon [6] and cerebellum [7]) and merges in the blowhole area and the upper and lower jaws (8-10). In the spine (11), the original segmentation is still obvious in the NMR images. In other, more lateral sections, the eyes and flippers are to be seen (not shown).

DISCUSSION AND CONCLUSION:

The anatomy of the late dolphin embryo and early fetus is well reflected in the acquired images. Since the different anatomical structures are clearly distinguishable, it is possible to perform a complete segmentation of the whole fetus. From the segmented dataset the volumes and surface areas of the different organs can be calculated easily. Thus, NMR application provides detailed insight into the organisation of embryonal and fetal specimens and the prenatal development of dolphins without altering or damaging these rare museum specimens.

Imaging of heart development in embryos with magnetic resonance microscopy at 7 (300 MHz) and 17.6 Tesla (750 MHZ)

Bianca. Hogers[1], Dieter Gross[2], Volker Lehmann[2], Huub J.M. de Groot[3], Kees Erkelens[3], Adriana C. Gittenberger-de Groot[1], Robert E. Poelmann[1]

[1] Department of Anatomy and Embryology, Leiden University Medical Center, Leiden, The Netherlands. [2] Brüker Analytische Messtechnik GmbH, Rheinstetten, Germany.[3]Leiden Institute of Chemistry, Leiden University, Leiden, The Netherlands.

Introduction: Although light and electron microscopy offer a high resolution necessary for studying embryonic development, there are certain drawbacks to these methods. Conventional microscopy is deleterious to the embryo, is subjected to fixation (artefacts), while (rare) specimens cannot be used for other studies and often requires a final reconstruction of 2D images into a 3D image. Magnetic resonance microscopy (MRM) makes it possible to study nondestructively embryos with an useful resolution and it has all signs of becoming the ultimate method to study longitudinally processes in time in one embryo *in vivo*.

Methods: We imaged both fixed embryos (chick, stage 15-37) of which the vasculature was contrast-enhanced with gadolinium and living mouse embryos (13-17 ED) at 7 Tesla (300MHz). Moreover, we explored the use of an ultra high magnetic field (17.6 Tesla, 750MHz) for MRM, to increase image quality per image acquisition time. Therefore, the stage 29 fixed chicken embryo was also images at 750 MHz, using the same parameters.

Results: For the fixed embryos we reached a resolution of 30μm and were able to discern the heart, pharyngeal arch arteries, dorsal aorta and the larger veins, from stage 15 onwards. For the in vivo measurements an isoflurane anesthetized pregnant mouse was mounted in a probe with an ID of 38 mm and connected to an ECG and respiration device. Body temperature was kept constant by tubes filled with circulating warm water. The multislice RARE method resulted in very detailed images of the placenta with the umbilical vessels, the head of the embryo with brain vesicles, heart, liver, arms, legs, spine, ribs and even the dorsal aorta and the carotid artery. In addition, we succeeded in demonstrating blood flow (without contrast agent) in a 13 day mouse embryo *in utero*. To this arm, we selected one slice from the RARE and subjected this region to very fast gradient echo. With postprocessing this image was colored and superimposed on the RARE image, revealing blood flow through the heart and the dorsal aorta of the embryo, through the umbilicus and the uterine arteries.

We show that at 750 MHz frequency an image with approximately three times better SNR can be obtained by T_1 weighting using a standard gadolinium contrast agent, compared to the same measurement at 300 MHz. The image contrast was improved by around 20 percent and the contrast to noise ratio by almost a factor of 3.5. Smaller bloodvessels of the vascular system are identified at the high field, which indicates a better image resolution.

Conclusions: Although at the limit of desirable resolution, MRM is applicable for in-vivo imaging of mice embryos. Moreover, imaging at 17.6 Tesla is beneficial for MRM and opens new areas for functional imaging research, in particular when SNR, resolution and contrast are limited by acquisition time.

NMR microscopic Imaging of the Honey-Bee Brain

D. Haddad, F. Schaupp, G. Manz*, R. Brandt*, R. Menzel*, A. Haase
Physikalisches Institut EP5, Universität Würzburg, Germany
*Institut für Neurobiologie, Freie Universität Berlin, Germany

INTRODUCTION:

Using 3D NMR microscopy, we were able to visualize the anatomy of the honey-bee brain in its natural shape. Since NMR microscopy allows to obtain anatomical images of the brain still surrounded by the intact cuticle, deformations introduced by dissecting the brain out of the head capsule could be avoided, thus revealing the brain's true *in-vivo* shape. Ensured by the high spatial resolution of the NMR images, detailed visualization of the different brain compartments was possible. Because of its fast and effective learning abilities, the honey-bee brain constitutes a very important model in neurobiology used to understand the neural processing, learning strategies and establishment of a stable memory.

MATERIALS AND METHODS:

The heads of honey-bee workers were fixated and evacuated after cutting them from the thoraxes. In order to fit the heads in the NMR tubes, the mandibles were removed. The NMR tubes were filled with iso-osmotic sucrose solution. A temperature of 5°C was maintained during the whole examination time. For the NMR experiments a specially designed NMR probehead with a solenoid coil (length: 5.5mm, inner diameter: 4mm) was used. The measurements were performed at 11.75 T on a Bruker AMX500 spectrometer with a maximum gradient strength of 0.66 T/m. Two- and three-dimensional spin echo images (matrices: 256x256, 256x256x15 and 256x256x30) were acquired with resolutions of $15.6 \times 15.6 \mu m^2$, $100 \mu m$ slice thickness, $15.6 \times 15.6 \times 60.0 \mu m^3$ and $15.6 \times 15.6 \times 30.0 \mu m^3$. TR 1.0-1.5s and TE 8.2-25.0ms. During data processing zero-filling by a factor of 2 was applied in each dimension. The Amira Graphics Software Package was used for the visualization and segmentation of the 3D datasets.

Figure 1: *Axial slice through a 3D data set of the honey-bee brain with a resolution of $15.6 \times 15.6 \times 30.0 \mu m^3$ with the following anatomical structures: 1) lateral ocellus, 2) median ocellar tract, 3) median calyx, 4) lateral calyx, 5) pedunculus and beta-lobe, 6) lobula 7) medulla*

RESULTS:

The very detailed anatomy of the honey-bee brain is revealed in the NMR images. The achieved resolution was sufficient to visualize substructures like the mushroom bodies consisting of the paired calyces, the peduncle and the *beta*-lobes, the ocelli and the optical lobes with the medulla and the lobula (see Figure 1). Other parts like the *alpha*-lobes and the antennal lobes appear in slices of different depth. Furthermore, structures like the compound eyes and supporting and protecting chitin plates are also clearly resolved. The different substructures of the bee brain were segmented manually and reconstructed to polygonal surface models. Figure 2 shows the reconstruction together with a volume rendering of the 3D dataset.

Figure 2: *Volume rendering of a 3D NMR dataset of the honey-bee brain together with a surface reconstruction of manually segmented brain structures.*

DISCUSSION AND CONCLUSION:

To our knowledge, the 3D structure of the honey-bee brain in its natural shape has been studied here for the first time. Since the head capsule surrounding the brain was still intact, the brain was still stretched between its attachment points. In this study, due to the high resolution used, we were able to obtain precise information not only about the shapes and volumes of the different parts composing the honey-bee brain, but also about their relative orientations and angles towards each other and towards the surrounding cuticle. A so called 'standard bee brain' model can be established using fully segmented 3D NMR datasets in combination with other 3D visualization techniques, e.g. confocal microscopy. This model will help to standardize data of a large number of honey-bees and different acquisition methods and will also help to facilitate the understanding of the honey-bee's learning strategies, neural processing and establishment of a stable memory.

References: Rybak J., et al., The Journal of Comparative Neurology,334, 444-465 (1993)

Application of NMR Microimaging to the Study of Water Transport in Developing Rice Caryopses

A.K. Horigane[1], W.M.H.G. Engelaar[2], S. Maruyama[2], A. Okubo[3], T. Nagata[1] and **M. Yoshida**[1]

[1] National Food Research Institute, Tsukuba, 305-8642, Japan.
[2] National Institute of Crop Science, National Agricultural Research Organization, Tsukuba, 305-8666, Japan.
[3] Department of Applied Biological Chemistry, Graduate School of Agricultural and Life Sciences, The University of Tokyo, Tokyo, 113-8657, Japan.

Introduction: The obstruction of assimilates transport during rice grain development causes imperfections in the morphological structure of the endosperm, which can affect the quality of cooked rice grain. Morphological structure and moisture distribution during development of rice caryopses were observed by nuclear magnetic resonance (NMR) microimaging, and moisture distribution patterns are discussed in relation to the morphological development and route of water or assimilates transport.

Methods: Rice plants (*Oryza sativa* L. cv. *Koshihikari*) were grown outdoors in pots, and spikelets were sampled at various times after anthesis. A spikelet from each sample was fixed on an acrylic sample holder, wrapped with polyvinylidene chloride film to prevent moisture loss, and inserted in a NMR tube (5 or 10 mm outer diameter). NMR microimaging was performed on a NMR spectrometer with a 7.1 Tesla magnet (Bruker DRX300WB). For the acquisition and processing of NMR data the ParaVision and Xwin-NMR programs were used. Three-dimensional (3D) images were produced by a 3D-spin echo pulse program.

Results and Discussion: Maximum intensity projection (MIP) images clearly showed the growth of the ovary without disturbance by the lemma or palea since the signal intensity of the hull (lemma and palea) was always lower than that of the caryopsis. As the caryopsis developed, its moisture content decreased resulting in lower signal intensities in MIP images from older caryopses compared to those from younger caryopses. A striped pattern of water was observed on the surface of the endosperm in the MIP images of the spikelets 10-25 days after anthesis. This finding supports a hypothesis that water flows from the pericarp vascular bundle onto the nucellus covering the surface of the endosperm, and these are the first 3D images of water flowing out of the vascular bundle. In the longitudinal images, young tissues, especially of the embryo, the pericarp vascular bundle, and the endosperm, were clearly observed up to 25 days after anthesis. The decrease in the signal intensity in the endosperm during the development of the caryopsis illustrated change in the physical property of the starch storage tissue from fluid to doughy. Water observed in a relatively narrow zone in the center of the caryopsis 25 days after anthesis was considered to indicate a route for water and assimilates supply or drain for the embryo. The fact that this band of water touched the corner of the embryo strengthened the above assumption. Future work should focus on elucidation of the direction of the water flow and function of this water route in the endosperm in the infiltration of water and hollow formation in rice grain during cooking[1,2].

References:
1) Horigane A. K. et al. J. Food Sci. 64, 1-5 (1999).
2) Horigane A. K. et al. J. Food Sci. 65, 408-412 (2000).

Water Uptake in Malting Barley – Environmental and Genotypic Variations

Sheila M. Glidewell[1], J. Stuart Swanston[1] & Jose-Luis Molina-Cano[2]

[1] Scottish Crop Research Institute, Invergowrie, Dundee, DD2 5DA,UK
[2] Universitat de Lleida-Institut de Recerca i Tecnologia Agroalimentàries, Av. Rovira Roure 177, 25196 Lleida, Spain

Introduction

Water uptake during steeping is the initial step in the malting of barley for beer and whisky production. It is a process that occurs in two overlapping phases, i.e. uptake of water by the outer grain layers and internal redistribution. Although the relative rates of each phase may be modified by steeping regimes, there are also genetic differences, so gross water uptake measurements can give misleading predictions of the extent of hydration across the endosperm. There are also environmental effects on hydration, with high nitrogen levels generally associated with reduced water uptake. However, barley grown under Mediterranean conditions has been shown to hydrate more readily than grain from Northern Europe, despite higher nitrogen and it was suggested that composition and deposition of protein may be more important than actual quantity. NMR imaging was therefore employed to consider differences in the water distribution during steeping of two barleys grown in both Spain and Scotland.

Materials and Methods

Grains of *cv* Triumph, an existing malting cultivar and TL43, a Triumph mutant selected for reduced dormancy were grown in northern Spain and eastern Scotland.. The spatial distribution of water uptake during steeping was studied by NMR imaging of the grains *in situ*. 2D spin echo images of longitudinal slices using an unweighted sequence (TE 10 ms, TR 2000ms) and 3D spin echo images with TE 6.56ms, TR 200ms were acquired at hourly intervals. Grain was also steeped in a laboratory micro-malting apparatus and the percentage moisture content of the grain was determined after each wet phase. Endosperm ultrastructure was visualised by SEM cryosections of dry grains. Grain nitrogen was determined by the Kjeldahl method and storage protein (hordein) proportions, semi-quantitatively by HPLC.

Results

Time-lapse animations of the 2D images showed that the initial swelling of the embryo was followed by the ingress of water into the endosperm principally from the scutellum towards the distal end of the grain with slower ingress from the ventral crease. The 3D images with shorter TE gave higher S/N in the short T_2 region of the dry endosperm and concomitant images of different slices showed water ingress along the ventral crease. Differences in both rate of water uptake and its distribution in the endosperm were apparent between the cultivars and their growth sites. Gross water uptake determined by changes in grain weight (micro-malting) during the first 8 hours under water, showed Spanish-grown grain of both genotypes to take up slightly more water than Scottish-grown. The SEM showed TL43 to have a more compacted grain structure than Triumph, with higher protein levels in the central endosperm. Storage protein levels were thus higher in TL43, especially in Spain, but the proportion of sulfur-rich B-hordein was higher in Triumph and located predominantly in the sub-aleurone region

Discussion

These data show that water distribution during the early stages of steeping may not relate to the total quantity of water entering the grain. The more rapid movement of water from the scutellar region in TL43, when grown in Scotland, may well relate to differences in grain nitrogen. Comparison of endosperm structure by SEM suggested that Triumph should modify more readily than TL43, but the high levels of B-hordein in the sub-aleurone may constitute a significant barrier to water movement during the initial stages of steeping.

References

Chandra,G.S. *et al., J. Sci. Food Agric.*, **79**,37-46, 1999
McEntyre, E. *et al., Cereal Chem* **75**, 792-795, 1998
Molina-Cano, J-L. *et al., J. Inst. Brew.*, **101**, 79-83, 1995
Yin *et al., Tech. Quart. Master Brewers Ass. Amer.* **33**, 236-240, 1996

Water content in Cucurbita and Petunia pollen during pollen life studied by MR Microscopy and T2 measurements

H. VAN AS[1], M. NEPI[2], T. SCHEENEN[1], F.J. VERGELDT[1], K. KEIJZER[3] AND E. PACINI[2].

1 Laboratory of Molecular Physics (Biophysics) and Wageningen NMR Centre, Wageningen University, 2 Department of Environmental Sciences, Botany Section, University of Siena, Siena, Italy, and 3 Laboratory of Plant Cytology and Morphology, Wageningen University, Wageningen, The Netherlands.

Pollen grains in intact flowers are situated in the anthers, which are filled with water before opening and pollen release. Two types of pollen grains can be recognised on the basis of water content: partially dehydrated and slightly dehydrated pollen grains. Partially dehydrated pollen grains are the more common, the water content ranging between 5 and 30 % of pollen fresh weight at the moment of anther opening. Slightly dehydrated pollen grains have a higher water content (30-50 %) and generally they survive for only a few hours. Here we report on the application of 3D MR microscopy and T2 relaxation time measurements to characterise the water status in the anthers, pollen and filament during the process of anther opening and pollen release.

Petunia hybrida (water content 10 %) and *Cucurbita pepo* (water content 43%) were chosen as representatives of the two different types of pollen. Both viability and water content remained much higher in Cucurbita pollen retained inside the flower, being 40 % and 58% respectively even 28 hours after anther opening. A role of anther filament and starch in the region of the filament close to the anthers in maintaining the pollen hydration state could clearly be demonstrated by 3D MR microscopy (0.7 T; resolution in the order of 60*60*200 μm) and T2 images of intact mature anther and filament systems, before, during the process of anther opening and after opening.

Pollen of the two species, collected at the moment of anther opening, was exposed to a relative humidity controlled air flow (30 and 75 %). 1H NMR combined FID-T2 measurements at 0.7 T was used to characterise the status of water by measuring the same pollen population during the exposure period. Both CONTIN and e-fit analysis was applied on the decay-curves. Because of the large spread in relaxation times (several μs up to 100 ms) the initial FID and first 16 echoes were acquired at high sampling rate and hardly no filtering, whereas the long echo train was acquired with much higher SNR. Both parts of the decay were analysed separately, because combined analysis under estimated the initial (fast) decay in the FID. To localise the water site inside the pollen grains they were observed with a high resolution cryo-SEM.

Cucurbita pepo pollen lost water quickly both at 30 and 75 % RH. The viability remained high until a water content of 15% was reached after which it decreased dramatically. A number of different water protons relaxation times (T2) were obtained, the main fractions had a T2 of 0.009, 0.3 and 6.5 ms. The latter had the higher amplitude in fresh pollen but it decreased constantly during the dehydration and it was comparable to the amplitude of the shorter component at 10-15 % water content. At this stage cytoplasmic water was no more detectable with the cryo-SEM. Petunia hybrida pollen lost a small quantity of water at 30 % RH but it re-hydrated at 75 %, the viability remained always high. Three main T2 components related to water protons: 0.006, 0.1 and 10 ms. These components showed great changes during the re-hydration process. The amplitudes of these fractions increased strongly during the first 120 minutes and then stabilised. The T2 values of the 0.006, 0.1 and 10 ms fractions changed at the same time to 0.009, 0.3 and 4 ms, respectively, comparable to those observed in Cucurbita pollen. It was concluded that at low water content (below 15 %) Petunia pollen remain viable because water was in a glassy state (water with T2 of 0.006 and 0.1 ms), which was not observed in Cucurbita pollen.

Functional Imaging of Intact Plant-Roots with Multi Spinecho Methods

Ilja Kaufmann, Lars Wegner, Ulrich Zimmermann, Axel Haase
Physikalisches Institut Universität Würzburg, Germany

Introduction

NMR-microscopy provides a wide field of methods that can also be applied to plant-research. Because of non-invasivity there is no need for direct contact to the sample. So NMR-methods can "easily" be applied to samples that are difficult to access, like plant roots, which are used to be beneath the earth or within a nutrient solution.

Methods

All experiments were performed at a vertical Bruker 11.75T AMX500 spectrometer with a homebuilt probehead comprising a climate chamber. We designed a special root-NMR-glas-tube (fig. 1). To optimize SNR a Helmholtz coil as RF-resonator was placed close to the root. To achieve this, the examination area of the tube is narrowed to D=5.0mm. A big cup shaped reservoir at the tubes top prevents the examination area from running dry and changing the coils filling factor and thus its match during the experiment.

Because of the inhomogenity of the roots (most are aerated), flaws in magnetic susceptibility and therefore very short T_2^*, only spinecho imaging sequences could be used properly. To achieve a high time resolution for functional studies, we used Turbo Spinecho Methods (TSE) [1] for high resolution microscopy (9min for a TSE-microscopy with 256*256points and a 4 echo train), and combined with saturation recovery [2] for T_1 maps. (8.5min for 128*128 points with an 8 echo train, T_E=9ms). T_2 maps were recorded with a Carr-Purcell spinecho sequence [3] that was improved by a phase cycle for the echo train pulses, to reduce additional signal from stimulated echos (15min for 128*128 points, T_E=26ms, T_R=1.6s, 8 T_2 weighted images).

Results

A TSE of the root of a 2 week old *Zea mays* plant (with nutriant solution supply capillary) is shown in Fig. 2. Daily T_1 and T_2 maps, while a root was growing into the tube, gave first information about the order of the values for different root tissues during their developement. To examine the dehydration of a root, a T_1 map sequence was recorded over half a day, with a dry tube. Fig 3a and 3b shows the root area of the T_1 and spindensity map at the beginning of this experiment (root still wet). The experiment was repeated once with and once without illumination of the plant. A diagram of the averaged T_1 value and spin-density for each radial value within the root shows the variation for different root tissues and the shrinkage of the root, fig. 4.

Discussion and Conclusions

We could show for the first time, that it is possible to apply functional NMR-imaging methods to intact plant roots which may help to learn about water management in root systems. The TSE is suitable for proton imaging of maize roots, and its spatial resolution is sufficient to resolve different types of tissues within the root. E.g. xylem and endodermis can be clearly identified in Fig. 2. The daily T_1 -maps show, that it takes about two days for the different tissues to differenciate completely (not displayed here). In Fig. 4 it is obvious, that the illuminated plant needs more water, that has to be taken out of the root tissue due to the dry tube. Most of the water seems to come out of the cortex (r in between 0.25mm and 0.4mm). In the observed plant without illumination, a decrease in spindensity could be observed at r=0.2mm which is the area (or little inside) of the endodermis.

[1] Hennig J, Nauerth A, Friedburg H, Magn Reson Med, 3:823-833, 1986
[2] Evelhoch JL, Ackerman JJH, J Magn Reson, 53 (1):52-64, 1983
[3] Carr H. Y., Purcell E. M., Phys. Rev. 94, 630 (1954)

Fig. 1: NMR-Root examination tube

HF coil

Fig. 2: Root of *Zea mays*
TSE with 4-echo-train,
slicethickness=0.5mm
256*256 points
duration=9min
FOV=5mm
T_R=513ms
T_E=9ms

Fig. 3a: T1 in s
4.0
3.0
2.0
1.0
0.0
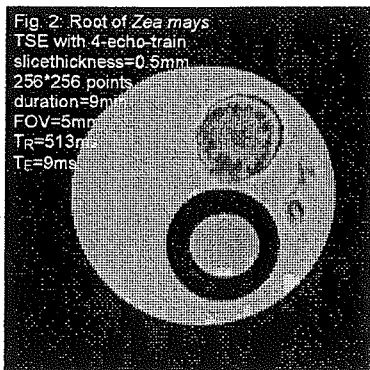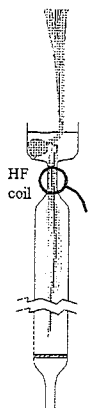
Fig. 3b: Spindensity map cutting
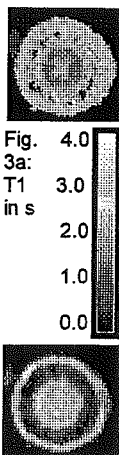
Fig. 4: dehydration with (right) and without (left) light.

T1 in Maize root
Spindensity in Maize root
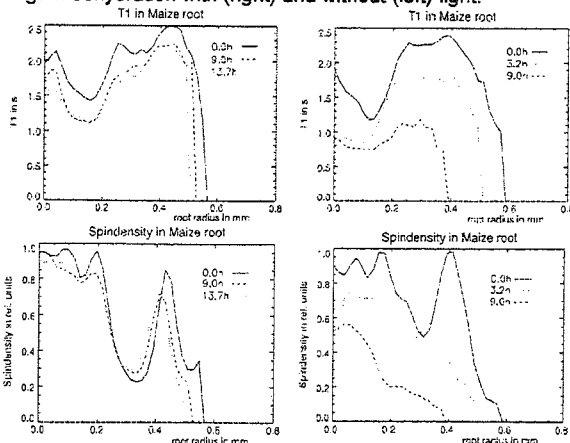
Some like it hot – Visualization of Combustion Processes and Combustion Products in Model Plant Materials

David Axelson[1], Bryce MacMillan[2], Bruce J. Balcom[2]

[1] MR_Consulting, Kingston Ontario, [2] MRI Centre, Department of Physics, P.O. Box 4400, University of New Brunswick, Fredericton, New Brunswick, Canada E3B 5A3

The ability to make non-invasive, real time, dynamic measurements to characterize combustion has been demonstrated with the implementation of new ^{1}H (proton) magnetic resonance imaging (MRI) protocols in model plant materials (SPRITE, half k-space SPRITE). Qualitative and quantitative analyses as a function of burn time (smoldering, driven combustion), spatial position, resolution, acquisition time and sample design/composition have been investigated. Combined with the use of multivariate data analysis and signal-to-noise enhancing post-processing filters, it is possible to generate information under realistic conditions not readily attainable by other methods.

Water Diffusion and Cell Swelling in Diffusion Weighted Imaging: The Erythrocyte Ghost Model

Peter E Thelwall & Stephen J Blackband

McKnight Brain Institute, Univeristy of Florida, Gainesville, Florida, USA

Introduction

Biological tissues are multicompartmental and heterogeneous. A change in the MR properties of a tissue component can indicate a pathology *in vivo*, ischemia in the brain results in a rapid decrease in the ADC of tissue water (1). This change is most commonly attributed to cell swelling increasing the fraction of water with low ADC, yet an understanding of the effects of tissue structure and microstructure on water diffusion remains elusive. Our previous studies of water diffusion involved perfused rat hippocampal slices subjected to physiological insult. Biexponential analysis of water diffusion was used to follow cell volume change (2,3).

We have developed a model tissue composed of erythrocyte ghosts to study the effects of compartmentalisation on water diffusion. The cell density, cell size and membrane permeability to water can be modulated. The constituents (and therefore biophysical properties) of both the intracellular and extracellular compartments can be controlled. Additionally, MR visible marker molecules can be localised to these compartments for measurement of extracellular tortuosity and intracellular restriction.

Methods

Erythrocyte ghosts were prepared from human blood by a hypotonic gel filtration method (4) and resealed by restoration of isotonicity. The resultant saline filled ghosts were suspended in iso-, hypo- or hypertonic pH buffered solutions to effect cell swelling and shrinkage. MR data were acquired from erythrocyte ghost suspensions using a 5 mm imaging probe interfaced to a Bruker 750-MHz widebore instrument and console. A pulsed gradient spin-echo (pgse) sequence was used to obtain the data; gradient strengths of up to 1480 mT/m were employed to produce b-values up to 7000 s/mm^2 over a 7ms diffusion time.

Results and Discussion

We have observed non-monoexponential water diffusion in the model tissue. To aid in a preliminary interpretation, data were fitted to a biexponential function. Ghost samples under hypotonic conditions show elevated signal at high b-values, as expected for an increase in intracellular volume. Biexponential analysis demonstrated a decrease in f_1, D_1 and D_2 on cell swelling. The trends are consistent with the changes in water diffusion observed in rat brain *in vivo* on ischemic insult (1). Although the erythrocyte ghost model differs from brain tissue - simplistic structure, smaller cell size, higher membrane permeability to water - the data presented here show changes in the diffusion profile on cell swelling analogous to the effects of cell swelling observed *in vivo* (1). Non-monoexponential water diffusion was recently observed in human brain (5) (albeit at long diffusion times, allowing for water exchange between compartments). Our goal is to understand the biophysical mechanisms that determine MR signal contrast in *in vivo* models and in the clinic, increasing the quantitative potential of such data.

Conclusions

We analysed water diffusion in a biological tissue model composed of erythocyte ghosts. The biophysical parameters of the model are easily controlled. We demonstrated non-monoexponential water diffusion from the samples. Biexponential fits indicated an increase in the fraction of slow diffusing water on cell swelling, as observed in the brain following ischemic insult. Current work focuses on comparing experimental data with mathematical models of water diffusion based on the biophysical parameters of the experimental model, such as those developed by Stanisz *et al.* (6).

(1) Niendorf *et al*, Magn Reson Med 36:847-857 (1996)
(2) Blackband *et al*, Magn Reson Med 38:1012-1015 (1997)
(3) Buckley *et al*, Magn Reson Med 41:137-142 (1999)
(4) Wood, Methods in Enzymology 173:346-355 (1989)
(5) Mulkern *et al*, Magn Reson Med 44:292-300 (2000)
(6) Li *et al*, Magn Reson Med 40:79-88 (1998)

Diffusion During the Development of Isolated *Xenopus* Oocytes

S.C. Grant[1], L.E. Carlson[2] and R.L. Magin[2]

UF McKnight Brain Institute[1], University of Florida, Gainesville, FL, U.S.A.

Department of Bioengineering[2], University of Illinois, Chicago, IL, U.S.A.

Introduction

The oocytes of the African clawed frog *Xenopus laevis* have been investigated previously though spectroscopy [1] and microscopy [2] as a single cell model for NMR analysis. Furthermore, multi-exponential diffusion has been observed in tissues [3,4] and single neurons [5], providing evidence of water compartmentation at even the subcellular level. In this study, the mechanism of water diffusion is examined throughout the stages of unfertilized development through the use of MR microscopy and localized spectroscopy to determine changes in water distribution during the oocyte growth cycle.

Methods

Following isolation, 15 oocytes were separated into three, five-member groups of Early (stages I and II; 100-450-micron diameter), Middle (stages III and IV; 450-1000-micron diameter) and Late (stages V and VI; 1000-1300-micron diameter) development (7). These cells were analyzed individually using appropriately-sized, susceptibility-matched RF microcoils at 11.75 T. Following scout images, 10 ^{1}H images with b values of up to 11,600 s/mm^2 were acquired at 21 ± 0.6 C in under 3 hours using a diffusion-weighted spin echo sequence. A 200-micron slice centered on the nucleus provided accurate localization with an in-plane resolution of at least 40x40 microns for all experiments. Regions within the cytoplasm and nucleus were segmented by hand, with the mean intensities fit to a bi-exponential function using a Levenberg-Marquardt non-linear algorithm. In addition to diffusion-weighted imaging, localized ^{1}H STEAM spectra were acquired from intracellular regions of Late oocytes with b values of up to 34,000 s/mm^2. These spectra were used to examine the Apparent Diffusion Coefficients (ADCs) of the major metabolic constituents (lipid and water) from subcellular voxels as a means of investigating the origins of imaging-based non-monoexponential diffusion in this single cell model.

Results

Diffusion analysis of the nuclear region yielded a constant and primarily mono-exponential ADC [mean $\pm$ SD (volume fractions $\pm$ SD)] of 2.17 ± 0.14 x 10^{-3} mm^2/s for all developmental groups. The cytoplasm yielded coefficients of 2.04 ± 0.31 ($87.6 \pm 8.0\%$) and 1.36 ± 0.10 ($83.3 \pm 3.5\%$) x 10^{-3} mm^2/s for the ADCs of the fast diffusing component and 0.57 ± 0.32 ($12.4 \pm 8.0\%$) and 0.025 ± 0.011 ($16.7 \pm 3.5\%$) x 10^{-3} mm^2/s for the ADCs of the slow diffusing component of the Early and Middle groups, respectively. The Late group, in which hemispheric differentiation is apparent in the cytoplasm, yielded 1.36 ± 0.78 ($32.7 \pm 16.0\%$) and 1.25 ± 0.06 ($85.2 \pm 3.5\%$) x 10^{-3} mm^2/s for the fast ADC and 0.14 ± 0.2 ($69.3 \pm 17\%$) and 0.024 ± 0.016 ($14.8 \pm 3.5\%$) x 10^{-3} mm^2/s for the slow ADC of the vegetal and animal poles, respectively.

Conclusions

Diffusion analysis of the oocyte nuclei displays constant values and a predominately mono-exponential decay, regardless of the developmental stage and in agreement with previous single cell studies (5,6). Because of the minimal large-scale structural development of the nucleus during the growth cycle of these unfertilized cells, this finding is consistent with the physiology of *Xenopus* oocyte (7). The increasingly non-monoexponetial nature of diffusion in the cytoplasm shows evidence of significant compartmentation that becomes more prominent with the development of organelles, cytoskeletal structures and hemispheric differentiation. In addition, studies involving the acquisition of diffusion-weighted localized STEAM spectra demonstrate that non-monoexponetial diffusion in Late developmental oocytes is partly, though not entirely, attributable to the vastly different ADCs of cytoplasmic metabolites.

[1] Posse and Aue, J. Magn. Reson. 83: 620-5 (1989).
[2] Pauser *et al.*, Magn. Reson. Imag. 13: 269-76 (1995).
[3] Buckley *et al.*, Magn. Reson. Med. 41:137 (1999).
[4] Bui *et al.*, Neurosci. 93:487 (1999).
[5] Grant, *et al.*, 41st ENC. 197 (2000).
[6] Schoeniger, *et al.*, J. Magn. Reson. 103(B):261-73 (1994).
[7] Dumont, J. Morph., 136:153-64 (1972).

Moisture Distribution in Raw and Cooked Potato Slices via MRI

Jeffrey H. Walton
Nuclear Magnetic Resonance
Facility
University of California
Davis, CA 95616 USA

Michael J. McCarthy
Department of Food Science and
Technology
University of California
Davis, CA 95616 USA

Petr Dejmek
Department of Food Engineering
Lund University
Box 124, 221 00 Lund Sweden

Introduction
Frying is a common method used in cooking foods with the potato being the most commonly fried food. During the frying process, potato looses moisture in a non-uniform manner with greater moisture from the outer regions and less moisture loss from the inner regions. Simultaneous with the moisture loss is the development of a crust with pores and uptake of oil into the potato. Quantification of the rates of moisture loss, oil uptake, and structure development are needed to improve current mathematical models of the frying process.

Methods
Raw russet potatoes (Idaho, USA) were obtained from a local market. The raw potato was sliced to nominally 2 mm thickness. The length and width were a minimum of 15 times the thickness. Proton images were acquired on a 7T Bruker Biospec imaging system using a multislice, spin echo protocol. Image slices were 0.5 mm thick. Raw potato slices were fried under standard conditions using vegetable oil.

Results and Discussion
The proton MR images shown were taken prior to (left) and after (right) frying. Under these conditions, the image intensity is from the water protons in the potato. The moisture distribution in the raw potato shows significant variation as primarily due to the structure of the potato. This variation is seen to persist in the center higher moisture region of the partially cooked potato. The initial average moisture content of the potato is 78% wet basis. Of particular interest to food scientists are the changes that occur in the internal potato moisture distribution and the development of the crust structure. From the image of the partially fried potato, it is evident the moisture is high at the center of the slice and low at the edges.

Conclusion
Although there is significant moisture variation in the image of the cooked potato, there was no clear evidence of pore structure development in the images.
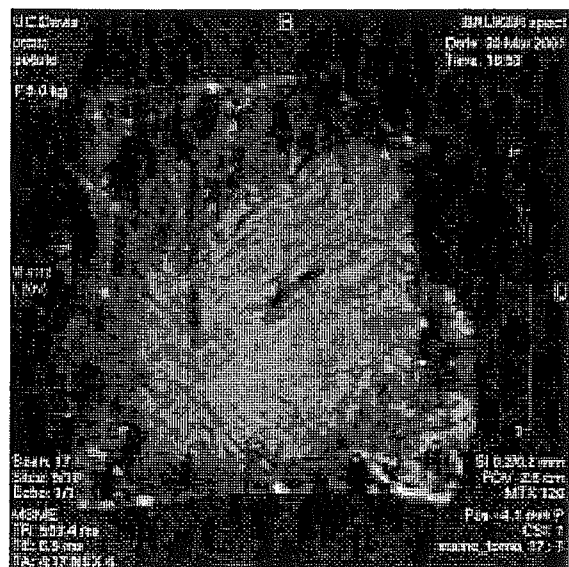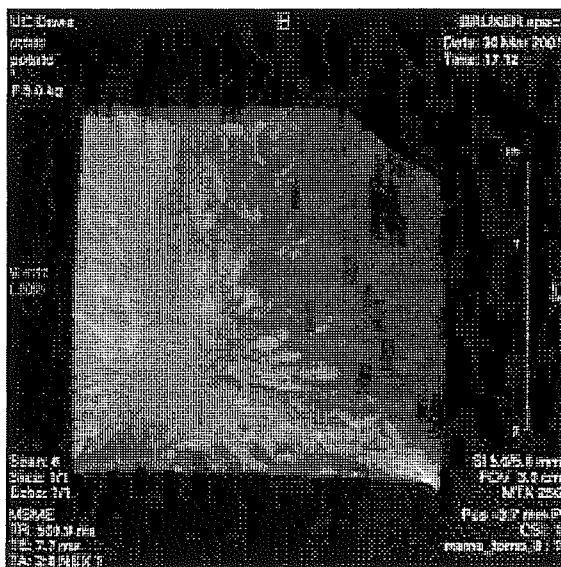
The Status of Water in Boiled Japanese Noodles Observed by NMR Microscopy: Comparison of Images Acquired with High and Low Magnetic Field MR Microscopes

Tokiko KOJIMA, Akemi K. HORIGANE(*), Mitsuru YOSHIDA(*), Yoshimasa MATSUDA(**),
Tomoyuki HAISHI(***), Katsumi KOSE(**), Akira NAGASAWA(****)
Saitama Industrial Technology Center-Northern Laboratory, Kumagaya, 360-0031 Japan
(*) National Food Research Institute, Tsukuba, 305-8642 Japan
(**) Institute of Applied Physics, University of Tsukuba, Tsukuba 300-2642 Japan
(***) MR Technology Inc. Tsukuba, 300-2642 Japan
(****) Department of Chemistry, Faculty of Science, Saitama University, Saitama, 338-8570 Japan

We have recently established the method for estimation of the moisture content from the correlation between the moisture content and water proton T_2 in standard wheat gel samples on a high field (7T) MR microscope (MRM) (Bruker DRX300WB). By using this method, the moisture distribution in a section of Japanese noodles after boiling was clearly observed through T_2 mapping (Fig.1). In the present study, we have tried the moisture distribution measurement on a compact MRM with a 1.0 T permanent magnet (installation space: less than 1 square meter) in order to make this method to be available in small laboratories or factories.

Figure 2 shows the relationship between the moisture content and water proton T_2 in wheat gel samples measured using DRX300WB, ARX400, and Compact MRM, of which proton resonance frequencies are 300, 400, and 43 MHz, respectively. The T_2 values were not dependent on the resonance frequency, but observed to be slightly varied with pulse sequences: the T_2 values measured with the CPMG sequences were about 1.2 times of those measured with the simple spin-echo sequences. This result shows that the moisture content can be also measured using the compact MRM. Figure 3 shows cross-sectional T_2 images of noodles prepared in the same procedure and acquired with two MRM systems: DRX300WB and the compact MRM. These images demonstrate that the compact MRM can be used for mapping of moisture content in Japanese noodles at the similar spatial resolution with the superconducting MRM
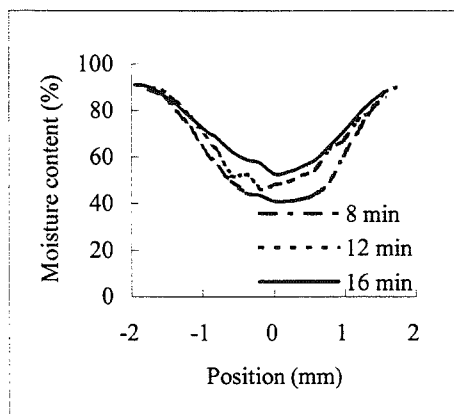
Fig.1 Moisture distribution in boiled Japanese noodles at different boiling time measured through T_2 using DRX300WB.
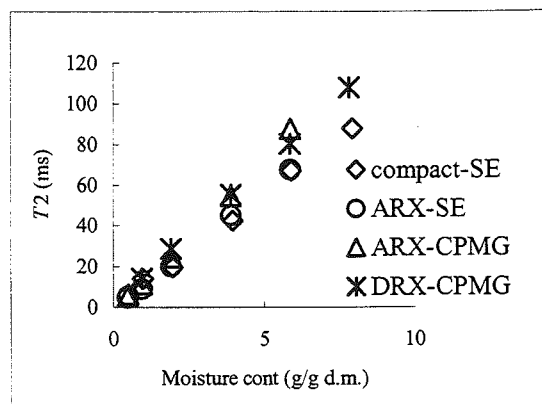
Fig.2 Relationship between the moisture content and T_2 values in wheat gel samples.
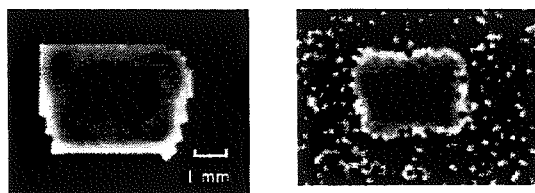
Fig.3 T_2 images of boiled noodles prepared in the same procedure. Left: DRX300WB (pixel size:195 microns square), Right: Compact MRM (pixel size: 200 microns square)

STUDIES OF MOISTURE CONTENT IN CEREALS
BY MAGNETIC RESONANCE MICRO-IMAGING

L. Foucat[1], C. Bonazzi[2], E. Triboi[3], J.P. Renou[1]

[1] SRV/STIM, INRA – Theix, 63122 St Genès Champanelle, France
[2] INRA ENSIA, 1 avenue des Olympiades, 91744 Massy Cedex, France
[3] Agronomie, INRA 63039 Clermont-Ferrand Cedex 2, France

Introduction

Moisture distribution was studied by magnetic resonance micro-imaging (MRI) during the maturation of wheat grain, and the drying process of rice grain. Although these two types of grain have initially similar moisture content (about 20% w/w), the bond state of water between them is very different (T_2 value is about 30 and 1 ms for wheat and rice grain, respectively). Hence, it is necessary to use two different MRI approaches to access the moisture distribution during the grain evolution. Classical Multi-Slice/Multi-Echo (MSME), and Constant–Time Imaging (CTI) were used for wheat and rice, respectively, in this study.

Materials and Methods

All NMR experiments were recorded on a Bruker AMX 400 spectrometer equipped with the micro-imaging accessory, and operating at a proton frequency of 400 MHz.

The moisture state in wheat grain was studied according to different temperature conditions during grain maturation. The MSME acquisition consisted of 8 transversal and 8 longitudinal images of 1 and 0.5 mm slice thickness and spatial resolution of 50 μm^2. The T_2 images were calculated from the acquisition of 20 echoes (first echo and inter-echo time of 6.6 ms), and water density images were derived.

The moisture profile kinetics of rice during drying was obtained using two-dimensional Constant–Time Imaging (CTI) techniques.[1] An internal RF shield (copper foil) was used to restrict excitation/detection to a central slice of 3 mm thick, which can be considered to have a cylindrical geometry. Acquisition time of each image was 14 min, in agreement with the drying kinetics, and had a planar resolution of 100 μm^2. Four drying experiments were performed at two different air temperatures (30 and 60°C).

Results and Discussion

Wheat grain maturation

Figure 1 illustrates the desiccation of a wheat grain with time expressed in total degrees per day. These images demonstrate that the MRI technique used is sensitive enough to resolve the different tissues within a single grain. For the moisture content of the whole grain, MRI results significantly correlated with conventional methods. The moisture content varied according to the tissue within the grain. Proton density images showed more pronounce desiccation in the endosperm layer.
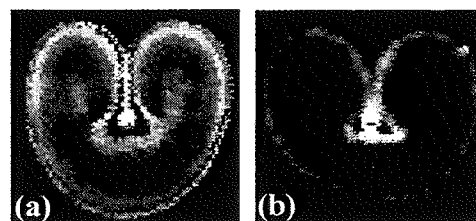
Figure 1: proton images density of a transverse slice of a wheat grain at (a) 340°day and (b) 650°day.

Rice grain drying

Figure 2 shows a rice grain at the beginning and after 30 h of drying at 30°C. Uni-dimensional water profiles from the short and the long axis of the elliptic section of the grain were extracted from the series of these images. A diffusive model was developed using a cylindrical geometry, taking into account the shrinkage during drying, in order to determine the diffusivity parameters associated with the different kinetics of drying processes studied.[2]
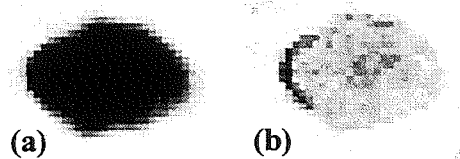
Figure 2: images of a rice grain from (a) the beginning to (b) the end of drying process at 30°C.

Conclusion

Two different MRI approaches were used to study distribution and mobility of water during maturation of wheat and kinetics of moisture profiles during drying of rice. For the latter, the choice of the CTI techniques was dictated by the short T_2 value of water protons. This work demonstrates that MRI is a well adapted technique to characterise water dynamics in cereals, even at low moisture content and low water mobility.

References

1. Gravina, S. and Cory, D.G., J. Magn. Reson., B 104, 53-61 (1994).
2. Frias, J.M., Foucat, L., Bimbenet, J.J., Bonazzi, C., Chem. Eng. J. (submitted).

Multidimensional q-space microscopy – correlations in diffusion and flow

Siegfried Stapf, Song-I Han, Christian Heine, and Bernhard Blümich

Lehrstuhl für Makromolekulare Chemie, ITMC, RWTH Aachen, Worringerweg 1, D-52056 Aachen, Germany

A powerful recent development of NMR pulsed-field gradient (PFG) experiments is found in the extension of conventional imaging or diffusion measurements toward a combination of position and displacement encoding modules within the same pulse sequence. Such sequences can be applied to the multiple encoding of position and velocity, as well as the measurement of space-dependent diffusivities or average velocities. The most general approach to follow transport processes, however, is to repeatedly interrogate particle positions at successive times by applying PFGs. Whether positional encoding is retained or replaced by displacement information depends on the choice of conditions imposed on the applied PFGs, thus reducing the degrees of freedom.

Possibly the most direct visualization of motion is obtained by a double-encoding of position, with a mixing time Δ being defined by the PFG separation. This so-called 2-D POsition eXchange SpectroscopY sequence (POXSY, [1]) can be employed to follow fluid motion through complex geometries which are within the limits of the NMR microscopy imaging resolution. If velocity changes are sufficiently slow, a similar information is obtained from combining position and velocity encoding in two successive steps, which leads to a map of the spatial dependence of velocity.

For many problems of diffusion and flow in structured media the localization of averaged motion properties is not sufficient and the determination of the temporal evolution of displacements is necessary in order to obtain a more complete understanding of the material transport processes. The method of choice can be regarded as multidimensional q space microscopy, where displacements instead of positions are encoded during different times within one single experiment and can then be related to each other in an appropriate coordinate system. The VElocity eXchange SpectroscopY experiment (VEXSY, [2]) is a 2D realization of this concept and allows the comparison of two velocities, or displacements, before and after a variable mixing time τ_m. In the three-pulse SERPENT sequence [3], a similar measure is found for interleaved intervals. As a particularly useful representation plots of the conditional probabilities have been suggested [4] which are accessible from the data of such two- or higher-dimensional experiments. With their help it is possible to discriminate between different subsets of spins based on the direction and magnitude of their initial or final displacements, and to clarify questions which could not be solved satisfactorily by analysing only the evolution of 1D propagator shapes as a function of time.

The potential of multi-dimensional NMR microscopy methods in k space, q space or combinations thereof is best demonstrated by discussing material transport in systems of increasing complexity. Poiseuille flow in cylindrical pipes is perfectly understood and can be treated analytically; the flow behaviour of Newtonian fluids was investigated by several of the above mentioned NMR methods and the agreement with theory is excellent. The cross-over towards turbulent flow conditions manifests itself in a sudden loss of correlation between displacements. Colloidal suspensions were used as model non-Newtonian fluids and were found to show strongly deviating flow properties both in the slow and the fast velocity regime.

The transport properties of fluids through porous matrices is of utmost interest for a wide range of engineering applications as well as for environmental sciences. Random packings of monodisperse spherical particles have been the systems of choice for the application of a variety of NMR methods. Although some statistical properties of dispersion processes within these arrays are now well understood, 2D q space microscopy was able to provide further insight into the details of the flow process and recently revealed information about heterogeneity, polydispersity and quasi-periodicity in such systems which are currently compared to numerical simulations. The expertise gained from the treatment of this relatively simple geometry can be invested into the understanding of flow processes in natural systems such as porous rocks.

As one further advantage of multi-dimensional q space microscopy its increased resolution as compared to imaging techniques can be stated. With appropriate gradient strengths being available, not only the degree of restrictions of fluids inside pores on the scale of micrometers can be measured, but also information about local anisotropy, pore shape and connectivities becomes available from combining two or more displacement encoding steps along different directions or in different times.

The development of time-saving 1D versions of the multiple q encoding techniques in order to routinely obtain correlation coefficients between arbitrary displacements demonstrates the potential of the described approach to investigate transport processes in complex systems.

1. S.Han, S.Stapf, and B.Blümich, J.Magn.Reson. **146**, 169 (2000).
2. P.T.Callaghan and B.Manz, J.Magn.Reson. A **106**, 260 (1994).
3. S.Stapf, R.A.Damion, and K.J.Packer, J.Magn.Reson. **137**, 316 (1999).
4. S.Stapf and B.Blümich, Magn.Reson. Imaging, *in press*

Sampling of q-space measurements for quantitative flow and diffusion studies in porous bio-systems

T.W.J. Scheenen, P.A. de Jager, F.J. Vergeldt and H. Van As
Laboratory of Biophysics and Wageningen NMR Centre,
Wageningen University, Dreijenlaan 3, 6703 HA, Wageningen, The Netherlands

In porous bio-systems (e.g. plants, bioreactors, soils) water can be stationary (only diffusion) or flowing at different velocities. For quantitative flow imaging under conditions of unknown flow profile diffusion and flow have to be discriminated and the full flow profile measured. A very powerful method for this purpose is q-space or displacement imaging. Fast q-space NMR microscopy has been demonstrated by Pulsed Field Gradients (PFG) for diffusion and flow encoding combined with a Turbo Spin Echo (TSE) pulse sequence (1). The unique feature in that PFG TSE sequence is the fact that phase-information, imposed by the PFGs, is recalled throughout the complete TSE train. A model-free analysis (2) of the displacement spectrum for every pixel results in images with the following parameters: the amount of stationary water, the amount of flowing water, the volume flow, the averaged linear flow velocity and the cross-sectional area of flow.

To discriminate between slowly flowing and diffusing water long observation times are needed. This can be measured by a stimulated echo (STE) version of the PFG TSE sequence (3). If linear flow velocities are high, short observation times can be used, for which the spin echo (SE) version of the sequence is more suited. However, at high flow velocities dynamic range problems in the shape of the displacement spectra can occur if truncation effects are not allowed (the signal of diffusing water has to be zero at the highest PFG step) and the number of PFG steps is limited (32 or 64). The consequence is that the higher velocities can exceed the higher edge of the displacement axis and displacement intensity emerges at negative displacements (wrap around). In unfortunate cases the displacement spectrum for flow can be stretched all over the displacement axis and is hard to discriminate from the base line. Quantification then will clearly result in an apparent velocity much lower than the actual value.
A solution for this dynamic range problem is an alternative way of sampling the signal as a function of PFG-steps: non-equidistant. If the smallest step is set at 1 a.u., this size has to be increased at larger PFG-values. Doing so, it is avoided to sample much more PFG steps (typically three a four times) in a linear way, increasing measurement time with the same factor. Before Fourier Transformation of the raw data into the displacement spectrum, the non-linear sampled data must be interpolated and can be filtered. If an equal amount of time is spent for the measurements, the SNR of the non-linear sampled q-space experiment is higher with respect to the linear sampled one, trading off with (high frequency) details in the displacement spectrum. This is not a serious problem since rapid, abrupt jumps or changes in these spectra are not to be expected.

Experimental results were obtained for flow studies in a cucumber plant under varying environmental conditions. Linear and non-linear q-space sampling resulted in comparable results at low evaporation conditions (night, lamps off) and were in good agreement with actual water uptake rates (linear velocities in the order of a few mm/s). However, under high evaporation conditions, linear q-space sampling resulted in systematically deviations from actual water uptake values, whereas non-linear sampled data were in good agreement with uptake rates (up to 20 mm/s). In this way air embolism and embolism repair in xylem vessels could reliably be studied even in single vessels.

1. Scheenen, T, de Jager, PA. van Dusschoten, D. and Van As, H. 2000. Microscopic displacement imaging with pulsed field gradient turbo spin-echo NMR. *J. Magn. Reson.* 142: 207-215.
2. Scheenen, TWJ. , de Jager, PA., van Dusschoten, D. and Van As, H. 2000. A model-free quantification of water transport in intact plants with NMR imaging. *J. Exp. Bot.* 51: 1751-1759.
3. Scheenen, TWJ. , Vergeldt, FJ., Windt, C., de Jager, PA. and Van As, H. 2001. Microscopic imaging of slow flow and diffusion: a pulsed field gradient stimulated echo sequence combined with turbo spin echo imaging. *J. Magn. Reson.* (accepted)

NMR imaging velocity profiles in the simulation of fluid dynamics in oil production

G. Maddinelli, F. Donaggio, N. Mancini and S. Correra
EniTecnologie S.p.A., via F. Maritano 26, 20097, S. Donato, Milan, Italy

NMR imaging technique can be usefully applied in solving complex engineering problems. One the most promising applications are certainly velocity measurements methods based on the superposition of pulsed field spin-echo (PGSE) and imaging experiments[1]. This type of technique is quite promising in applications to complex fluid dynamics studies[2], especially when multiphase flow is involved. In fact, engineering applications generally require several simulations assessment to better investigate line assembly of industrial plants. A better understanding of phenomena related to flow during oil production operations could be significantly beneficial for economics and efficiency of technology in this field. Improvements in the knowledge of multiphase flow are especially required, due to the complex behaviour of fluids near the well-head production. Moreover, multiphase systems can result from technologies applied to make heavy oil less viscous and therefore easily transportable, producing dispersions or emulsions[3]. MRI has great potential in discriminating oil/water mixtures even in optically opaque media (e.g. by chemical shift and relaxation differences) and also in measuring velocity profiles over a wide range of values without any kind of interference with the flowing system[4]. This feature associated with high spatial resolution makes MRI more attractive than other conventional techniques (e.g. laser Doppler methods). In this research project, we have assembled a flow loop line inside a 31 cm horizontal-bore magnet. Space was sufficient to place a 9 mm (I.D.) tubing with different geometrical features as straight and round lines inside. Flow was assured by a screw pump in a velocity range of 10-100 cm/sec. Preliminary studies were realised using a fluid constituted by a mixture of water/glycerine to ensure the appropriate parameters (e.g. viscosity and Reynolds number) to be well inside a laminar flow regime. Velocity profiles were measured in different points of the flow line and compared with data calculated from Computational Fluid Dynamics (CFD) methods. Also the introduction of simulated obstacles on the flow regime was investigated.

1. Callaghan P.T., Eccles C.D. and Xia Y. J. "NMR microscopy of dynamic displacements". Phys. Sci. Instrum. 21, 820-822, 1988;
2. Xia Y., Callaghan P.T., and Jeffrey K.R., "Imaging velocity profiles: flow through an abrupt contraction and expansion". AIChE Journal, 38, 9, 1408-1420, 1992;
3. F. Donaggio, N. Mancini G. Maddinelli, S. Correra "Fluent CFD Code Performance Evaluation in Describing Oil in Water Dispersions Flow" Proceeding of 3rd International Conference on Multiphase Flow, Pisa, April 99.
4. Newling, B., Hall L.D. et al., "Chemical Resolved NMR velocimetry". Chemical Engineering Science, 52, 13, 2059-2072, 1997.

Microscopic imaging of slow flow and diffusion: a pulsed field gradient stimulated echo sequence combined with turbo spin echo imaging

T.W.J. Scheenen, F.J.Vergeldt, **C.W. Windt**, P.A. de Jager and H. van As

Laboratory of Biophysics
Department of Agrotechnology and Food Sciences
Wageningen University and Research Centre
The Netherlands

Abstract

We present a pulse sequence that combines a displacement-encoded stimulated echo with rapid sampling of k-space by means of turbo spin echo imaging. The stimulated echo enables the use of long observation times between the two pulsed field gradients that sample q-space completely. Propagators, constructed with long observation times, can discriminate slowly flowing protons from diffusing protons, as shown in a phantom in which a plug flow with a linear velocity of 50 um/s could clearly be distinguished from stationary water.

As an example of a biological application the apparent diffusion constant in longitudinal direction of a transverse image of a maize plant stem was measured as a function of observation time. Increasing contrast in the apparent diffusion constant image with increasing observation times were caused by differences in plant tissue: although the plant stem did not take up any water, the vascular bundles, concentrated in the outer ring of the stem, could still be discerned because of their longer unrestricted diffusional pathways for water in the longitudinal direction compared to cells in the parenchymal tissue.

For a second example the movement of slow flowing water in a tomato pedicel was measured. After the pedicel of a green-mature tomato was excised from the plant a small water pressure gradient was applied, inducing a slow flow of water through the piece of stem tissue. In the xylem region of the pedicel flowing water could be distinguished from a large amount of stationary water. Linear flow velocities up to 0.67 mm/s were measured with an observation time of 180 ms, opening up the possibility of, for instance, measuring and quantifying *in vivo* water flow towards growing tomato fruit.

MR Imaging of wetting front dynamics: The effect of gravity

A. Caprihan[1], N.E. Daidzic[2], E. Fukushima[1], J.I.D. Alexander[2]

[1]New Mexico Resonance, 2301 Yale Boulevard, SE, Suite C-1, Albuquerque, NM 87106, U.S.A., www.nmr.org

[2]The National Center for Microgravity Research on Fluids and Combustion (NCMRfc) at NASA John H. Glenn Research Center, 21000 Brookpark Road, Mail Stop 110-3, Cleveland, OH 44135, U.S.A., www.ncmr.org, Email: Nihad.Daidzic@grc.nasa.gov

The ability to efficiently control water and nutrient supply in plant production systems in microgravity is necessary in long-duration manned missions. For such a long-duration missions (e.g. Mars), the re-supply of life support consumables is not a viable option, regeneration, reuses and autonomous production becomes essential. However, it has recently become evident that the macroscopic dynamic behavior of the temporal and spatial under-saturation levels in soils strongly depends on the physical behavior of the fluid at the microscopic level. The experience from previous space missions also has shown that one needs much deeper understanding of the flow of water, air and solute transport in an unsaturated porous soil media. Ultimately, the stability and break-up of liquid-bridges, -columns and -films, dynamic rearrangement of particles, contact angle dynamics, capillary fingering and entrapment of the non-wetting phase together with the complex geometry of porous media will determine the saturation levels on macroscopic (pore-size) scales. However, it is not yet clear how much some of these microscale fluid physics phenomena are gravity dependent. The purpose of this study is to examine some wetting front dynamics under simulated variable gravity conditions.

Terrestrial Magnetic Resonance Imaging (MRI) experiments were used to visualize studies of the moisture transport in thin porous sections. Such thin sections were positioned horizontally and vertically to simulate variable gravity conditions and the wetting front dynamics has been imaged. Experiments with various porous samples (Aquafoam-Oasis^{TM}, Zeoponics^{TM}, ZeoPro^{TM}, and Profile^{TM}) were performed in a 30 cm, 1.9T Oxford super-conducting magnet with a TECMAG Libra spectrometer (Tecmag, Inc., Houston, TX). Two different imaging strategies were used depending on whether the water in the foam sample was static or moving. Wet foam samples with stationary water distributions were imaged with the standard Fourier imaging method (*Callaghan, 1991*). 2D and 3D images were obtained with a resolution of 0.5 mm in each direction. This method acquires data from all parts of region of interest in the time domain. The data is then Fourier transformed, where each frequency corresponds to a different location in space. Because the Fourier method collects data from the full region of interest at each scan, artifacts can arise in the image if the water distribution in the sample changes during a scan. Therefore, time-resolved imaging to study water uptake dynamics of the foam was done by line-scan imaging technique (*Caprihan et al, 1997*). Unlike Fourier imaging, line scan techniques spatially scan the sample space, more in analogy with most other imaging techniques. Our line scan technique takes a one-dimensional (1D) projection image of a thin slice, i.e., a line, then shifts to a new position and takes another 1D image. Thus, a 2D image can be generated by sequentially sweeping the line over the object. The successive 1D images in the line-scan technique can be taken rapidly without regard to magnetization recovery limitations because the measurement will not be repeated in that slice until all the other slices are scanned. In other words, the time available for magnetization recovery for each line is the product of number of lines and the time between imaging successive lines. Our line was 2.5 mm thick and there were 256 points along it with a spatial resolution of 0.5 mm. The line was swept over 32 positions to make a 256x32 image every 1.8 s. The image was interpolated to give equal resolution in each direction. We did not resolve the third dimension of the 7.5mm thick foam sample in preliminary study.

The terrestrial MRI experiments in thin porous soil medium sections will facilitate and provide necessary information for the development of the new physical-mathematical models that will account for discontinuous phases, effects of (launch) vibrations, solitary ganglion dynamics, pore network behavior, fingering capillary instabilities, air entrapment, medium anisotropy and heterogeneity, and the hyperbolic nature of moisture transport. We are also looking into the possibility to perform MRI experiments in parabolic flights using NASA KC-135 zero gravity simulator.

1. P.T. Callaghan, Principles of Magnetic Resonance Microscopy (Clarendon, Oxford 1991).
2. A. Caprihan, E. Fukushima, A.D. Rosato, and M. Kos, Rev. Sci. Instrum. **68**, 4217 (1997).

Characterisation of Locally Anisotropic Structures Within Isotropic Porous Solids Using 2-D Pulsed Field Gradient NMR

R. G. Graham, W. M. Holmes, **C. De Panfilis**, K. J. Packer

School of Chemistry, University of Nottingham, Nottingham NG7 2RD, UK

Pulsed magnetic field gradient (PGSE) NMR has been used to probe the scale of structures in the range 1-500 μm ever since it was first introduced by Stejskal and Tanner [1]. It has been widely used to investigate both flow and diffusion of fluids contained within porous solids and other structures, characterising the effects through the probability density $P_\Delta(X)$ for displacements, X in a time Δ, where the direction X is given by the direction of the applied field gradient. For a system which is isotropic overall, the choice of the gradient direction in the determination of such 1-D propagator is a matter of convenience. The determination of the joint probability $P_\Delta(X,Y)$ [2] of displacements in two directions X and Y in time Δ seems particularly appropriate for fluid flow in porous solids because of the clear difference between the axial mean flow direction and the perpendicular direction.

In this work, self-diffusion in water, occupying 25% of the pore space within a random packing of 100 μm diameter glass beads, is characterised using PGSE NMR to determine the joint probability, $P_\Delta(X,Y)$ of displacements X and Y in time Δ.

It is demonstrated that the detailed features exhibited by the correlation distribution $C_\Delta(X,Y) = P_\Delta(X,Y) - P_\Delta(X)P_\Delta(Y)$ reflect the anisotropic microscopic structures of the water phase despite the overall isotropy of the sample. It is suggested that this will allow detailed structural characterisation of restricting environments, such as porous solids, via the diffusion and flow contained in fluids

---

[1] E. O. Stejskal, J. E. Tanner, *J. Chem. Phys.* **42** (1965) 288.

[2] S. Stapf, K. J. Packer, *Appl. Magn. Reson.* **15** (1998) 303.

Study of molecular exchange of the liquid in zeolite NaX.

A. V. Ouriadov*, V. D. Skirda**

*University of New Brunswick Department of Physics, MRI Research Centre, Fredericton, New Brunswick, Canada
**Kazan State University Department of Physics, Kazan, Russia

One of the specific features of the mobility of liquid molecules inside zeolite is that zeolite is characterized by biporous structure: intra- and intercrystallite pore structure. The aim of this work is to study the specific features of the translation mobility of n-decane molecules in NaX zeolite within wide ranges of diffusion times and concentration of a liquid. Measurements were conducted by PMFG ^{1}H NMR at a frequency of 60 MHz. The maximal value of pulse gradient (g) was 100 T/m. In experiments we registered diffusion decays Diffusion decays (DDs) were registered by scanning of g value at fixed parameters of pulse duration and diffusion time. Diffusion times varied from 2 to 450 ms. Measurements were performed within temperature range 303–363 K. A special attention was paid to the study of molecular exchange between intra- and intercrystallite-confined liquids [1].

The DDs obtained for the case when liquid completely filled the all zeolite porous are non-exponential and in the most general form, the DDs quite adequately described by the expression:

$$A(k^2) = p_a \exp(-k^2 D_a t) + p_c \exp(-k^2 D_c t) + \int p_b(D_b) \exp(-k^2 D_b t) dD_b \qquad (1)$$

where p_a is the population of the phase with the lowest self-diffusion coefficient D_a and p_c is the population of the phase with the largest self-diffusion coefficient D_c. The third term in expression (1) characterizes the phase population ($1-p_a-p_c$) with the intermediate (between D_a and D_c) values of self-diffusion coefficients D_b. As the DDs for these samples demonstrate distinct to an increase in population p_a with a decrease in n-decane content in the samples This circumstance makes it possible to attribute components with the observed self-diffusion coefficients D_a and D_c to liquid molecules confined in intracrystallite and intercrystallite spaces, respectively, taking the zeolite biporous structure and the predominant sorption of a liquid in narrow pores into account.. It was found that there is the dependence of p_a on time and this dependence is exponential. It means that the lifetime distribution function is also exponential and the exchange process between intra- and intercrystallite-confined liquids is not limited by the diffusion of molecules to the interface. Thus it can be conclude that a certain barrier exists at the interface (crystallite surface) preventing the free diffusion of n-decane molecules to the intercrystallite space [1].

We disclosed also that self-diffusion coefficients D_a and D_c are the functions of diffusion time. The analyses of D_a performed using scaling approach, [2] allows to define the reason or completely restricted self-diffusion of fluid molecules in to the intracrystallite space of NaX, and to calculate the resultant size of a region, where the confined diffusion occurs.

The genuine self-diffusion coefficients of fluid in the channels of zeolite NaX have been determined from analysis of experimental time dependencies of self-diffusion coefficients [1]. For the first time on an example of the system "NaX/n-decane" it has been established, that concentration dependence of the genuine self-diffusion coefficients of fluid molecules in zeolite with three-dimensional network of channels, qualitatively coincides with concentration dependence for self-diffusion coefficient of liquid, predicted for the single-file diffusion regime in the zeolites with one-dimensional channels [3].

1. Uryadov A.V. et al., Colloid Journal, Vol. 63, № 2, 233–241. (2001
2. Valiullin R.R. et al., *Phys. Rev.* E, Vol. 55, № 3,. 2664-2673 (1997).
3. Uryadov A.V. et al., Mag. Res. Imag., in publishing

FROM ORGANIC TO INORGANIC. WATER AND ITS INTERACTION BY NMR

Maristella Gussoni[1], Fulvia Greco[2], Francesca Bonazzi[2] and Lucia Zetta.[2]

[1] Dipartimento di Scienze e Tecnologie Biomediche, Università di Milano, Milan, Italy

[2] Istituto di Chimica della Macromolecole, CNR, Milan, Italy

Purpose

Water is a major component of many organic and inorganic systems. It plays a dominant role in determining their physical and chemical properties. Nevertheless it is not just the amount of water that is important but its availability to interact with the studied matrix. In a high water content matrix, water may be considered to be bound, because it is held within a structure and physically encased in the matrix, so that it is free to move over many molecular dimensions, but it is restrained in the structure by impermeable or semipermeable barriers. Aim of the present study was to determine the status and the structural role of water interacting with both organic and inorganic matrices. The study could be carried out on samples involving quite different scientific and technological fields, like biology, food industry or material science. Indeed, a biological tissue, that is the cells constituting a seed, during its germination and development to become a plant, was assumed as an example of organic matrix. On the contrary, the porous structure of a hydrated cement paste was assumed as an example of inorganic matrix. ^{1}H NMR, by means of Microimaging technique (MRM) and relaxation time measurements, well characterized both the matrices as concerning water distribution and the effects of the interaction between water and matrix. The information from water signals in biological samples is related to water compartimentation.[1] Water tissue from different compartments shows relaxation times T_1 and T_2 related to the metabolic state of the compartment itself that changes with tissue development. The result of compartimentation is a multiexponential behaviour of the relaxation decay. As regard as inorganic matrices, water can be considered physically trapped in the pores that can be seen like inorganic barriers.[2] With respect to other inorganic matrices like zeolites, sandstones etc., hydrating cement can be considered an evolving porous system, as it reacts with the filling water.

Methods

MRM and relaxation time T_1 and T_2 experiments were carried out on a 4.7 T Bruker AM WB spectrometer equipped with a probehead tuneable at the ^{1}H resonance frequency (200.13 MHz) and a gradient drive unit. A 15 mm insert was used putting the sample in a 10mm tube.

Results and Discussion

Organic matrix: MRM and T_1 relaxation time experiments allowed to monitor the water tissue metabolic state of a Morning Glory seed germinating and growing in the NMR tube. The non-invasive NMR method does not alter hydrostatic and osmotic forces driving the water flux. Thus the growth of the plant was imaged through cellular differentiation, monitoring water and lipid distribution and metabolic changes through T_1 variations in different cellular compartments. Moreover a model of water transport through the plant stem was designed by following the progress of tracers absorbed by the roots. The model described a parabolic water transport where the peak position was determined by the upward axial transport and the parabolic tail width was determined by the radial water transport component caused by both diffusion and permeation.

Inorganic matrix: MRM and T_2 relaxation studies provided information on the chemical and physical state of water during the hydration process in Portland cement entirely occurring in the NMR tube. Soaking the dried sample, water was physically absorbed back into the sample, suggesting an open porous structure for the multimodal pore distribution in cement. Moreover, the effect of the addition of large amounts of a liquid organic waste, like 2-monochloroaniline, to the cement paste was assessed. In fact among the adopted techniques for the neutralization of liquid wastes, the so called "cement based solidification/stabilization" technique is increasingly adopted.[3] In particular, the influence of the organic compound on the hydration process and on the physical and permeability properties of cement materials was investigated. NMR results showed a very good agreement with separate analyses performed on similar samples, in particular thermogravimetric methods.

References

1.Macfall, J.S.,Van As, H.: in Nuclear Magnetic Resonance in Plant Biology, ed by Y.Shachar-Hill and P.E.Pfeffer (Am Soc Plant Physiologists, Maryland). 33-76 (1996)

2.McDonald, P, Strange, J. Physics World, 29-34 (1995)

3.Pollard, S.J.T., Montgomery, D.M., Sollars C. J. et al., J of Hazardous Materials 28, 313-327 (1991).

Point Spread Function Analysis of Spiral-SPRITE Sequence

Pavol Szomolanyi, Igor Mastikhin, Bruce J. Balcom

MRI Centre, Department of Physics, P.O. Box 4400, University of New Brunswick, Fredericton, New Brunswick, Canada E3B 5A3

Point spread function analysis of Single-Point Ramped Imaging with T_1 Enhancement [1] sequence with spiral k-space sampling (Spiral-SPRITE) is introduced. This analysis is useful for optimization of the measurement parameters TR and flip angle for a given T_1. By optimization of these parameters, blurring effects caused by the point spread in resulting images can be minimized.

Spiral-SPRITE is rapid imaging technique, particularly advantageous for very short T_2^* samples. This technique is substantially free from artifacts due to B_0 inhomogeneity, chemical shift and susceptibility variations because of phase encoding. K-space sampling in the form of one spiral or several spirals interleaf gives possibility of magnetization preparation [2] and at the same time, speeds up measurement, since sampling of high frequency components in the periphery of k-space is omitted.

Polymers [3], concrete samples, pharmaceutical pills, H-gas, SF6-gas or food are typical samples, which has been successfully measured by the Spiral-SPRITE sequence. All of these measurements employed one spiral or several spirals interleaf k-space sampling [4].

Point spread function in Spiral-SPRITE sequence is governed by the exponential decay of longitudinal magnetization along the path of spiral trajectory. At the time TR after the application of 'n' excitation RF pulses, the longitudinal magnetization will be in steady state. Evolution of z-magnetization during Spiral-SPRITE acquisition depends on the number of applied RF pulses. This fact influences image resolution. Attenuation of M_z magnetization along the spiral trajectory will result in a blurring of the image. The Spiral-SPRITE image resolution is affected by the finite sampling function U(t) and function R(t) , which represent the effect of T_1 contrast or saturation of longitudinal magnetizaton through respective RF pulses. The Fourier transform of U(t) and R(t) yield the sampling point spread functions (SPSF) and the evolution point spread function (EPSF). Resulting 2D image will be convolution of the Fourier transformation of idealized k-space representation of our object $F\{M(k_X, k_Y)\}$ with the SPSF due to discrete sampling of k-space and an EPSF, which will be the Fourier transform of the two-dimensional k-space damping.

$$M(x,y) = F\{M(k_X, k_Y)\} \otimes SPSF \otimes EPSF \qquad (1)$$

The effect of incomplete k-space sampling with attenuation of longitudinal magnetization through successive RF pulses was simulated given knowledge of the k-space trajectory. Computer simulations of point spread function were done for K-space trajectory optimization.

[1] Balcom B. J., MacGregor R. P., Beyea S. D., Green D. P., Armstrong R. L., and Bremner T. W., J. Magn. Reson. A 123, 131 (1996)
[2] Mastikhin I., Balcom B. J., Prado P. J. and Kennedy C. B., Journal of Magnetic Resonance 136, 159-168 (1999)
[3] Kennedy C. B., Balcom B.J. and Mastikhin I.V., Can. J. Chem. 76, 1753 – 1765 (1998)
[4] Szomolanyi, P., Goodyear D., Balcom B.J., Matheson D., Magnetic Resonance Imaging,, in press

Magnetic Resonance Imaging of Layered Materials using SE SPI Techniques

Alexei Ouriadov, Bryce MacMillan, Yuesheng Cheung, Bruce Balcom

MRI Research Centre, Department of Physics, University of New Brunswick, Fredericton, New Brunswick, Canada

Polymer composite layered materials are widely using in many industrial applications. Magnetic Resonance Imaging is amenable to the study of the solid-like materials and holds great potential for the study of polymer composite layered materials which naturally present a 1 dimensional imaging problem.

Polymer composite layered materials frequently have low proton density and consequently a poor SNR magnetic resonance signal. We have employed a spin echo modified signal point imaging[1] technique to partially overcome these difficulties which are exacerbated when attempting high resolution imaging..

The Signal Point Imaging method is a pure phase encoding technique and due to this it does not contain artifacts as chemical shift, magnetic field inhomogeneity, susceptibility variations[2] and molecular self-diffusion[3]. Besides the signal point imaging technique does not have line width restriction on resolution general time sampling in comparison with frequency encode method[4]. The using of SE SPI (Spin Echo Signal Point Imaging) technique and also Multi SE SPI technique permits 1D high resolution images from a variety of layered materials including nafion.

As Nafion has quite a large T_2 value it permitted high-resolution images using SE SPI and Multi SE SPI with 6 micron resolution with a FOV of 390 μm. Sample thickness was 300 μm. The use of Multi SE SPI technique allowed to obtain high resolution 1D image in quite a short time period. The time necessary for getting image in case when we acquired 4 echoes was approximately 10 minutes. It should be noted that the obtaining of 1D image with good S/N ratio took approximately 40 minutes when using SE SPI method.

These measurements employ small radio frequency coils placed on the surface of sample with pure phase encode gradients applied perpendicular to the sample surface to encode depth information. We note that the B_1 magnetic field generated by radio frequency coil was perpendicular to the samples ie perpendicular to the sample surface. The detected signal is thus effectively integrated over the diameter of the RF coil increasing the available SNR. Detection of the pure phase encoded echoes permits optimal setting of the audio filter further enhancing the experimental SNR. And decreasing the number of signal averages. All the measurements were done in 2.4 Tesla MRI magnet with a resonance frequency of 100 MHz for ^{1}H at the room temperature.

Reasonable image acquisition times, tens of minutes, for typical applications permit time resolved visualization of a variety of dynamic phenomena, such as wetting and drying, in a wide range of composite layered materials.

1.   Balcom B.J. Spatially Resolved. Magnetic. Resonance, 75-86, Wiley-VCH, Weinham (1998)
2.   Gravina S. et al., J. Mag. Res., B 104, 53-61 (1994)
3.   Callaghan P.T. et al., J. Mag. Res., B 104, 34-52 (1994)
4.   Beyea S. D. et al., J. Mag. Res., 144, 255-265 (2000)

Application of Magic Echo and Single Point Imaging (SPI) to Study Solid Materials with Standard MRI Devices

Z. Fang, D. Hoepfel
FH Karlsruhe - Hochschule für Technik
FB Mechatronik und Naturwissenschaften (MN)
Moltkestr. 30, 76133 Karlsruhe, Germany

Introduction: Due to reduced molecular motion the T_2 relaxation time in solid materials is normally shorter by a factor of 10^3 to 10^5 comparing to those in liquids, resulting in a large intrinsic NMR line-width about 20kHz. In the case of solid state MRI the transversal magnetisation M_x/M_y decays so fast ($\leq$1ms) that only a small amount is left before any conventional MRI sequences can be successfully applied, therefore the achievable spatial resolution and signal-to-noise ratio are strongly degraded. Two classes of methods are commonly used to do solid-state MRI: (i) using large gradients and (ii) using line-narrowing techniques. The class of imaging methods characterized with large gradients includes stray-field imaging (STRAFI), pure phase-encoding imaging such as single point imaging (SPI)[1], and mutli-quantum imaging. The class of imaging methods characterized with line-narrowing techniques includes magic-angle spinning (MAS) imaging, magic-angle rotating-frame imaging, multi-pulse line narrowing imaging, and magic-echo phase-encoding imaging[2]. Most of these solid-state MRI methods require additional hardware, therefore difficult to be realized with standard MRI devices. From an experimental point of view, pure phase-encoding methods like SPI and magic-echo phase-encoding are the most suitable methods to do solid-state imaging of abundant nuclei ^{1}H.

Applied methods: Single point imaging (SPI) is a 3D pure phase-encoding imaging method. A single data point in the k-space is acquired with a minimum phase-encoding time (~50μs) after each broadband, small flip angle (normally ≈10°) RF excitation pulse. The main advantages of SPI are: no additional hardware necessary, an ultra short phase-encoding (detection) time, no chemical shift artefacts, no susceptibility artefacts and insensitive to B_o-inhomogeneity. The limiting disadvantage is a long total acquisition time. SPI has proved to be suitable for imaging soft solid materials. However, even with SPI method, ^{1}H imaging of rigid solid materials requires very strong gradients and therefore sets stringent requirements on spectrometer hardware. To improve phase-encoding efficiency and S/N, the combination of pure phase-encoding and solid-echo approach was proposed by PJ Mcdonald[3]. Another approach is the combination of magic-echo and phase-encoding technique. With these two echo techniques, due to the refocusing of dipolar interaction, M_x/M_y transversal magnetization will decay with a prolonged T_2 time constant.

Preliminary results: In our research group, SPI, solid echo + SPI and magic echo + SPI are applied with a standard MRI device in order to study the spatial structure of various solid materials, such as low water content food materials (chocolates), earth samples used as filters in waste-water processing, industrial polymer foams, etc.
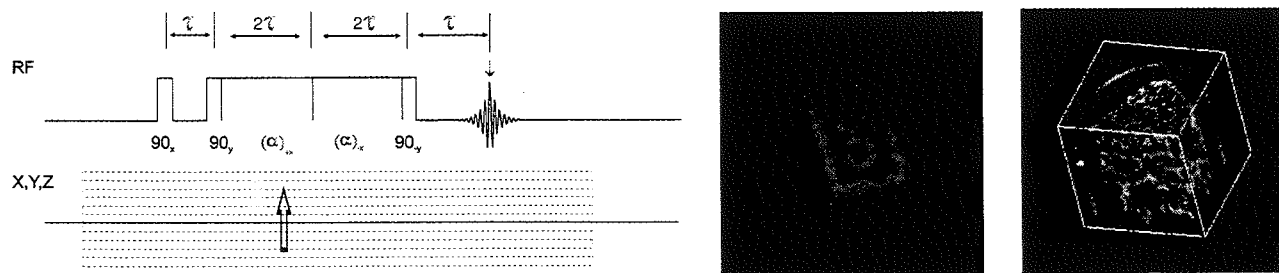
Fig. 1 On the left hand side is the Magic-Echo Phase Encoding Solid imaging sequence, X, Y, Z represent three spatial phase encoding directions, 2τ is the phase encoding time. On the right hand side are two SPI images of a Lego block measured on a 0.35T electro-magnet system, FOV is 4.0×4.0×4.0cm^3, resolution is 625×625×625μm, and a Milka-Luflee chocolate sample measured on a 4.7T superconducting magnet system, FOV is 2.2×2.2×2.2cm^3, resolution is 176×176×352μm.

References:
1. Emid, S. and Creyghton, J.H.N., Physica 128B, PP81-83 (1985)
2. Demco, D. E., Hafner, S. and Kimmich, R., JMR 96, PP307-322 (1992)
3. McDonald, P. J., Attard, J. J. and Taylor, D. G., JMR 72, PP224-229 (1987)

Symmetric Echo Acquisition for Absolute-Value Display in Solid-State NMR Imaging

Seiji Saito and Shigeru Matsui

*Institute of Applied Physics, University of Tsukuba, Tsukuba,
Ibaraki 305-8573, Japan*

In liquid-state MRI, imaging signals are generally acquired in the form of an echo rather than an FID. In solid-state MRI, on the other hand, an FID is usually acquired and few experiments are reported on the echo acquisition (1). The echo acquisition is superior to the FID acquisition: (i) The sensitivity is gained by $\sqrt{2}$, since the acquired echo can be regarded as a back-to-back sum of two complementary FID's. (ii) The digital resolution is doubled. (iii) The phase correction for the real component (absorption) display becomes unnecessary. Here, we present an improved method of solid-state MRI which enables the symmetric echo acquisition under the magic-echo line narrowing (2).

In the previously reported magic echo imaging (TREV-16TS) (2), the signal sampling points obtained at the magic echo peaks followed a k-space trajectory which was not symmetric with respect to the k origin. Therefore, only the even-numbered sampling points were taken to form an FID while the odd-numbered sampling points were discarded. In the improved method, however, the gradient pulse sequence is modified so that all the sampling points can be used to follow a symmetric k-space trajectory. This allows a symmetric echo to be acquired. Unlike the previously reported method, the gradient pulses are applied only during the second halves of the selected RF-free windows, analogously with the echo acquisition performed in liquid-state MRI using the CPMG spin-echo sequence (3). For obtaining the same FOV as in the previous method, the gradient amplitude must be increased by a factor of 4.

One- and two-dimensional imaging experiments have been conducted on a homebuilt NMR imager, operating at 59.85 MHz for protons. Three samples, natural rubber, adamantane, and polycarbonate were used. The relaxation times T_2 for these samples, 1 ms, 50 μs, and 30 μs, respectively, were prolonged by the magic-echo line narrowing to about 20 ms, 15 ms, and 1.5 ms. The experimental results obtained on the three samples have confirmed the superiority of the echo acquisition mentioned above and revealed a TREV-16TS adjustment parameter which is critical for the successful echo acquisition.

REFERENCES
(1) G. C. Chingas, J. B. Miller, and A. N. Garroway, *J. Magn. Reson.* **66**, 530-535(1986).
(2) S. Matsui, *Chem. Phys. Lett.* **179**, 187-190 (1991);
   S. Matsui, *J.Magn Reson.* **95**, 149-153 (1991);
   S. Matsui, *J.Magn Reson.* **98**, 618-621 (1992);
   S. Matsui, Y. Ogasawara, and T. Inouye, *J. Magn. Reson.* **A 105**, 215-218 (1993);
   S. Matsui, M. Nonaka, T. Nakai, and T. Inouye, *Solid State NMR* **10**,39-44 (1997);
   M. Nonaka, S. Matsui, and T. Inouye, *J. Magn. Reson.* **145**, 315-318 (2000) and references
      therein.
(3) D. J. O. McIntyre, F. Hennel, and P. G. Morris, *J. Magn. Reson.* **130**, 58-62 (1998).

NMR Imaging of Snowpack Structures

Toshihiro Ozeki[1], Akihiro Hachikubo[2], Katsumi Kose[3],
Tomoyuki Haishi[3], Shunichi Nakatsubo[4], Kouichi Nishimura[4]

[1]Hokkaido University of Education, Iwamizawa, 068-8642, Japan
[2]Kitami Institute of Technology, Kitami, 090-8507, Japan
[3]Institute of Applied Physics, University of Tsukuba, Tsukuba, 305-8573, Japan
[4]Institute of Low Temperature Science, Hokkaido University, Sapporo, 060-0819, Japan

Introduction

Microstructure of the snowpack should be better understood because it affects the mechanical and physical properties of snow. The avalanche release mechanism also depends on the microstructure of snowpack. Thin sections and plane-surface sections are currently used to investigate. However, they give only two-dimensional information; therefore, a large number of operations are necessary to reconstruct the three-dimensional structure. In this study we have developed a NMR imaging technique to visualize and quantify the 3D structure of snowpack.

Method

Because the NMR signal from the ice was very weak, the airspaces in the snow were filled with dodecane doped with iron acetylaetonate $C_{12}H_{26}$, which has a good infiltration property and a low freezing point (about -12 °C). Thus, the NMR images the space occupied with dodecane instead of ice particles. The 3D images were obtained with a homebuilt NMR imaging system (Kose, 1996) using a 4.74-T superconducting magnet. The result of test imaging of dodecane showed 0.5 to 2 hours were needed to obtain the one 3D image, and hence we developed a specimen-cooling system to keep the temperature below 0 °C. This system has a double-pipe cylinder made of acrylic plastic with outer diameter of 40 mm and inner diameter of 20 mm through which cold air was passed. Two types of snow were prepared: ice spheres of about 3-mm diameter and depth-hoar crystals. In particular, because the ice spheres are sufficiently large and uniformly sized, they were ideal for test imaging.

Results

3D microscopic images were obtained successfully; the image matrix was 128^3 and voxel size was 0.2 mm^3. We could recognize the 3D structure of the packed ice spheres clearly by viewing from various angles and cross sections (Fig. 1). Continuous measurements for the ice spheres melting in 110 minutes were also carried out; the image matrix is 64^3 and the voxel size is 0.4 mm ^{3}. Both experiments showed that the NMR imaging could be a powerful technique to study the structure of snowpack.

Reference

Kose, K., 3D NMR imaging of foam structures.
J. Mag. Resonance A118, 195-201(1996)
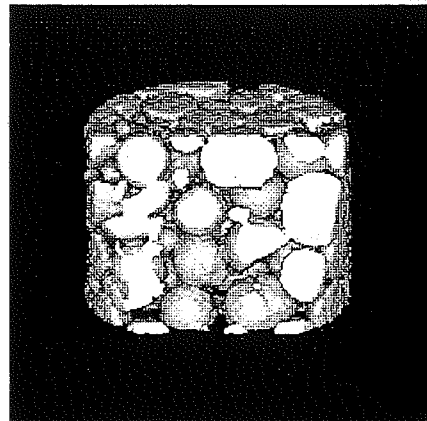
Figure 1: Negative image of ice spheres.

THE KINETICS OF PARACETAMOL DISSOLUTION IN WATER STUDIED BY THE FLASH TECHNIQUE

Narcyz Piślewski, Jadwiga Tritt-Goc, Joanna Kowalczuk

Institute of Molecular Physics, Polish Academy of Sciences, Poznań, Poland

Introduction

The subject of the presented study was the paracetamol tablets purchased from the pharmaceutical firms existing on the Polish market : Biofarm Poznań, Polfa Kutno S.A., Polfa Łódź, Polfa Grodzisk Maz. and GlaxoWellcome Poznań. The tablets are characterised by the same amount (500mg) of the main component pestanal with the chemical formula C_6H_2NO, but they can differ as to the amount of additional components. However, the total weight of the single paracetamol tablet is the same.

With the present work, we had two principal goals. First we wanted to examine the distribution of pestanal within the tablets. Second, we investigated the *in situ* dissolution behaviour of paracetamol tablets in specific conditions.

Methods

The experiments were performed on Bruker 300 MHz spectrometer equipped with macroimaging accessories. The method used was NMR imaging. The 1D spin density profiles of studied paracetamol tablets were obtained using Single Point Imaging pulse sequence useful for imagine of solid materials. The dissolution process of the paracetamol was followed by Snapshot FLASH method in water solution of hydrochloric acid (pH=2) which corresponds to the condition in the stomach. With repetition times of 50 ms the method is fast and in our case the total experimental time was 452 ms. The 2 D FLASH images of dissolved paracetamol tablets were measured in the function of time at two temperatures 19°C and 37°C.

Results and Discussion

The comparison between ^1H NMR spectra of paracetamol tablets and pestanal itself shows that the proton spectrum of tablets comes from active component. The 1D SPI profiles of all studied tablets prove the homogeneous distribution of pestanal within the tablets. Some representative 2 D FLASH images of paracetamol tablets from Polfa Kutno S.A. taken at 37 °C are presented on the Fig. 1. These images and others measured for all studied tablets serve for calculation of the dissolution profiles. Tablets from Polfa Łódź, Polfa Grodzisk Maz. and GlaxoWellcome Poznań are characterised by the same rate of the dissolution. The tablets from Polfa Kutno S.A. have the dissolution times four times longer than the tablets mention above. All these tablets when exposed to contact with water decrease their surfaces in time. Quite a different dissolution behaviour is shown by the paracetamol tablets from Biofarm Poznań. At first stage of contact with water they swell and increase their surface and after some time follow the dissolution process as other studied tablets. The dissolution process for all paracetamols under investigation is faster at 37°C than at 25°C.

Conclusion

In this work we show that paracetamol tablets when exposed to aqueous solution undergo fast dissolution. However, the kinetics of this process depend on the farmaceutical firms the tablets come from. The porosity of the tablets can be responsible for the different dissolution behaviour of paracetamol tablets and it will be the subject of our next study. Furthermore, we demonstrate that Snapshot FLASH method can be successfully used to follow the dissolution process for paracetamol as well as for other compact tablets.

(a)   (b)   (c)   (d)
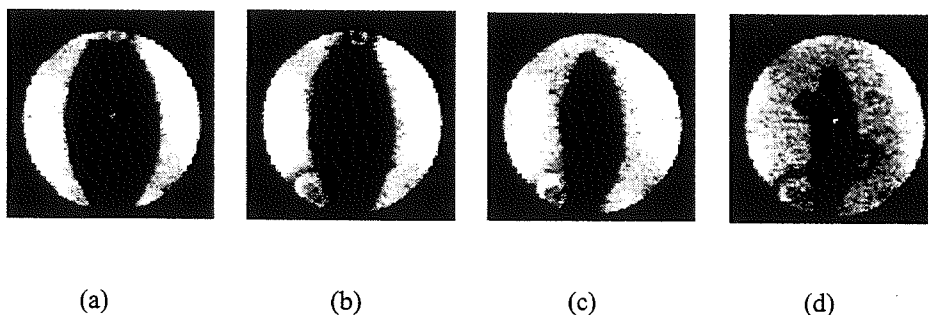
Fig. 1. Time-resolved FLASH images of the dissolution process of paracetamol tablets from Polfa Kutno. The images were taken 90 s (a), 8min (b), 25min (c) and 45min (d) after immersion of the tablets into water.

P-39

MAGNETIC RESONANCE IMAGING OF WATER INGRESS INTO HPMC

Jadwiga Tritt-Goc and Narcyz Piślewski
Institute of Molecular Physics Polish Academy of Sciences, Poznań, Poland

Introduction
Hydroxypropylmethylcellulose (HPMC) belongs to the industrially important class of hydrogel-forming polymers and recently is increasingly used to produce controlled release drugs. When exposed to water or body fluids, the polymer forms a gel layer around the tablets and greatly influences the dissolution and diffusion of the drug. The system's reaction to solvent ingress can be measured in terms of swelling and diffusion.

Experimental techniques
The method used was magnetic resonance imaging. The experiments were performed on a Bruker 300MHz NMR spectrometer equipped with imaging facilities. The MSME pulse sequence allows to study the water diffusion and the swollen behavior of the hydroxypropylmethylcellulose by two-dimensional mapping of NMR properties such as spin-density and T_2 relaxation times of the solvent in the function of time. All the recorded images have an in-plane pixel resolution of about was 117 μm×117 μm. The measurements were performed for two temperatures 25°C and 37°C, and two pH values 6 and 2.

Results and discussion
As an illustration, typical images of time-resolved diffusion of water at pH=2 into a 8 mm diameter HPMC cylindrical rod with a length of 9 mm for 25 °C is presented in Figure 1.
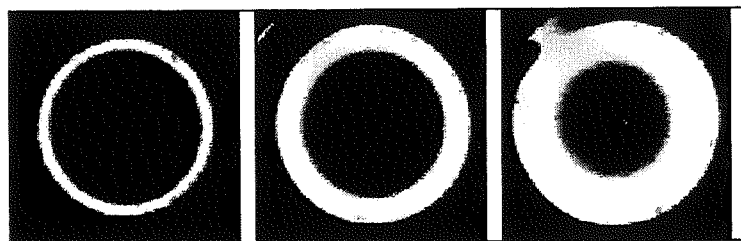
Figure1. Time–resolved MSME images of the diffusion process of water into HPMC rod taken after 10, 35 and 190 min after immersion of the rod into the solvent.

On the basis of such images taken for the studied temperatures and pH values, the penetration distances of the solvent into HPMC were calculated. It is shown that transport behavior for water at pH=6 and both studied temperatures obeys Fick's law - Figure 2a. The linearity of the penetration distance of the detectable water into the HPMC as a function of the square root of time is the standard proof for a Fickian diffusion process. On Figure 2b the distance diffused by the water at pH=2 is shown. The solvent front advances linearly into the matrix with time, which confirms that Case II or relaxation-controlled diffusion is occurring. The behavior of the penetration distance at the beginning of the experiment is indicative of an initial Fickian diffusion process. There is also an increase in the solvent concentration going from the polymer core to the fully swollen region of the polymer for pH = 6, whereas T_2 remains almost constant in the swollen region. For water with pH = 2 the solvent concentration is constant throughout the swollen region and T_2 relaxation rate decreases toward the polymer core. These observed phenomena further justify Case I and Case II diffusion processes for pH = 6 and 2, respectively.
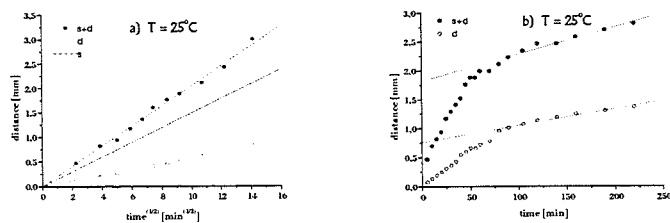
Fig.1. Progress of the diffusion front as a function of the square root of time for HPMC with H_2O at pH = 6 a) and pH = 2 b). s –swollen distance; d – diffusion distance.

Conclusion
Usually, Fickian diffusion applies to rubbery polymers whereas Case II to the polymers in the glassy state. Our measurements show that the change in the acidity of the water solution has the same effect on the diffusion as the change in temperature when going from above to bellow glassy temperature.

NMR SORP:
Automated NMR and MRI Experiments as a Function of Relative Humidity

Johannes Leisen and Haskell W. Beckham
Georgia Institute of Technology, School of Textile & Fiber Engineering,
Atlanta, GA, 30332-0295 USA

Mike Benham
Hiden Analytical, Warrington, WA5 7UN, UK

Many material properties depend strongly on moisture absorbed from the environment. Such dependencies have been studied extensively for many technical applications ranging from the wearing comfort of textiles to the stability of epoxy resins used for electronic packaging. Routinely, moisture sorption by a material is studied gravimetrically following exposure to varying temperatures and relative humidities. Information obtained this way provides no direct information on the spatial distribution of moisture, nor the properties of the moisture within the substrate. NMR spectroscopy and NMR imaging provide such information.

By integrating a commercial moisture sorption balance (Hiden Analytical) with a Bruker DSX-400 NMR spectrometer, an experimental setup was developed for the automated recording of NMR data at defined levels of relative humidity.

Initial experiments were conducted on the moisture uptake of a cotton fabric. The sample was exposed to a cycle of increasing and decreasing levels of relative humidity (RH); NMR data were recorded after the equilibrium moisture content had been reached at each RH level. The free induction decay can be approximated by a combined Gaussian and exponential decay, arising from the cellulose fibers and the sorbed moisture, respectively. Hence, the amount of sorbed moisture may be extracted from the NMR data. Moisture uptake or desorption may be observed by performing experiments at increasing or decreasing levels of relative humidity. Different amounts of a mobile proton fraction are found depending on the direction of RH changes, so that a hysteresis loop is formed (cf. Figure 1A). This hysteresis corresponds well to results established by measuring the moisture uptake gravimetrically. The decay constant T_2^* of the exponential decay, which reflects the rotational mobility of the sorbed water, was evaluated and plotted as a function of RH; a hysteresis loop is also observed for these data (cf. Figure 1B). Since the rotational mobility will be influenced by the binding interaction between sorbed water molecules and the substrate, T_2^* may be used to quantify this binding interaction. A plot of T_2^* versus the moisture content (from Figure 1A) provides data that fall on a single curve; no hysteresis loop is observed in Figure 1C. Hence, while the amount of sorbed moisture depends on the history of exposure to different RH levels, there is clear evidence that the mobility of water molecules sorbed onto the cotton depends only on moisture concentration.

(A)   (B)
(C)
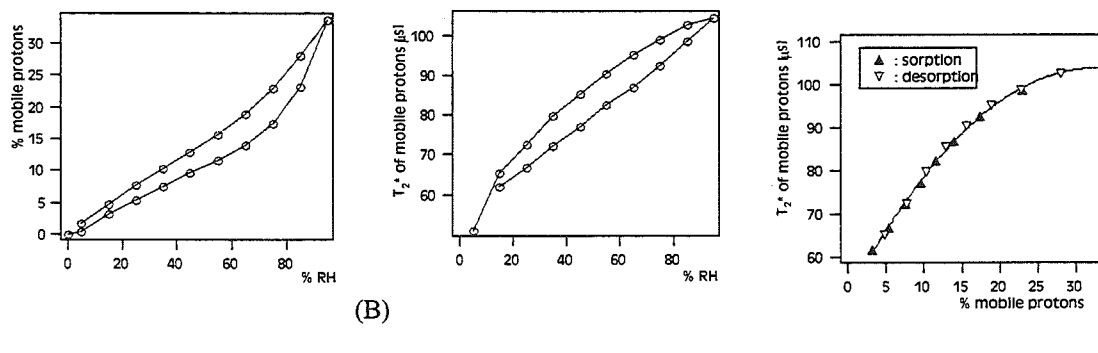
Figure 1. *Amount and mobility of moisture in a cotton fabric with different histories of exposure to different levels of RH at 20 °C.*

Further experiments were conducted to determine the sizes of domains formed by the sorbed water within the cotton fabric. This was achieved by measuring the spin diffusion between the protons of the cellulose fibers and those of the sorbed water molecules. This type of experiment has been described for the measurement of spatial heterogeneities on the nm length scale in polymers [1]. The magnetization transfer observed for the water-cellulose system was very similar for all levels of relative humidity. Hence, at least in the cotton fabric under investigation, sorbed water tends to form the same size domains at all RH levels. These findings should prove useful for discriminating between various models currently proposed to explain the hysteresis observed in moisture sorption curves [2].

References:
[1] Schmidt-Rohr, K. and Spiess, H.W. "Multidimensional Solid State NMR and Polymers", Chapter 13, Academic Press, 1994.
[2] Skaar, C. "Wood-Water Relations", Chapter 2, Springer-Verlag, 1988.

NMR FRINGE-FIELD IMAGING OF WATER INGRESS IN VARIOUS CEMENTITIOUS MATERIALS

D.A. Verganelakis, A. Leventis, M.R. Halse, M.J.D. Mallett, J.H. Strange
School of Physical Sciences, University of Kent at Canterbury, Kent, UK.

G. Hunter and M.R. Jones
Departments of Chemistry and Civil Engineering, Dundee University, Dundee, UK.

ABSTRACT
The Nuclear Magnetic Resonance (NMR) Fringe-Field Imaging method has been used successfully to image and compare water concentration profiles in dry hardened Portland cement samples and cements containing pozzolanic additives. Further experiments using the technique of NMR Cryoporometry provided a pore-size distribution. A simulation computer model based on capillary imbibition was developed where experimental and theoretical results were compared.

INTRODUCTION
The corrosion of the reinforced concrete is a problem still under investigation. The mechanism of water and chloride ions transport within the concrete microstructure is ill understood. The potential of the NMR fringe-field imaging was explored due to its non-destructive nature, high accuracy, good resolution and repeatability of the experiment.

FRINGE-FIELD IMAGING
The principle of fringe-field imaging is making use of the static and large magnetic field gradient near the windings of a superconducting magnet. This large gradient dominates all other internal gradients which are generated by paramagnetic ions and/or susceptibility gradients. FFI as a technique has many advantages, such as good resolution, lack of saturation effects etc. It proved to be an ideal tool for studying cements and overcoming all the problems generated by their composition (Fe^{+3}) and by their porous structure.

EXPERIMENTAL WORK
Various cement samples were made at different w/c ratios using pozzolanic additives, such as PFA (Pulverised Fuel Ash) and GGBS (Ground Granulated Blastfurnace Slag), which it is believed to inhibit water imbibition.

1-Dimensional water profiles were accumulated at a frequency of 103 MHz, 18T/m gradient, 6µs pulses separated by a tau of 7µs. Comparing the water profiles useful results could be deduced about the efficiency of the various pozzolanic additives in lowering water permeability and the effects of w/c ratios.

Further experiments were conducting using the technique of NMR Cryoporometry which gave a better insight in the cement's porous microstructure. Various pore-size distributions were recorded.

SIMULATION MODEL
A computer simulation model was developed based on spherical capillary pores being connected by varying cylindrical pore throats. Capillary pore-size distributions derived from Cryoporometry were introduced into the simulation model and its effects on the simulation master curve were compared [1,2].

SUMMARY
This work constitutes a small step towards understanding the mechanism of water transport in cementitious materials. The importance of Fringe-Field Imaging in studying heterogeneous materials with short T_2 was proved. Overall, it supports the use of pozzolanic additives in Portland cement at low w/c ratios for the cases where low permeability is required.

REFERENCES
[1]   Leventis A., Verganelakis D.A., Halse M.R., Webber J.B., Strange J.H., *Transport in Porous Media* 39:143-157 (2000).
[2]   Hammecker C., Jeannette D., *Transport in Porous Media* 17:285-303 (1994).

Use of SPRITE to study the penetration of ^{1}H, [23]Na and [35]Cl in Portland Cement Mortar.

F. de J. Cano[a,b], **B. J. Balcom**[a], T. W. Bremner[b], and R. P. McGregor[a]

[a]MRI Centre, Department of Physics and [b]Civil Engineering, P.O. Box 4400, University of New Brunswick, Fredericton, New Brunswick, Canada E3B 5A3

Penetration of chloride ions into reinforced concrete may contribute to corrosion of the steel, which reduces the service life of the structures(1). In order to assess the chloride content destructive, low spatial resolution methods are routinely used (2). Some work has been done using traditional Magnetic Resonance Imaging techniques to study penetration of chlorides into brick (3), which are not suitable for concrete, due to the shorter lifetime signal of chlorides in cement based materials compared to those in brick. The SPRITE technique has demonstrated to be suitable to image materials possessing short lifetime signals (4,5), including portland cement based materials[6].

The first Magnetic Resonance Imaging profiles of chloride penetration by absorption of 20% NaCl solution in low and high permeability Portland cement mortar were obtained using the SPRITE technique[7]. In this study the penetration of water as well as chloride and sodium ions into mortar specimens was monitored for a period of 72 hours. Marked differences in penetration depth were observed in low and high permeability mortar. These preliminary experiments show also significant differences between the extent and nature in the penetration of chlorides compared to water and sodium. In the high permeability specimen there was a decrease in the chloride signal intensity with time, which could be related to chemical binding of chlorides [8]. It was also found that the sensitivity of the measurement needs to be improved to image chlorides in low w/c ratio mortar, an improvement which may be achieved either by the use of a larger specimen or a higher field magnet.

In addition, recent experiments indicate that the technique can be used to image the distribution of chlorides in concrete/mortar containing normal Portland cement, which makes it possible to study the penetration of chlorides in cores taken from field concrete.

In conclusion, SPRITE is a very powerful non-destructive magnetic resonance imaging technique capable of imaging the penetration of aggressive ions like chlorides into Portland cement concrete/mortar, which possess short signal lifetime.

[1]   Mehta, P. K., Concrete International, Vol. 19, No. 7, 27-33 (1997).
[2]   Scanlon, J. M. and Sherman, M. R., Concrete International, Vol. 18, No 6, 57-62 (1996).
[3]   Pel, L., Kopinga, K. and Kaasschieter, E. F., Journal of Physics D; Applied Physics, 33, 1380-1385 (2000).
[4]   Balcom, B. J. , MacGregor, R. P. , Beyea, S. D., Green, D. P., Armstrong, R. L., and Bremner, T. W., Journal of Magnetic Resonance, Series A 123, 131-134 (1996).
[5]   Balcom, B. J., Spatially Resolved Magnetic Resonance, Methods, Materials, Medicine, Biology, Rheology, Geology, Ecology, Hardware, Wiley-VCH, pp. 75-86 (1998).
[6]   Beyea, S. D., Balcom, B. J., Prado, P. J., Cross, A. R., Kennedy, C. B., Armstrong, R. L., and Bremner, T. W., Journal of Magnetic Resonance, 135, 156-164 (1998).
[7]   Cano, F. de J., Bremner, T. W., McGregor, R. P. and Balcom, B. J., To be published in Cement and Concrete Research.
[8]   Midgley, H. G., and Illston, J. M., Cement and Concrete Research, Vol. 14, No. 4, 546-558 (1984).

Deuteron NMR study of a Holographically-formed Polymer Dispersed Liquid Crystal

Marija Vilfan[1], Adam K. Fontecchio[2], Mojca Vilfan[1], Michael J. Escuti[2], Bostjan Zalar[1], Gregory P. Crawford[2], and Slobodan Zumer[1,3]

[1]J. Stefan Institute, Jamova 39, 1000 Ljubljana, Slovenia
[2]Department of Physics and Division of Engineering, Brown University, Providence, RI 02912, USA
[3]Department of Physics, University of Ljubljana, Jadranska 19, 1000 Ljubljana, Slovenia

Holographically-formed polymer dispersed liquid crystals (HPDLCs) are an important stratified optical material incorporating nanodroplets of nematic liquid crystal in a polymer host, thus enabling switchable reflection/diffraction gratings. Whereas conventional PDLC materials consist of a homogeneous distribution of liquid crystal droplets, HPDLCs are composed of alternating planes of liquid crystal droplets (surrounded by a rigid polymer shell) and of pure polymer regions [1,2]. Such an arrangement is achieved by exposing the mixture of liquid crystal and reactive monomer to two opposing laser beams. The laser light forms an interference fringe pattern within the sample, which initiates the polymerisation process in the bright fringes. In the dark fringes the liquid crystal phase diffuses out into droplets [3]. The liquid crystal forms distinct Bragg planes, resulting in specific wavelengths of light being reflected or transmitted through the cell according to the Bragg condition.

We report here on the deuterium NMR study of an HPDLC formed from a homogeneous mixture of urethane oligomers, liquid crystal (EM Industries BLO38), and of selectively deuterated liquid crystal pentyl-cyanobiphenyl (5CB). Deuterium NMR spectra of a stack of thin HPDLC layers were recorded in a broad temperature range between 380 K and 280 K. Dynamic light scattering method was applied to the same sample in order to follow the onset of nematic order upon cooling. The morphology of the sample was investigated using scanning electron microscopy (SEM) and atomic force microscopy (AFM). Liquid crystal regions were found to be 50-200 nm in diameter and of irregular shape. They are arranged into planes separated by roughly 1 micrometer.

Above the nematic-isotropic bulk transition temperature the deuteron NMR linewidth in the HPDLC sample is considerably larger than in the bulk, and exceeds also the linewidth in a normal PDLC, which is a uniform droplet dispersion of the same BLO38-5CB mixture. The broadening is due to the weak surface induced order in small voids which persists far above T_{NI} [4]. The most amazing point, however, is the lack of a phase transition at ~ 358 K where both the bulk and the normal PDLC exhibit a discontinuous phase transition into the nematic phase. As shown by dynamic light scattering, liquid crystal in HPDLC voids remains isotropic down to ~342 K, where it partly turns into the nematic phase whereas the complete transition does not occur before 317 K. This is also the temperature at which the deuteron linewidth starts to increase indicating the onset of static broadening on the NMR time scale. At the lowest temperatures under study NMR spectra become a well resolved powder pattern as in normal PDLC. Our data show that the holographic formation of a liquid crystal dispersion produces a pronounced impact on the formation of orientational order upon cooling.

1. Sutherland, R. L., Natarajan, L. V., Tondiglia V. P., and Bunning, T. J., Chem Mater. 5, 1533 (1993).
2. Crawford, G. P., Fiske, T. G., and Silverstein, L. D., SID International Symposium Digest of Technical Papers 27, 99 (1996).
3. Bowley, C. C. and Crawford, G. P., Appl. Phys. Lett. 76, 2235 (2000).
4. Vilfan, M., Vrbancic, N., Zalar, B., Zumer, S. and Crawford, G. P., Phys. Rev. E 59, R4754 (1999).

Diffusion in hydrogel materials in dependence on structure, crosslinking, and swelling degree

M. Knörgen, K.-F. Arndt*, H. Schneider
Department of Physics, Martin-Luther-Universität Halle-Wittenberg, Friedemann-Bach-Pl. 6, D-06108 Halle
*Department of Chemistry, Technische Universität Dresden, D-01062 Dresden, Germany

Hydrogels have attracted considerable attention due to various physical and chemical properties/1/. Among others this is an extreme volume alteration by swelling/deswelling. The swelling behavior depends on a variety of parameters like the crosslink density of the gel, pH-value, and temperature/2/. Also, there is a wide range of applications, starting at temperature depending outlets, artificial muscle and not least at special dosimeter gels for medical purposes.

Our special interest was focused on the diffusion behavior in PNIPAAm (Poly(N-isopropylacrylamide)) gels of different degree of crosslinking. The pulse sequence mainly used was a 2D-Fourier imaging variant of the PGSE-method. The diffusion maps were calculated from an image series obtained from a gradient strength series.

The results show the dependence of the diffusion on the degree of crosslinking and swelling. It could be shown, that these (swelling/deswelling) processes can be locally inhomogeneous (as an example: skin effect during deswelling).

Further, the diffusion process was also investigated by observing a diffusion front of heavy water entering the gel matrix. The time course of this process shows inhomogeneities on a macroscopic scale.

/1/   Zhang, J., et.al., Macromolecules **33**, 102-107 (2000)
/2/   Knörgen, M., et.al., Journal of Molecular Structure **554**, 69-79 (2000)

NMR imaging of swollen superabsorbing polymer gels

Ruediger Voelkel, Rudolf Berg, Sergey Evsyukov, H.-Joachim Haehnle

BASF Aktiengesellschaft, Polymer Research Division
D67056 Ludwigshafen, Germany

NMR microscopy is a suitable technique to investigate swollen polymer gels such as polyacrylics which are the active ingredient of many articles of hygiene. Standard imaging techniques and equipment can be used to visualise the material in the swollen state. Contrast is based on the concentration of water, relaxation (T_1 or T_2^*) or diffusion.

3D maps based on multi-slice-multi-echo experiments reveal patches with a long apparent T2 located on the surface of commercial superabsorbent particles [1]. The same spots show slowed diffusion of water. T2 maps based on a slice-selective single echo Hahn-spin-echo sequence are obtained as well. The latter look very similar to published images [2] which have been interpreted as an indication of a gradient in crosslink density.

Some new developments try to avoid the drawbacks of the existing superabsorbents: Mixed bed ion exchange (MBIE) superabsorbents which consist of a "mixture" of a cationic and an anionic polymer are known to be less sensitive to salt in the liquid than the standard material in use today. NMR microscopy reveals a domain structure inside this new superabsorbent and thus provides an explanation of the swelling of this material. Another line of development is to integrate the distributing function of the fluff into the active absorbing material in order to reduce the volume of diapers. A foam made from superabsorbent material serves this purpose. NMR images of such a material allow to distinguish the filled paths from the empty ones, although the concentration of water is practically the same in the channels as in the swollen gel itself.

NMR microscopy is a promising tool on the route to establish structure – property relationships in the field of polymer gels and to support the development of better products.

[1]   Szayna M., Berg R., Voelkel R., 39th ENC Asilomar CA (USA) 1998
[2]   Traub B., Fritzhanns T., Hafner S., Spiess H.W., Colloid Polym Sci 278, 547 (2000)

T_1s of inert fluorinated gases are sufficiently predictable to aid quantitative imaging

Dean O. Kuethe and Tanja Pietraß

New Mexico Resonance, Albuquerque, USA; Dept. of Chemistry, New Mexico Tech, Socorro, USA

Introduction The T_1s of some perfluorinated gases are not only unaffected by chemical environment, but they are also highly predictable. Accurate predictions of T_1 are useful for correcting images for relaxation weighting and can also be used to estimate the composition of gas mixtures from experimentally measured T_1s. They may also provide measurements of pore sizes in the 1 to 50 nanometer range. By fitting curves to T_1s measured at different pressures, temperatures, magnetic field strengths and in different mixtures, we are finding that they can be predicted using only a handful of parameters.

Methods Previous works (review: ref. 1) suggest that T_1s from spin-rotation relaxation in symmetric perfluorinated gases will fit an equation of the form $T_1 = (1/aT)$ $(cf + \omega 2/cf)$, where f is molecular collision frequency, a is a coupling parameter, c is a collision cross-section parameter, ω is Larmor frequency, and T is temperature. However, experimentally determined parameters vary with temperature in ways that are difficult to model. In hopes that some of this temperature dependence can be accounted for by how Lennard-Jones molecules differ from hard spheres, we derived collision frequencies accordingly and sought to minimize the number of additional parameters. A thesis (2) provided a treasure trove of data and we filled gaps with additional measurements.

Results Within 3%, T_1s fit the curve, $T_1 = (1/aT)$ $(f_e + w2/f_e)$, where f_e is an effective collision frequency $f_1/b_1 + f_2/b_2 + ... + f_n/b_n$, and each f_i is the collision frequency of the fluorinated gas molecules with molecules of species i; f_1 and b_1 represent self collisions. b_1 is mildly temperature dependent, requiring one additional parameter. Parameters z_i (between 0.7 and 1.4), one for each additional species, yield the b_is as $b_i = z_i \sqrt{(m_1/m_i)}$, where m_is are molecular masses. For most biological imaging, $T_1 = T_2$, because f_es are above the T_1 minimum at $f_e = \omega$. Figure 1 shows an exemplary curve fit for T_1s of C_2F_6 at a variety of pressures. Physiologically relevant T_1s for SF_6, and CF_4 are between 0.5 and 2 milliseconds, ideal for extensive signal averaging but with T_2s suitably long for projection imaging with good resolution. C_2F_6 and c-C_4F_8 T_1s are about 4.5 times 29.5 times longer, respectively.

By including collisions with the pore walls, $f_e = f_e + f_w/b_w$, we can model T_1 changes observed when a gas is introduced to pores similar in size to the mean free path of bulk gas. Figure 2 shows T_1s of CF_4 at 3 different pressures, in fumed silica, differentially compressed to yield five different pore sizes (courtesy, Doug Smith, Nanopore Inc., Albuquerque), along with those from the b_w that yielded the best fit.

Discussion Short T_1s of inert fluorinated gases have been exploited to quantify obstructed ventilation in lungs, and measure lung volume (3). With accurate predictions of relaxation weighting, similar quantitative techniques may benefit from shorter repetition times. In some situations (*e.g.*, lung gas composition as a function of ventilation-perfusion ratio), the expected T_1 will be a monotonic function of a variable of interest, and T_1 can yield a measurement of that variable. Our T_1 *vs.* pore size model displays appropriate qualitative characteristics but accuracy requires further refinement. Nonetheless, measured T_1s are monotonic functions of pore size and can be calibrated.
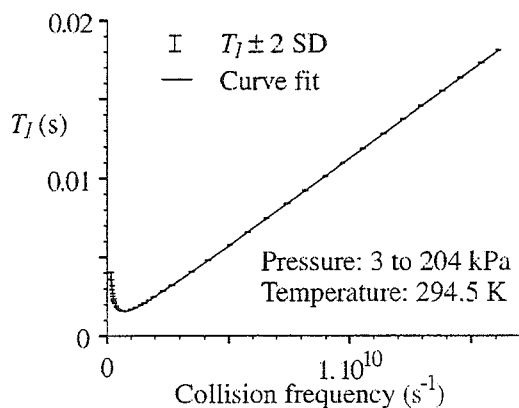
Figure 1. A bulk gas T_1 curve fit, T_1 of C_2F_6 at various pressures.
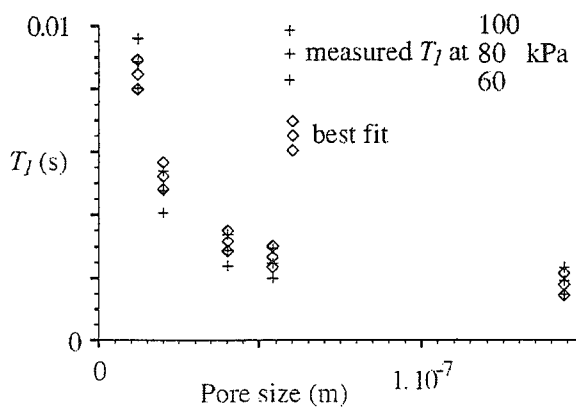
Figure 2. T_1 lengthening in small pores approximately modeled by including collision frequency with walls.

1. Armstrong, R. L. Magn. Reson. Rev. 12: 91-135. (1987).
2. Johnson, M. D. Gas phase longitudinal ... Ph.D. Thesis, UC Davis, CA, USA. 310p. (1987).
3. Kuethe, D. O. et al. J. Appl. Physiol. 88:2279-2286 (2000).

Chemically-resolved multicomponent NMR diffusion imaging in gel-stabilized microreactors

Markus Küppers, Song-I Han, Christian Heine, Siegfried Stapf, Bernhard Blümich

Lehrstuhl für Makromolekulare Chemie, ITMC, RWTH Aachen, Worringer Weg 1,
D-52074 Aachen, Germany

The optimization of fluid multiphase reactions is of major economic importance. A wide variety of geometries for industrial reactors has been designed in order to combine a maximum of both quantity and quality of reaction products with the need of minimizing the consumption of resources and energy. One widespread example is the esterification reaction which is known to be most efficient in the presence of suitable enzymatic catalysts. These enzymes, however, are only active in aqueous environments and within a limited range of reactant concentrations.

A well-established approach employs a physical separation of the organic solvent and the aqueous reaction compartment by immobilizing the enzyme in a hydrogel matrix. By dispersing the matrix as spherical drops within the reactant solution, diffusion-driven exchange of reactants and reaction products through the gel allows for a constant replacement of reactants and thus leads to a maximum efficiency in product concentration [1].

A major problem, however, in designing such microreactors is the lack of understanding of the exact properties and timescale of material transport within the spherical gel particles and to the enzymatic sites. In this study, we have investigated the model esterification reaction

$$\text{propionic acid} + \text{1-butanol} \rightleftharpoons \text{propionic acid butyl ester} + \text{water}$$
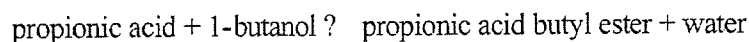
within alginate gel beads of 3 mm diameter. The beads were produced using D_2O, and cyclohexane-d_{12} was used as a solvent, with typical concentrations of both propionic acid and butanol of $10 \, \text{ml} \, l^{-1}$ (~ $1.1 \, \text{mol} \, l^{-1}$). Equivalent experiments were performed using a gel of cylindrical shape representing a one-dimensional geometry.

The ingress of both reactants as well as the reaction product from the solution into the deuterated hydrogel was first investigated separately by means of 1D ^1H concentration mapping [2] and 2D FLASH imaging, hereby acquiring typically 50-100 images over a period of 12-24 h. The ingress was shown to be fully symmetric in the imaging plane, which allowed us to reconstruct the time-resolved radial concentration profile of all components in the spherical particle by Inverse Abel Transformation [3]. The experiments were then repeated using both reactants, where chemical-shift resolved images were employed to follow the concentration dependence $c(t)$ of all reaction partners with a spatial resolution of 75 µm. The reaction rates computed from these measurements were shown to depend on radial position, which corresponds to an inhomogeneous enzyme distribution in the gel drop as a consequence of the manufacturing process. The results of the presented investigations enter the development of even smaller microreactors with improved enzyme distribution in order to achieve more efficient ester production and release rates for potential industrial-scale applications.

1. K. Buchholz, V. Kasche, Biokatalysatoren und Enzymtechnologie, VCH Verlagsgesellschaft, Weinheim, 1997.
2. B. Blümich, NMR Imaging of Materials, Clarendon Press, Oxford, 2000.
3. P.D. Majors, A. Caprihan, Fast Radial Imaging of Circular and Sperical Objects by NMR, J. Mag. Res., 94, (1991), 225-233.

INDIRECT ^{13}C IMAGING BY DOUBLE EDITING OF ^{1}H-^{13}C BONDS.

C. Casieri[1], C. Testa[2,3], A Knijn[2], G. Carpinelli[2], F. Podo[2] and F. De Luca[3]

[1] INFM and Department of Physics, University of L'Aquila, 67100 L'Aquila (Italy)
[2] Laboratory of Cell Biology, Istituto Superiore di Sanità, 00161 Rome (Italy)
[3] INFM and Department of Physics, University "La Sapienza", 00185 Rome (Italy)

NMR Spectroscopy (MRS) and Imaging (MRI) are efficient techniques to study the metabolism of living organisms. Among the nuclides useful as NMR metabolic probes, the ^{13}C and ^{1}H are especially able to provide direct information on *in vivo* glucose metabolic pathways. On the other hand, it is also known that ^{13}C detection is very time spending while that of ^{1}H is chemically quite imprecise. The detection of the ^{1}H nuclei bound to ^{13}C can increase considerably the sensitivity of ^{13}C-MRS and ^{13}C-MRI. To this aim, we propose an editing approach based on the heteronuclear scalar coupling selectivity, i. e. a J-editing sequence or X-filter, which selects only the protons coupled to ^{13}C nuclei (1,2) whose chemical shifts fall within a certain interval (3). This has been realized by introducing a double resonance pulse sequence (T-SEDOR: Twin Spin Echo DOuble Resonance) equipped with selective ^{13}C pulses. This approach, which works either for MRS or MRI, has shown a great enhancement of the chemical resolution of the ^{1}H-^{13}C bonds detection. In this work we present the MRS and MRI results obtained on aqueous solutions of different glucose metabolites. The results show that this technique permits a high sensitivity and chemical selectivity of the indirect ^{13}C detection and make it a promising tool for *in vivo* studies of metabolic topics (4).

(1) A. Knijn, C. Casieri, G. Carpinelli, C. Testa, F. Podo and F. De Luca, *NMR Biomed.*, **13**, 123 (2000).
(2) C. Testa, C. Casieri, R. Canese, G. Carpinelli, F. Podo and F. De Luca, *Magn. Res. Imag.*, **19**, 000 (2001). In print.
(3) C. Casieri, A. Knijn, F. Podo and F. De Luca, *Chem. Phys. Lett.*, **338**, 137 (2001).
(4) C. Casieri, C. Testa, G. Carpinelli, F. Podo and F. De Luca, *J. Magn Res.* Submitted.

Magnetic Resonance Imaging of Solid Polymers at Elevated Temperatures Using SPRITE

Bryce MacMillan, Meghan Halse, Bruce Balcom

MRI Centre, Department of Physics, University of New Brunswick, Fredericton, New Brunswick, Canada

Polymers and polymer science are becoming increasingly more important in many industrial and manufacturing processes, and research and development of new composites and new applications of these materials has accelerated accordingly.

Magnetic Resonance Imaging (MRI) of solid polymers is difficult due to their very short spin-spin relaxation times[1]. In some instances, this has been overcome by imaging the polymers at elevated temperatures[2]. This traditionally has required exceeding the glass transition temperature, and so the number of polymers with which this approach is successful is limited.

Single Point Imaging (SPI) sequences, particularly the SPRITE[3] sequence (Single Point Ramped Imaging with T_1 Enhancement) have proven effective in imaging a variety of solid polymers[4]. However, there are still many more polymers which cannot be imaged due to their very short spin-spin relaxation times.

When combined with the sample heating approach, SPRITE has the potential to successfully image a much wider variety of solid polymers. With the SPRITE sequence, the only requirement is that T_2^* becomes long enough that the signal can be phase encoded. The minimum phase encoding time in these methods is limited by the instrument deadtime which is usually tens of microseconds at present, but which may be greatly reduced in future.

We have found that T_2^* in a wide variety of polymers increases sufficiently upon heating to be successfully imaged. A typical T_2^* change (which still varies greatly with the polymer) would be 15 μs at room temperature to 240 μs at 84 C and 330 μs at 124 C.

We use the SPRITE technique to image solid polymers by elevating the sample temperature. Polymers that are invisible to these methods at room temperature are readily imaged at higher temperatures.

1. Jackson, P. et al., Polymer International, 24, 139-143 (1991)
2. Jezzard, P.J. et al., Polymer Communications, 32, 74-76 (1991)
3. Balcom, B.J., et al., J. Mag. Res., A123, 131-134 (1996)
4. Kennedy, C.B., et al., Can. J. Chem., 76, 1753-1765 (1998)

Multi-channel Gradient Probe for the Super-Parallel MR Microscope

Yoshimasa MATSUDA, Tomoyuki HAISHI(*), Yukako YAMAZAKI, Katsumi KOSE
Institute of Applied Physics, University of Tsukuba, Tsukuba 305-8573,
(*) MR Technology Inc. Tsukuba, 300-2642 JAPAN

The super-parallel MR microscope, in which a large number of samples (up to 100) can be imaged at the same time, has been proposed by our group (1). One of the key units is the multi-channel gradient probe, in which gradient coils are attached to each RF coil to achieve a high efficiency and low inductance. In the present study we have developed an eight-channel gradient probe and measured the performance using imaging experiments.

The eight-channel gradient probe consists of the 2 x 4 array of the gradient probe units: each unit can be used for a usual MR microscope (Fig.1). The gradient coils for z direction (static magnetic field direction) are Maxwell pairs and those for x and y directions are parallel four wires. The coils of each gradient probe unit are so connected that gradient fields are cooperatively generated at the sample zones: Figures 2 and 3 show the directions of the electrical currents for Gz and Gx (Gy) coils.

We performed imaging experiments to test the gradient probe using a 1.5 T magnetic field of a clinical MRI. Eight water phantom images (Fig.4) were acquired one by one at eight sample zones when all of the gradient coils were driven at the same time. This figure demonstrates that the design concept is fine.

(1) K. Kose, T. Haishi, Y. Matsuda, I. Anno, 9th ISMRM, 609.
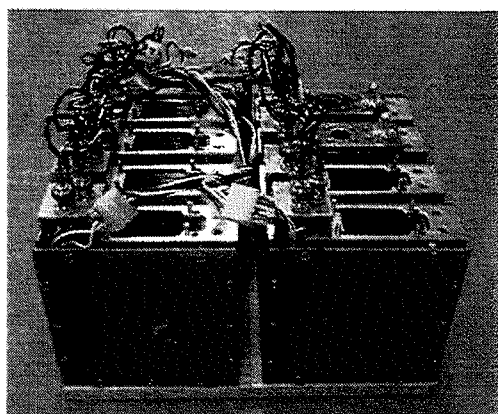
Fig.1 Eight-channel gradient probe.
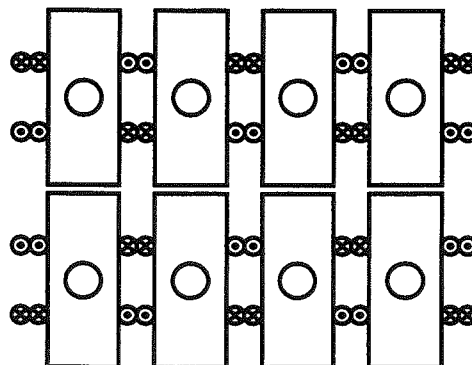
Fig.2 Current directions for Gz coils.
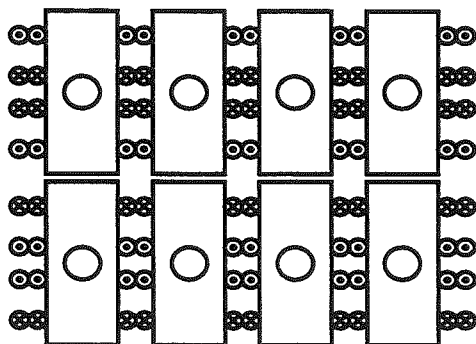
Fig.3 Current directions for Gx coils.
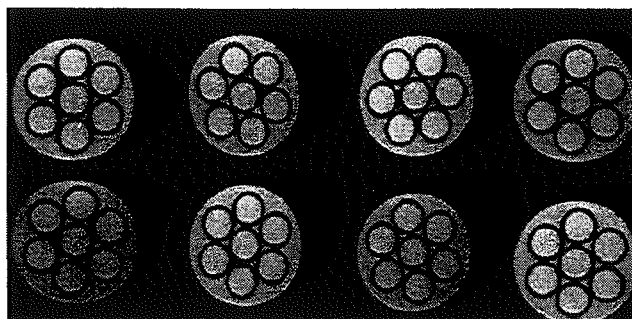
Fig.4 Phantom images acquired at eight sample zones.

P-52

Multi-channel Digital Receiver for the Super-Parallel MR Microscope

Shin UTSUZAWA, Yoshimasa MATSUDA(*), Tomoyuki HAISHI, Katsumi KOSE(*)
MR Technology Inc. Tsukuba 300-2642
(*)Institute of Applied Physics, University of Tsukuba, Tsukuba 305-8573, JAPAN

The super-parallel MR microscope, in which a large number of samples (up to 100) can be measured at the same time, has been proposed by our group (1). One of the key units is the multi-channel digital receiver system, in which NMR signal detection is essentially performed by high-speed signal sampling at the intermediate frequency. In the present study we have developed a four-channel digital receiver unit using a single AD converter board.

Figure 1 shows one transmitter-receiver unit for the super-parallel MR microscope for a 1.5 T static magnetic field. The 800 kHz intermediate frequency was determined by the sampling frequency of 3.2 MHz: a PC-431 AD converter board (DATEL Inc.) can simultaneously sample four-channel NMR signal at the 3.2 MHz sampling clock. The AD converter board configured on a PCI card was installed to a PC and an image reconstruction program for the sampled data was developed on Windows98 operating system.

The digital receiver system was tested using an "MRI signal simulator" which used a DSP board (DSP6031) and I/Q modulator. Figure 2 shows the reconstructed image using the 800 kHz intermediate frequency signal. Although some artifacts are seen because of system noise and some timing errors, these artifacts will be removed by synchronous operation of the whole digital system. Since the four-channel digital receiver system can be constructed on a single PCI card, this system has a good space and cost performance for the super-parallel MR microscope.

(1) K. Kose, T. Haishi, Y. Matsuda, I. Anno, 9th ISMRM, 609.
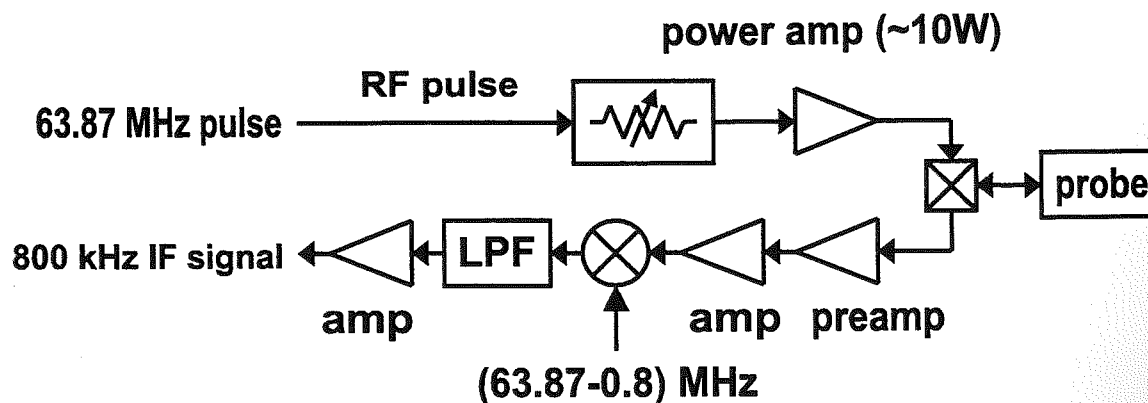
Fig. 1 Transmitter-receiver unit for the super-parallel MR microscope.
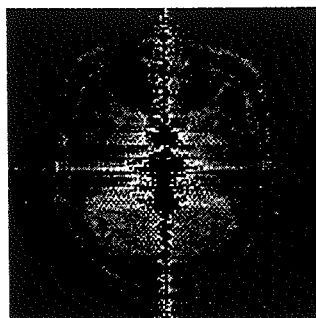
Fig. 2 Reconstructed image using the 800 kHz intermediate-frequency MRI signal.

NMR MOUSE : Developing the Mobile Surface Explorer

M.C.A. Brown, M.J.D. Mallett and P. Blümler
School of Physical Science, University of Kent at Canterbury, Canterbury CT2 7NR, U.K.

Abstract

The MOUSE is a new technique that was designed to non-destructively analyse surfaces of arbitrarily shaped and large samples. The probe not only provides the static inhomogeneous B_0 field, it includes an integral rf coil for excitation and detection. The inhomogeneous B_1 field the coil produces excites a very small volume of space to perform in situ measurements upon. The probe is also a very compact and cheap to manufacture item. The advantages of this configuration are primarily in the field of materials sciences, because traditional measurements are performed in a standard spectrometer which have a small sample volume (notably for MAS spectrometers), and therefore large samples would have to be cut down to size.

The current objective involves redesigning the MOUSE to become imaging capable. The developmental work involved in this task includes the modelling and experimentally determining the magnetic properties of the MOUSE as well as testing and analysing new designs. Also involved is the configuration of a set of gradient coils and writing a pulse sequence to obtain spatially resolvable data and thus produce the images. A number of preliminary designs have already been constructed and some of the results are shown within.

References

[1]   G. Eidmann, R. Savelsberg, P. Blümler,and B. Blümich; J. Magn. Reson. **A122**:104-109; (1996).
[2]   B. Blümich, P. Blümler, G. Eidmann, A. Guthausen, R. Haken, U. Schmitz, K.Saito, and G. Zimmer; Magn. Reson. Imag, **16** (5/6); 479-484; (1998).

The Construction of Portable MRI devices.

G. Dunn, M.J. Mallett.
School of Physical Sciences, University of Kent at Canterbury, Kent, UK.

P. Blümler.
Max-Planck Institute for Polymer Research, Mainz, Germany.

ABSTRACT
Hand held MRI devices such as the NMR-Mouse have already been developed at the Magnetic Resonance Centre at Aachen, Germany and at the University of Kent at Canterbury [1]. These devices are, however, only capable of penetrating a few millimetres into a sample. To investigate an entire sample requires a different concept for portable NMR devices.

A computer simulation model has been developed using Opera-3d by Vector Fields Ltd. Several configurations of permanent magnets and the resultant magnetic fields were investigated. The most promising arrangement was selected and a prototype constructed. The new device consists of two magnetic rings separated by an air gap. This arrangement results in an acceptably homogenous static polarization field B_0. A solenoidal coil is placed in the center of the rings to deliver the rf field B_1. The primary aim of the project is to produce two-dimensional images via repositioning of the device and so gradient coils will be required.

The device has been used to measure transverse relaxation times in a variety of fruits and work is continuing to map the B_0 field in order to compare it with the computer simulation.

The important advantages of this type of device are portability and low cost. Further uses include the investigation of objects *in situ* such as fruit, trees, pipe work and animal limbs.

REFERENCE
[1] Blümlich B. *NMR Imaging of Materials*. Oxford Science Publications, Clarendon Press, Oxford 2000. ISBN 0 19 850683 X

Dedicated MRI System for On-Line Selection of Female Salmons

Katsumi KOSE, Yusuke AKITA, Tomoyuki HAISHI(*), Yoshimasa MATSUDA
Institute of Applied Physics, University of Tsukuba, Tsukuba 305-8573
(*) MR Technology Inc. Tsukuba, 300-2642 JAPAN

Salmon roe is a favorite food for Japanese people, often served with sushi. Salmons are captured in the ocean (about 1,000 salmons for one ship) and separated into females and males in fishing ports, because female salmons are much more expensive than male salmons. However, since the selection by the appearance (Fig.1) is a very time-consuming task (at least 30 seconds for one salmon even by an expert), development of a high-speed selection system has been desired. For this requirement, we have developed an MRI specially designed for on-line selection of female salmons.

Figure 2 shows the overview of the system. A 0.2 T C-shaped permanent magnet with a 25 cm gap (50 ppm homogeneity for 15 cm dsv) was used for the magnet. For the RF coils, two solenoid coils with a 14 cm circular aperture and a 14 cm x 22 cm oval aperture were developed. Figure 3 shows cross-sectional images of male and female salmons acquired with a gradient echo sequence (TR=30ms, TE=15ms, acquisition time=3.84 sec). Salmon roe was clearly visualized as a dark region because the T_2 is shorter than that of the surrounding tissue (muscle). However, since the requirement for the selection speed for one salmon is less than one second, we imaged salmons using a much faster gradient-echo sequence (TR=12.3ms, TE=10ms, acquisition time=0.8s). Figure 4 show the results: the presence of salmon roe is barely seen. The poor image contrast is due to T_1 saturation and the short echo time. Although faster T_2 weighted imaging sequences, such as EPI, RARE, snapshot FLASH, are desirable for salmon roe visualization, the total system cost could not allow the use of a high performance gradient system. To solve the problem, we are now planning to use a fast line-scan method in the next season (from October to February in the northern hemisphere).
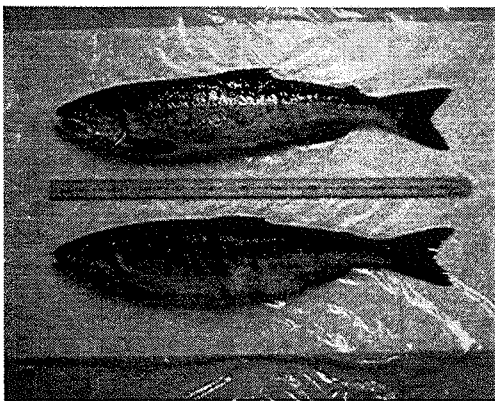
Fig.1 Male (upper) and female (lower) salmons.
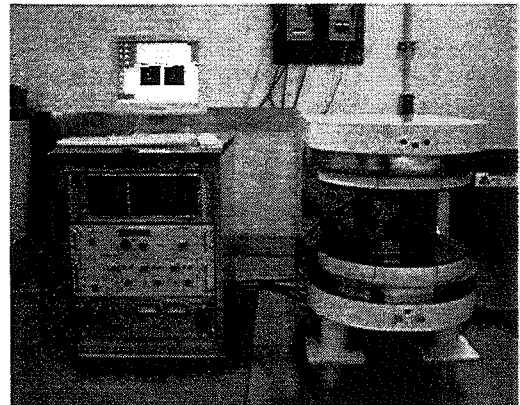
Fig.2 MRI for on-line salmon selection.
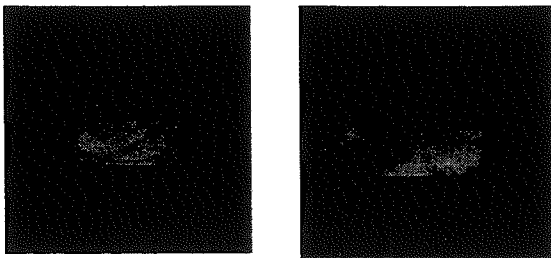
Fig.3 Male (left) and female (right) salmons.
TR/TE=30ms/15ms, 128x128 pixels
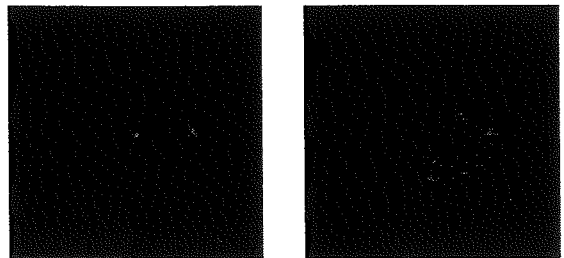
Fig.4 Male (left) and female (right) salmons.
TR/TE=12.3ms/10ms, 64x64 pixels

Compact MRI System for Trabecular Bone Density Measurements

Tomoyuki HAISHI, Yukako YAMAZAKI(*), Yoshimasa MATSUDA(*), Shin UTSUZAWA
Katsumi KOSE(*), MR Technology Inc. Tsukuba 300-2642
(*) Institute of Applied Physics, University of Tsukuba, Tsukuba 305-8573, JAPAN

Osteoporosis is a common disease associated with aging. About 50% of women above age of 70 are osteoporosis in Japan and many countries are in the similar situation. For the diagnosis of osteoporosis, DEXA (Dual-Energy X-ray Absorptiometry) is the standard method, but cannot be used repeatedly nor for young women because of the radiation problem. Measurement of sound velocity or attenuation of ultrasound through a bone is another diagnostic tool. However, this method cannot measure the trabecular bone density which is a good index for diagnosis of osteoporosis. MRI is thus expected for a new diagnostic tool.

MR measurements of trabecular bone density or structure have been studied by several groups for more than ten years (1,2). However, as far as we know, an MRI system specially designed for diagnosis of osteoporosis has never been reported. In the present study we have developed a compact MRI system to image a heel and performed preliminary measurements of trabecular bone density for 16 normal volunteers.

Figure 1 shows the overview of the MRI system developed in this study. A 0.2 T permanent magnet with 116 mm gap was used for the magnet. An RF solenoid coil with an oval aperture (68 mm x 88 mm) was developed to image a heel. To identify the anatomical structure of a heel, 3D images of heels (1 mm cube resolution) were acquired using a 3D gradient echo sequence. Figure 2 shows a 2D slice image selected from the 3D data set. This image clearly shows the position of calcaneus. To measure the relative bone density, 2D cross-sectional images of heels of 16 normal volunteers were acquired using a 2D spin-echo sequence together with a water phantom (Fig.3). The imaging time for one 2D image was 102.4 seconds. Although corrections for relaxation times and RF coil sensitivity are required to quantify the trabecular bone density, our results have demonstrated a possible use of the MRI system for the diagnosis of osteoporosis.
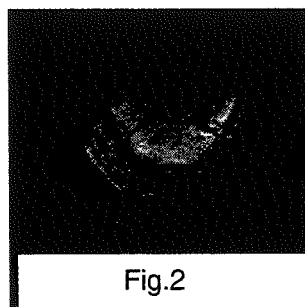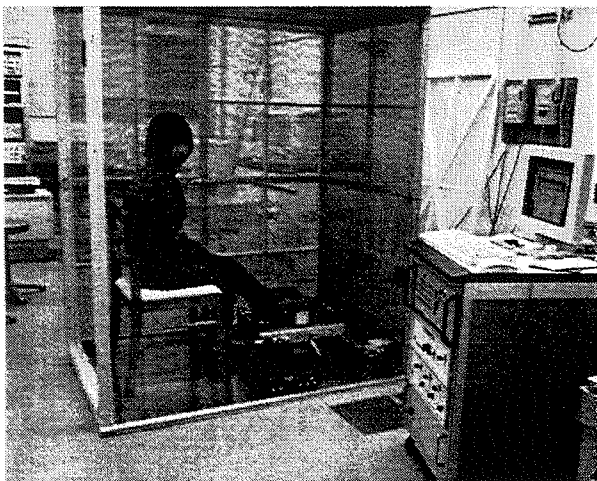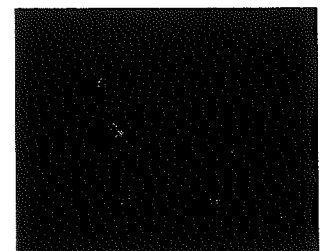
Fig.2   Fig.3

(1) Chung H, Wehrli FW, Williams JL, et al. Proc Natl Acad Sci USA 1993; 90: 10250-4.
(2) Wehrli FW, Ford JC, Haddad JG. Radiology 1995;196;631-41.

Quadrupole Resonance Explosive Detection Systems.

Quantum Magnetics, 7740 Kenamar Court, San Diego, CA 92104, USA.
Email: ahudson@qm.com, Phone:+01-858-566-9200, Fax:+01-858-566-9388

Alex Hudson, Hector Robert, Chin Wu, Tim Rayner and Lowell Burnett

The effect of quadrupole resonance may be used to detect the presence (or absence) of crystalline substances. Whilst similar to the technique of NMR, the signal may be detected without the use of a static (DC) magnetic field. This has considerable benefits in some scenarios. For example, quadrupole resonance may be used to screen a large item for the presence of crystalline narcotics or explosives.

The technology has seen significant development in the field of aviation security for the detection of plastic and sheet explosives, concealed within baggage. Its utility has also been demonstrated for the detection of buried land mines. The development and commercialization of these technologies is the main focus of Quantum Magnetics Inc.

In order to realize this goal, significant advances have been made both in the RF hardware and pulse sequences required to take quadrupole resonance out of the lab and to make it work in an operational environment.
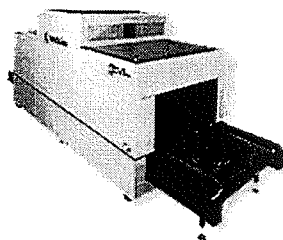
A Quantum Magnetics QScan 500^{TM} explosives detection machine

The Quantum Magnetics landmine detection prototype.

Index of Authors and Abstract Titles